High Density Fluctuations in Neutron Stars

Masterthesis im Fach Physik

vorgelegt von

Konstantin Otto

Betreuer und Erstbegutachter:

PD Dr. Bernd-Jochen Schaefer

Zweitbegutachter:

Prof. Dr. Christian Fischer

23. November 2017

Institut für Theoretische Physik
Justus-Liebig-Universität Gießen

JUSTUS-LIEBIG-
UNIVERSITÄT
GIESSEN

Abstract

High Density Fluctuations in Neutron Stars
The impact of thermal and quantum fluctuations at high baryon chemical potential on neutron stars is studied in the framework of the quark-meson model. Mean field and functional renormalization group (FRG) solutions are presented for both an $N_f = 2$ and an $N_f = 2 + 1$ version of the quark-meson model in order to determine the role of strangeness in compact objects. It is found that already the inclusion of vacuum fluctuations in mean field approximation alters the mass-radius relationships of neutron stars to lower maximum masses. The inclusion of mesonic fluctuations in the FRG approach significantly increases neutron star radii and masses such that a maximum mass of $2.5\,M_\odot$ could be attained. Although the addition of strangeness is observed to reduce the stiffness of the equation of state in general, it is found that in the FRG approach this effect only occurs at high chemical potentials above the stability region of the given neutron star solutions and the influence of strangeness is negligible.

Fluktuationen bei hoher Dichte in Neutronensternen
Der Einfluss von thermischen Fluktuationen und Quantenfluktuationen bei hohem baryonischen chemischen Potential auf Neutronensterne wird im Rahmen des Quark-Meson-Modells untersucht. Ergebnisse in Mean-Field-Näherung und unter Anwendung der Funktionalen Renormierungsgruppe (FRG) werden sowohl für eine Version des Quark-Meson-Modells mit $N_f = 2$ als auch eine Version mit $N_f = 2 + 1$ dargelegt, um die Rolle von Strangeness in kompakten Objekten zu bestimmen. Es wird beobachtet, dass schon die Mitnahme von Vakuumfluktationen in der Mean-Field-Näherung die Masse-Radius-Beziehung von Neutronensternen zu niedrigeren maximalen Massen verschiebt. Die Einbindung mesonischer Fluktuationen durch den FRG-Ansatz vergrößert die Radien und erhöht die Massen von Neutronensternen deutlich, sodass Massen bis zu $2.5\,M_\odot$ erreicht werden können. Obwohl durch das Hinzufügen von Strangeness im Allgemeinen eine Verringerung der Steifigkeit der Zustandsgleichung beobachtet werden kann, wird im Falle des FRG-Zugangs festgestellt, dass dieser Effekt nur bei hohen chemischen Potentialen über der Stabilitätsregion der berechneten Neutronensterne auftritt und der Einfluss von Strangeness somit zu vernachlässigen ist.

Contents

1 Introduction

The cosmos has always been the largest laboratory known to humankind. From the precise description of planet orbits by Johannes Kepler to their mathematical explanation in form of Isaac Newton's law of gravity, cosmological observables have already influenced the early physics of classical mechanics. These findings, however, should not be the only significant contributions to new theories. A generalization to graviationally interacting objects lead Einstein from special relativity to general relativity and allowed the successful description of many cosmological effects such as gravitational lensing [1]. Next to classical large-scale physics as described by general relativity, effects from small-scale quantum theories are essential in the explanation of various stellar observations. Among those are the nuclear fusion processes required to understand stellar nucleosynthesis as well as the ability of white dwarfs to withstand gravitational collapse via Pauli degeneracy pressure. The modern description of quantum effects is accomplished with the help of quantum field theories. In the standard model we know three elementary forces that can be transmitted via the exchange of gauge bosons and allow a quantum field theoretical description: the weak force transmitted via the Z and W bosons, the electromagnetic force transmitted via photons in quantum electrodynamics, and the strong force that is described by the interaction of quarks and the gauge bosons of quantum chromodynamics, the gluons. At very high energies, a unification of the weak and electromagnetic forces has already been achieved by Glashow, Salam and Weinberg [2–4] in the framework of an electroweak interaction. Nevertheless, a unified description of all elemental forces in nature fails to this day because the quantization of gravity using a Graviton exchange boson yields non-renormalizable interactions. Hence, the study of stellar object always encompasses a transfer from microscopical, quantized interactions to a macroscopical classical description that includes gravity as known from general relativity. This is achieved by calculating the thermodynamical equation of state from the quantum theory and applying it to a differential equation for the pressure and mass distribution of a stellar object, i.e. the Tolman-Oppenheimer-Volkoff (TOV) equation.

In modern day research, the study of the stars with the highest known density (except black holes), so-called neutron stars, is of great interest. The reason for this is that at the densities expected in such cold and dense compact objects, nuclear physics is pushed to its boundaries and the emergence of new degrees of freedom from the strong interaction is expected. As already mentioned, the strong interaction is described by a quantum field theory called quantum chromodynamics (QCD). It is a local gauge theory of the $SU(3)$ gauge group and includes quarks of multiple flavors interacting via gluons as well as gluon self-interaction. It knows three different color charges (and anticharges) of which each quark carries one and color neutrality can be achieved by a combination of all three different elementary charges. Furthermore, it displays unique features like asymptotic freedom and confinement. While the former means that at asymptotically large energies, the theory becomes weakly coupled and perturbative, the latter means that quarks are confined to color-neutral states at low energies. This explains the occurence of baryonic and mesonic degrees of freedom at low energies and a transition to free quark-gluon matter, the quark-gluon plasma, is conjectured for matter of very high temperature or chemical potential. While the phase diagram of this non-perturbative theory is already well understood at chemical potentials close to

zero thanks to e.g. lattice QCD calculations, the low temperature and high density region can neither be accessed by experiment nor by first principle calculations to this day. Hence, data from neutron stars which live in this regime can constrain possible equations of state which in turn constrains effective theories and models that aim at describing the complex phase structure that is expected in the high density region of the QCD phase diagram. In that way, the study of neutron stars can be understood as interdisciplinary research combining the fields of small-scale quantum physics and large-scale general relativity.

This work aims at conducting a first study of the properties of neutron stars with an equation of state obtained from the quark-meson (QM) model, a low-energy effective theory of interacting constituent quarks and mesons which displays a chiral phase transition similar to the one expected in QCD. In particular, the influence of thermal and quantum fluctuations at high density on the thermodynamics of the theory and their impact on mass-radius relationships of neutron stars are of interest. On top of that, the role of strangeness shall be investigated as well. To this end, the quark-meson model is formulated and solved for both two light quark flavors ($N_f = 2$) and two light flavors plus a heavier strange quark flavor ($N_f = 2 + 1$). The solution is acquired in mean field approximation both without consideration of the divergent vacuum term and with a renormalized version of the vacuum contribution included. Furthermore, both versions of the model are solved with a functional renormalization group (FRG) flow equation that allows the inclusion of meson fluctuations. The TOV equation is solved for all these configurations and a comparison between the mass-radius relationships of neutron stars based on the individual equations of state allows for a determination of the role of various fluctuations and strangeness in this framework.

In Sec. 2 of this work, the modern research status and important properties concerning neutron stars are conveyed. The TOV equation is derived and important restrictions on possible equations of state are considered. In Sec. 3, the features of quantum chromodynamics are detailed and chiral symmetry is investigated. The Lagrangian of Nambu–Jona-Lasinio type models is made plausible as an effective low-energy description of QCD and a bosonization procedure leads to a Lagrangian close to that of the quark-meson model. The QM model is further elaborated on in Sec. 4 where the two- and 2+1-flavor versions are defined. A solution in standard mean field approximation (without the vacuum term) is derived in Sec. 5. The functional renormalization group flow equation is then calculated in Sec. 6 and from its fermionic part, the idea of a renormalized mean field approximation is followed. Sec. 7 details the numerical setup used in this work and introduces the thermodynamic relations used in the calculation of the equation of state. The numerical results are discussed in Sec. 8 and a summary and an outlook to future investigations are given in Sec. 9. The appendices pick up technical details such as the conventions of the Matsubara formalism employed in this work (App. A) and analytic limits for vanishing temperature of flow equations and integrals (App. B). The calculation of meson masses is explained in App. C and starting parameters are given in App. D.

2 Neutron Stars

The study of neutron stars has experienced considerable research interest in recent years. Cold and dense objects that underlie the quantum nature of the strong interaction on the one hand and are subject to their own gravitational pull on the other hand, they connect the physics of microscopic interactions with the macroscopically relevant theory of general relativity. Various experiments are aimed at gathering important neutron star data such as mass-radius relations. The Neutron Star Interior Composition Explorer (NICER) experiment at ISS is specifically designed to probe the inner structure of such compact objects with precise x-ray measurements [5]. Gravitational wave detectors such as LIGO, Virgo, GEO, and several others that are in planning or construction like the space-based experiment LISA are searching for cosmic events like mergers of black holes and neutron stars. Very recently, the first neutron star merger has successfully been detected by the LIGO-Virgo collaboration and confirmed by electromagnetic telescope measurements [6]. Furthermore, pulsar timing arrays use fast-spinning neutron stars that are spread out over large distances as a clock to detect low-frequency gravitational waves [7]. Ultimately, new collider experiments like the CBM (Compressed Baryonic Matter) experiment that is currently built at FAIR in Darmstadt aim to probe strongly interacting matter at higher densities and lower temperatures than previous collider experiments [8]. Findings about e.g. the expected phase transition to a quark-gluon plasma are of relevance for the description of processes in the inner core of neutron stars [9]. This is the case because there is still no clarity on the state of matter at high densities and low temperatures. Traditionally, neutron stars are described by nuclear models, but at high densities unbound quarks, the elementary building blocks of protons, neutrons and other hadrons, should emerge. Observations of neutron stars with masses greater than two solar masses, such as the pulsar (rotating neutron star) J0348+0432 at $\sim 2.01\, M_\odot$ [10], demand a stiff equation of state, i.e. a high pressure per unit of energy density, in order to withstand gravitational collapse. At the densities present in the inner core of a neutron star, strange quarks are expected to play a role. If they first appeared in the confined phase in strange baryons (hyperons), this would according to previous studies weaken the equation of state significantly and one could not reach two solar masses [11]. If a deconfinement phase transition to quark matter happened first and strangeness appeared in the form of strange quark degrees of freedom, this could potentially resolve the problem which is commonly referred to as the "hyperon puzzle". In that case, one would speak of hybrid stars as those objects do not purely consist of nucleonic matter anymore. Unfortunately, the equation of state of hybrid stars and pure neutron stars tend to look very similar, which means it is hard to distinguish between such objects from experimental results like mass-radius relationships. This issue is also called the "masquerade problem" [12]. A search for gaps in the mass-radius curves of observed neutron stars has been proposed, which would allow a classification of compact objects into groups and indicate a first order phase transition from hadron to quark matter, thereby proving the existence of a critical endpoint in the phase diagram of Quantum Chromodynamics (as elaborated further in Sec. 3) [13].

2.1 Properties

Neutron stars stand at the end of the life cycle of many heavy stars that do not possess enough mass to collapse into a black hole. Main-sequence stars like the sun primarily consist of hydrogen and helium and develop sufficient thermal pressure to fight gravity

via nuclear fusion of hydrogen to helium [14]. If this reaction stops due to a lack of fuel, stars with a mass of $8\,M_\odot$ or lower usually collapse and shed all remaining layers until only an iron core remains. This remainder, a white dwarf, is kept from collapsing by ultrarelativistic electron degeneracy pressure, which works up to the Chandrasekhar limit that determines a maximum white dwarf mass of $\sim 1.4\,M_\odot$ [15]. Heavier stars oftentimes feature high enough core temperatures for the iron nuclei to disintegrate with the help of high energy photons into protons and neutrons. The protons in turn can capture electrons which gives a neutron and a neutrino. The loss in electron pressure triggers a second collapse. The sudden stop of this collapse around nuclear density is accompanied by a supernova, shockwaves that violently propel remaining outer layers away from the core [14]. The remainder that now has densities of the order of nuclear matter is a neutron star. Note that assuming the object in question has a constant nuclear density of $10^{18}\,\mathrm{kg/m^3}$, the Schwarzschild radius

$$R_S = \frac{2MG}{c^2} \tag{2.1}$$

becomes greater than the object's actual radius at a mass of approximately $4.3\,M_\odot$ and above. This serves as a rough upper bound for possible neutron star masses, because anything more massive becomes a black hole. However, it does not mean that neutron stars up to this mass are actually stable and can exist. As already stated, neutron stars of $2\,M_\odot$ already pose significant theoretical constraints on possible equations of state of cold and dense matter.

Typical temperatures of neutron stars are below 1 MeV, which is close to zero in scales of the strong interaction [16]. The radius is of order 10 km and one distinguishes three different layers in the modern description of compact stars. The outer crust has a radius of about 0.5 km and its mass is only $\sim 0.01\,M_\odot$ [17]. Here, separate nuclei can exist, but going to higher densities, neutrons start "dripping" out into the continuum. Close to the outer core, protons and neutrons build complex nuclei that resemble pasta [18]. From the crust to the outer core, a phase transition to liquid nuclear matter occurs. The outer core can be described by nuclear models up to densities of twice the nuclear matter density n_0. Typically, one employs one isospin symmetric and one pure neutron matter model in beta equilibrium [16]. This allows for the conversion process of protons into neutrons under electron capture which renders the interior of the star very neutron rich. The inner core starts at densities of $2\,n_0$ and to incorporate the emergence of quark degrees of freedom, one includes a quark model equation of state that is expected to hold at $\sim (4-7)\,n_0$. Then, either the state of matter that gives the lower energy density at each chemical potential is chosen or an interpolation between the two equations of state is performed. The first method requires a Maxwell construction and results in a first order transition from hadronic matter to deconfined quark matter while the second matter represents a continuous (crossover) transition [16]. Note that the given densities are not high enough for perturbative QCD calculations. Hence, typical low-energy approximations of the strong interaction that neglect the gauge sector like the Nambu–Jona-Lasinio (NJL) model [19, 20] come into place, allowing for chiral and, optionally, diquark condensates [21]. Phenomenological approaches are applied as well. For example, the energy difference of the non-perturbative and the perturbative vacuum can be expressed by a bag constant [16]. NJL type approaches that feature an effective bag constant are also utilized [22, 23]. Furthermore, the phenomenological string-flip model [24, 25] has recently been extended to strange quark flavors and

applied to neutron stars [26].

2.2 Tolman-Oppenheimer-Volkoff Equation

A relation between external properties of stellar objects, specifically mass and radius, and internal properties of matter can be established with the Tolman-Oppenheimer-Volkoff equation [27–29]. It is a differential equation for the pressure $p(r)$ of spherically symmetric, non-rotating heavy objects in hydrostatic equilibrium and follows from general relativity (GR). In general relativity, we define the covariant derivative of a vector [1]

$$\nabla_\mu V^\nu = \partial_\mu V^\nu + \Gamma^\nu_{\mu\lambda} V^\lambda \quad , \tag{2.2}$$

such that the object $\nabla_\mu V^\nu$ itself transforms like a tensor. The $\Gamma^\nu_{\mu\lambda}$ are the connection symbols. The connection is, from a perspective of differential geometry, not unique. If we demand it to be symmetric in the lower indices and render the covariant derivative of the metric zero, $\nabla_\rho g_{\mu\nu} = 0$, we obtain the Christoffel connection that also renders the proper time of a physical path extremal and is therefore used in GR. The Christoffel symbols are

$$\Gamma^\sigma_{\mu\nu} := \frac{1}{2} g^{\sigma\rho} (\partial_\mu g_{\nu\rho} + \partial_\nu g_{\rho\mu} - \partial_\rho g_{\mu\nu}) \quad . \tag{2.3}$$

From these definitions, the covariant derivative of a one-form can be shown to behave like

$$\nabla_\mu \omega_\nu = \partial_\mu \omega_\nu - \Gamma^\lambda_{\mu\nu} \omega_\lambda \quad . \tag{2.4}$$

Consequently, the covariant derivative of a general tensor is just the sum of its partial derivative and one Christoffel term per upper and lower index, respectively. Given a connection, one can define the Riemann curvature tensor

$$R^\rho{}_{\sigma\mu\nu} := \partial_\mu \Gamma^\rho_{\nu\sigma} - \partial_\nu \Gamma^\rho_{\mu\sigma} + \Gamma^\rho_{\mu\lambda} \Gamma^\lambda_{\nu\sigma} - \Gamma^\rho_{\nu\lambda} \Gamma^\lambda_{\mu\sigma} \quad . \tag{2.5}$$

With the Christoffel connection in use, it is a measure for the curvature of spacetime and vanishes if the metric becomes coordinate independent (flat spacetime). The Ricci tensor follows from contracting the upper index with the second lower index:

$$R_{\mu\nu} := R^\lambda{}_{\mu\lambda\nu} \tag{2.6}$$

and the Ricci scalar is just the trace

$$R := g^{\mu\nu} R_{\mu\nu} \quad . \tag{2.7}$$

They are the defining terms of the Einstein tensor

$$G_{\mu\nu} := R_{\mu\nu} - \frac{1}{2} R g_{\mu\nu} \quad . \tag{2.8}$$

The Einstein equation of general relativity now relates the curvature of spacetime to the presence of matter, expressed by the energy-momentum tensor $T_{\mu\nu}$:

$$G_{\mu\nu} = 8\pi G T_{\mu\nu} \quad , \tag{2.9}$$

with G being Newton's gravitational constant. For flat spacetime in the vacuum, $T_{\mu\nu} = 0$, Einstein's equation $G_{\mu\nu} = 0$ is trivially fulfilled. The general non-trivial vacuum solution under the assumption of spherical symmetry is the Schwarzschild metric

$$\mathrm{d}s^2 = -\left(1 - \frac{2GM}{r}\right) \mathrm{d}t^2 + \left(1 - \frac{2GM}{r}\right)^{-1} \mathrm{d}r^2 + r^2 \mathrm{d}\Omega^2 \tag{2.10}$$

with

$$\mathrm{d}\Omega^2 = \mathrm{d}\theta^2 + \sin^2\theta\,\mathrm{d}\phi^2 \quad . \tag{2.11}$$

Note that here we use the Minkowski metric $\eta_{\mu\nu} = \mathrm{diag}(-1,+1,+1,+1)$ that is obtained asymptotically for large distances r from the coordinate center and a transformation to Euclidean coordinates. In the rest of the work we will use the $(+,-,-,-)$ signature that is more common in hadron physics. There are two singularities, one at $r = 2GM$ that can be identified with the Schwarzschild radius, cf. Eq. (2.1) (with natural units where $c = 1$), and one at $r = 0$. The Schwarzschild radius is just a coordinate singularity and can be circumvented by switching to different coordinates, but it also signifies the event horizon that no time- or lightlike trajectories can traverse from the inside. Hence, spherically symmetric objects that are smaller than the Schwarzschild radius can not be directly observed from the outside and are classified as black holes. It shall be mentioned that if an object is larger than its formal Schwarzschild radius, there does not have to be an event horizon at all since the metric is governed by the presence of matter, $T_{\mu\nu} \neq 0$, and the Schwarzschild solution is invalid in that regime. The second singularity can be associated with a true singularity in spacetime [1] but we do not have to worry about that because we want to describe objects of finite proportions. Typically, stars are described as perfect fluids with the ansatz

$$T^{\mu\nu} = (\varepsilon + p)U^\mu U^\nu + p g^{\mu\nu} \tag{2.12}$$

for the energy-momentum tensor where

$$U^\mu := \frac{\mathrm{d}x^\mu}{\mathrm{d}\tau} \tag{2.13}$$

is the four-velocity and τ the proper time. This makes sense since in Minkowski space in the rest frame of the fluid the four-velocity becomes $U^\mu = (1,0,0,0)^T$ and therefore the components of the energy-momentum tensor are $T^{\mu\nu} = \mathrm{diag}(\varepsilon, p, p, p)$. ε is the energy density and p is the isotropic pressure in the rest frame. Inside such a star, we can also take a spherically symmetric ansatz and ensure correct signs in the Lorentzian metric by using exponential functions:

$$\mathrm{d}s^2 = -\mathrm{e}^{2\alpha(r)}\mathrm{d}t^2 + \mathrm{e}^{2\beta(r)}\mathrm{d}r^2 + r^2\mathrm{d}\Omega^2 \quad . \tag{2.14}$$

The energy-momentum tensor changes compared to the tensor in flat spacetime but we can still move into the fluid's rest frame such that the four-velocity only has one component and exploit its normalization:

$$-1 = U_\mu U^\mu = g_{\mu\nu}U^\mu U^\nu = -\mathrm{e}^{2\alpha(r)}(U^0)^2 \quad \Rightarrow \quad U^0 = \pm\mathrm{e}^{-\alpha(r)} \quad \Rightarrow \quad U_0 = \mp\mathrm{e}^{\alpha(r)} \quad . \tag{2.15}$$

Hence the energy-momentum tensor reads

$$T_{\mu\nu} = \mathrm{diag}\left(\mathrm{e}^{2\alpha(r)}\varepsilon\ ,\ \mathrm{e}^{2\beta(r)}p\ ,\ r^2 p\ ,\ r^2\sin^2\theta\, p\right) \quad . \tag{2.16}$$

The calculation of the left-hand side of the Einstein equation is a more tiresome task. First, all Christoffel symbols $\Gamma^\sigma_{\mu\nu}$ as defined in Eq. (2.3) with indices in spherical coordinates (t, r, θ, ϕ) must be computed. Afterwards, all elements of the Riemann tensor $R^\rho{}_{\sigma\mu\nu}$ given in Eq. (2.5) must be calculated. The Ricci tensor and scalar can then be inferred from the contractions (2.6) and (2.7). All non-vanishing components

of above quantities can be found in Ref. [1]. Just like in the energy-momentum tensor on the right-hand side, only diagonal components remain:

$$\begin{aligned}
G_{tt} &= \frac{1}{r^2}\mathrm{e}^{2(\alpha-\beta)}\left(2r\partial_r\beta - 1 + \mathrm{e}^{2\beta}\right) \\
G_{rr} &= \frac{1}{r^2}\left(2r\partial_r\alpha + 1 - \mathrm{e}^{2\beta}\right) \\
G_{\theta\theta} &= r^2\mathrm{e}^{-2\beta}\left[\partial_r^2\alpha + (\partial_r\alpha)^2 - \partial_r\alpha\partial_r\beta + \frac{1}{r}(\partial_r\alpha - \partial_r\beta)\right] \\
G_{\phi\phi} &= \sin^2\theta\, G_{\theta\theta} \quad .
\end{aligned} \tag{2.17}$$

The fourth relation is just $\sin^2\theta$ times the third relation on both sides of the Einstein equation. Consequently, there are only three independent equations. This makes sense since we have four parameters α, β, ε, and p, but there should be one degree of freedom left that is related to the structure of the matter in the star. Specifically, we assume that our perfect fluid follows a relation $p(\varepsilon)$, the equation of state. Since the factor of $\exp(2\alpha)$ can be dropped on both sides of the equation in the tt sector,

$$\frac{1}{r^2}\mathrm{e}^{-2\beta}\left(2r\partial_r\beta - 1 + \mathrm{e}^{2\beta}\right) = 8\pi G\varepsilon \quad , \tag{2.18}$$

we can just set ε as the free parameter for now and solve for β without consideration of the other equations. From a physical perspective, it proves reasonable to redefine β since we want the metric to look like the Schwarzschild metric outside the star where the energy-momentum tensor vanishes. Hence we write

$$\mathrm{e}^{2\beta(r)} = \left(1 - \frac{2Gm(r)}{r}\right)^{-1} \quad . \tag{2.19}$$

Assuming a sharp boundary of the star, say $T_{\mu\nu} = 0$ for $r > R$, we have to have $m(r) = M$ for all $r > R$. Note that $r > 2Gm(r)$ must be fulfilled for all r in order to render β real. In other words, the radial coordinate r must always be greater than the Schwarzschild radius of the mass inside the sphere of radius r. Thus, this ansatz already includes the condition that there can not be a event horizon inside the star. Inserting our redefinition into Eq. (2.18) we obtain

$$\frac{1}{r^2}2G\partial_r m = 8\pi G\varepsilon \quad \Longleftrightarrow \quad \partial_r m(r) = 4\pi r^2\varepsilon \quad . \tag{2.20}$$

One could integrate

$$m(r) = 4\pi\int_0^r \mathrm{d}r'\,(r')^2\varepsilon(r') \quad , \tag{2.21}$$

but usually the relation $\varepsilon(r)$ is unknown (instead, the equation of state that relates p and ε is known) and we need to solve the system in conjunction with the remaining equations. Interestingly, the integral looks just like a three-dimensional integral of the energy density in flat space. Moreover, we now see that

$$M = m(R) = 4\pi\int_0^R \mathrm{d}r\, r^2\varepsilon(r) \tag{2.22}$$

can indeed be interpreted as the mass M that is felt from outside the star and it becomes constant for $r > R$ as suspected, because $\varepsilon(r > R) = 0$. Turning to the second

of the three independent equations,

$$\frac{1}{r^2}\left[2r\partial_r\alpha + 1 - \left(1 - \frac{2Gm(r)}{r}\right)^{-1}\right] = 8\pi G p \left(1 - \frac{2Gm(r)}{r}\right)^{-1} \quad , \tag{2.23}$$

we obtain

$$\partial_r\alpha(r) = G\frac{4\pi r^3 p + m(r)}{r(r - 2Gm(r))} \quad . \tag{2.24}$$

The remaining equation in the $\theta\theta$ sector includes second derivatives of α and complicates the matter. Luckily, we can use energy-momentum conservation to obtain the third relation in an easier fashion. The relation

$$\nabla_\mu T^{\mu\nu} = 0 \tag{2.25}$$

yields four conserved quantities. First, we have to raise the indices of $T_{\mu\nu}$, which gives

$$T^{\mu\nu} = \mathrm{diag}\left(\mathrm{e}^{-2\alpha}\varepsilon\ ,\ \mathrm{e}^{-2\beta}p\ ,\ \frac{1}{r^2}p\ ,\ \frac{1}{r^2\sin^2\theta}p\right) \quad . \tag{2.26}$$

The only equation that does not trivially cancel to zero on both sides is

$$\nabla_\mu T^{\mu r} = 0 \quad \Longrightarrow \quad \partial_r p = -(\varepsilon + p)\partial_r\alpha \quad . \tag{2.27}$$

This is the Tolman-Oppenheimer-Volkoff equation. Usually, one combines the two relevant differential equations

$$\begin{aligned} \frac{\mathrm{d}p(r)}{\mathrm{d}r} &= -G\frac{(\varepsilon(r) + p(r))\left[m(r) + 4\pi r^3 p(r)\right]}{r\left[r - 2Gm(r)\right]} \quad , \\ \frac{\mathrm{d}m(r)}{\mathrm{d}r} &= 4\pi r^2\varepsilon(r) \quad . \end{aligned} \tag{2.28}$$

Given an equation of state (EoS) $p(\varepsilon)$, the inversion $\varepsilon(p) = \varepsilon(p(r)) = \varepsilon(r)$ is the missing function. Both differential equations become coupled and have to be solved numerically. Starting at $r = 0$, the initial value $m(0) = 0$ is a reasonable physical condition. The value $p_0 = p(0)$ remains a parameter that can be chosen for solutions of e.g. neutron stars of varying mass and radius. The equations are evolved until the pressure drops to zero (or becomes sufficiently low). This determines the radius R and the mass $M = m(R)$. Interestingly, as there is only one non-trivial initial condition for two observables, M and R are not independent. Plotting possible M on one axis and R on the other axis, a fixed equation of state produces a line in the diagram, a relation $M(R)$. Moreover, not all values of M or R necessarily have to be attainable. Typically, one observes a maximal mass M for which the mass decreases both for larger and smaller radii. That can be understood directly from the competing system of equations. We have learned that $r > 2Gm(r)$ has to be fulfilled at each point, hence $p(r)$ will decrease monotonously while $m(r)$ increases monotonously until the pressure is close to zero. Given a relation $\varepsilon(p)$, increasing the central pressure p_0 will make the mass rise more quickly, but also make the pressure drop more quickly. At some point, the decrease in pressure "wins" and the mass can not increase for shorter radii anymore. Of course, the maximum mass depends on the equation of state, i.e. its stiffness. An important observation is the unintuitive result that a higher mass can correspond to a lower radius.

2.3 Stability

Even though the TOV equation delivers possible mass-radius relationships, not all points on the curve necessarily correspond to a stable neutron star. To determine the stability of a star, it can be tested for small perturbations in the radial direction. This allows for the formulation of a simple necessary criterion [30]:

$$\frac{\mathrm{d}M}{\mathrm{d}p_0} > 0 \quad . \tag{2.29}$$

For a perturbation that renders $p_0 \to p_0 + \delta p_0$, the compact object moves infinitesimally along the $M(R)$ line. Note that in the last section we made plausible that higher central pressures actually correspond to lower radii and higher masses up to a maximum mass when the mass decreases with decreasing radii. From that argument, if condition (2.29) is fulfilled and the mass increases, we should be in the area where the radius decreases. Now the central pressure is too high for the given actual mass that has not changed and the star expands back to its original size. The same argument holds for $p_0 \to p_0 - \delta p_0$ when the star becomes too heavy for the new radius and gravity shrinks it to original size. Should $\mathrm{d}M/\mathrm{d}p_0$ be negative, an infinitesimal increase in central pressure $p_0 \to p_0 + \delta p_0$ would lead to a star that is actually too heavy to be in equilibrium at the new radius. The stronger gravitational attraction would lead to a collapse. Of course, this is only a plausibility argument that is not worked out rigorously here.

2.4 Restrictions on Equation of State

Several conditions can be posed that further restrict possible equations of state. Specifically, the conditions

$$\frac{\partial n_B}{\partial \mu_B} = \frac{\partial^2 p}{\partial \mu_B^2} > 0 \quad , \quad c_s^2 = \frac{\partial p}{\partial \varepsilon} \leq 1 \tag{2.30}$$

are common [16]. The first condition is just the thermodynamic statement that the baryon density should increase with increasing baryon chemical potential and that the pressure which is a thermodynamic potential should not have an inflection point with increasing μ_B. The second condition states that the speed of sound c_s shall not exceed the speed of light (given in natural units). This means causality ultimately restricts the stiffness of the equation of state, although it has to be noted that according to Ref. [16] several works indicate that $c_s > c$ might not violate causality after all. All EoS that are derived from the thermodynamics of a physical theory should fulfill these conditions automatically. However, they become important if one attempts to interpolate between two equations of state. As already stated, such unified constructions can be used in the description of a crossover transition from hadron to quark matter. As laid out in Ref. [16], a first-order phase transition can be described in this approach as well, but the given restrictions greatly limit the strength of the transition to a very weak first-order kink in the $p(\mu_B)$ curve. Then again, a hybrid star approach featuring a Maxwell construction actually requires the two EoS to intersect at some reasonable chemical potential and pressure. This further limits the stiffness of the quark matter EoS [16]. Concerning the minimal radius of a neutron star, we have already found the condition $R > 2GM$ (otherwise it would be a black hole). This can be further restricted by applying the causality condition. In order to stay in a reasonable regime, one can e.g. take a well-understood model $p_m(\varepsilon)$ for the equation of state up to a maximum

energy density ε_m. The pressure stays fixed up to an energy density ε_c at which point one assumes a maximally stiff equation of state where $\partial p/\partial\varepsilon = 1$:

$$p(\varepsilon) = \begin{cases} p_m(\varepsilon) & \varepsilon \leq \varepsilon_m \\ p_m(\varepsilon_m) & \varepsilon_m \leq \varepsilon \leq \varepsilon_c \\ \varepsilon - \varepsilon_c + p_m(\varepsilon_m) & \varepsilon \geq \varepsilon_c \quad . \end{cases} \tag{2.31}$$

This procedure is detailed in Ref. [31] among other possibilities of determining a reasonable maximally stiff EoS. Furthermore, a resulting minimal radius for physical parameter choices in the approach taken above is given as $R \geq 2.87GM$ therein. We will use this value as the causality constraint for the mass-radius relationships we compute.

3 Quantum Chromodynamics

Quantum chromodynamics is the theory of the strong interaction. It is a quantum field theory based on a local $SU(3)$ gauge symmetry. The corresponding charges are called color charges, which gives quantum chromodynamics (QCD) its name. We denote the color gauge symmetry as $SU(3)_c$. The QCD Lagrangian reads (in Minkowski space) [32]

$$\mathcal{L}_{\mathrm{QCD}} = \bar{q}(\mathrm{i}\partial\!\!\!/ - m)q - \frac{1}{4}F^a_{\mu\nu}F^{\mu\nu}_a + g\bar{q}\gamma^\mu A^a_\mu T_a q \quad , \tag{3.1}$$

with the $SU(3)_c$ generators

$$T_a = \frac{\lambda_a}{2} \tag{3.2}$$

and the Gell-Mann matrices λ_a. The elementary fields in the theory are the fermionic quarks q and the gauge bosons $A_\mu = A^a_\mu T_a$ called gluons. The pure gauge interaction term $F^a_{\mu\nu}F^{\mu\nu}_a$, with the field strength tensor

$$F^a_{\mu\nu} = \partial_\mu A^a_\nu - \partial_\nu A^a_\mu + g f^{abc} A^b_\mu A^c_\nu \tag{3.3}$$

and the $SU(3)$ structure constants f^{abc}, is named after Yang and Mills who considered local $SU(N)$ gauge theories already in 1954 [33]. The quarks live in the fundamental representation of the gauge group $SU(3)_c$. This means that they transform according to

$$q \to U_c(x)\, q \quad , \quad \bar{q} \to \bar{q}\, U_c^\dagger(x) \tag{3.4}$$

where

$$U_c(x) = \exp\left(-\mathrm{i}\omega_a(x) T_a\right) \tag{3.5}$$

is a unitary 3×3 matrix with determinant 1. Due to the spacetime dependence (locality) of the transformation, the kinetic term in the quark sector is not invariant under it:

$$\bar{q}\,\mathrm{i}\partial\!\!\!/\, q = \bar{q}\,\mathrm{i}\gamma^\mu\partial_\mu\, q \longrightarrow \bar{q}\, U_c^\dagger(x)\,\mathrm{i}\gamma^\mu\partial_\mu\, U(x)\, q = \bar{q}\,\mathrm{i}\gamma^\mu\partial_\mu\, q + \bar{q}\, U_c^\dagger(x)\,\mathrm{i}\gamma^\mu\left(\partial_\mu U(x)\right) q \quad . \tag{3.6}$$

Gauge invariance is achieved by coupling the gauge boson A_μ to the quarks. This can be seen by pulling the last term of the QCD Lagrangian, Eq. (3.1), into the derivative by defining the covariant derivative

$$D_\mu := \partial_\mu - \mathrm{i}g A_\mu \quad . \tag{3.7}$$

The gluon lives in the adjoint representation and has to transform like

$$A_\mu \longrightarrow U(x)\, A_\mu\, U^\dagger(x) - \frac{\mathrm{i}}{g}\left(\partial_\mu U(x)\right) U^\dagger(x) \tag{3.8}$$

such that $\bar{q}\,\mathrm{i}D\!\!\!/\, q$ stays invariant. From this relation, a gauge invariant action in the gluon sector can be constructed. The field strength tensor as defined in Eq. (3.3) can be followed from the commutator of two covariant derivative operators:

$$[D_\mu, D_\nu] = -\mathrm{i}g\left(\partial_\mu A_\nu - \partial_\nu A_\mu - \mathrm{i}g\,[A_\mu, A_\nu]\right) = -\mathrm{i}g T_a F^a_{\mu\nu} = -\mathrm{i}g F_{\mu\nu} \tag{3.9}$$

with the relation $[T_b, T_c] = \mathrm{i}T_a f^{abc}$ and the definition $F_{\mu\nu} := T_a F^a_{\mu\nu}$. It can easily be worked out from the commutator that the transformation behavior of the covariant derivative just transfers to the field strength tensor:

$$F_{\mu\nu} \longrightarrow U(x)\, F_{\mu\nu}\, U^\dagger(x) \quad . \tag{3.10}$$

In order to construct a quantity that is gauge invariant and Lorentz contracted we take the trace

$$\frac{1}{2}\mathrm{Tr}\left(F_{\mu\nu}F^{\mu\nu}\right) \tag{3.11}$$

which does not change under local gauge transformations by virtue of the cyclic invariance of the trace operation. The relation

$$\mathrm{Tr}\left(T_a T_b\right) = \frac{1}{2}\delta_{ab} \tag{3.12}$$

allows us to identify

$$\frac{1}{2}\mathrm{Tr}\left(F_{\mu\nu}F^{\mu\nu}\right) = \frac{1}{4}F^a_{\mu\nu}F^{\mu\nu}_a \quad . \tag{3.13}$$

In contrast to abelian gauge field theories like QED, the generators of $SU(3)$ do not commute and thus the structure constants do not vanish, which leads to the additional term $gf^{abc}A^b_\mu A^c_\nu$ in the field strength tensor. This can be understood as the reason for direct gluon self-interaction in form of three- and four-gluon vertices at the action level: the term $F^a_{\mu\nu}F^{\mu\nu}_a$ features gluon fields of power three and four. The complexity of the theory follows in large parts from this feature of self-interacting, massless gauge bosons. Note that there is another subspace that is not denoted here: there are N_f different sorts of quarks, where N_f denotes the number of flavors. Originally, the Gell-Mann matrices were introduced to successfully describe the baryon and meson octets that were found in collider experiments in a group theoretical approach [34, 35]. Today, we know six different quark flavors, but the first three (up, down, and strange) are sufficient to describe most thermodynamic processes due to their comparably low mass. The flavor space underlies chiral flavor symmetry which is spontaneously broken in some areas of the phase diagram and explicitly broken by a quark mass term in the Lagrangian. It will be discussed in detail in Sec. 3.1. Further symmetries of QCD include an approximate $Z(3)$ global center symmetry, which can be related to confinement, and scale invariance (dilation symmetry). The latter is only a symmetry of the classical Lagrangian which is anomalously broken by quantum effects and its order parameter is the gluon condensate [8].

3.1 Chiral Symmetry

Chiral (flavor) symmetry is a global symmetry under independent $U(N_f)$ flavor space transformations of right- and left-handed spinors. In the chiral basis, the Dirac spinor of the quarks can be written as two two-component Weyl spinors. One of them lives in the right-handed representation of the Lorentz group, the other one in the left-handed representation:

$$q = \begin{pmatrix} q_R \\ q_L \end{pmatrix} \quad . \tag{3.14}$$

The projectors

$$P_L = \frac{\mathbb{1} - \gamma_5}{2} \quad , \quad P_R = \frac{\mathbb{1} + \gamma_5}{2} \tag{3.15}$$

can be used to extract purely right- or left-handed Dirac spinors in a basis-independent way:

$$q_R = P_R q \quad , \quad q_L = P_L q \quad . \tag{3.16}$$

Consider a symmetry transformation

$$U_{L/R} = \exp\left(-\mathrm{i}\omega^a_{L/R} T_a\right) \tag{3.17}$$

in flavor space that rotates left- and right-handed parts independently. The T_a now denote the N_f^2 generators of $U(N_f)$ transformations. This $U(N_f)_L \times U(N_f)_R$ transformation renders

$$q = P_R q + P_L q = q_R + q_L \longrightarrow U_R q_R + U_L q_L = (U_R P_R + U_L P_L) q \quad . \tag{3.18}$$

Under infinitesimal transformations, the term in ellipses can be rewritten:

$$(\mathbb{1} - \mathrm{i}\delta\omega^a_R T_a)\,\frac{\mathbb{1}+\gamma_5}{2} + (\mathbb{1} - \mathrm{i}\delta\omega^a_L T_a)\,\frac{\mathbb{1}-\gamma_5}{2} = \mathbb{1} - \mathrm{i}\frac{\delta\omega^a_R + \delta\omega^a_L}{2} T_a - \mathrm{i}\frac{\delta\omega^a_R - \delta\omega^a_L}{2} T_a \gamma_5 \quad . \tag{3.19}$$

We see that the chiral flavor symmetry can also be expressed as a symmetry under rotations that treat left- and right-handed spinors equally and those that treat them oppositely. The former are called vector, the latter axial vector transformations: $U(N_f)_V \times U(N_f)_A$. This symmetry is commonly split into a $U(1)_V$ phase factor, a $U(1)_A$ axial current and the remaining $SU(N_f)_V \times SU(N_f)_A$ symmetry. The $U(1)_V$ symmetry just corresponds to a global phase factor

$$q \longrightarrow \mathrm{e}^{-\mathrm{i}\omega^0_V} q \quad . \tag{3.20}$$

The Noether current and conserved charge of this symmetry are

$$j^\mu_V = \bar{q}\gamma^\mu q \quad , \quad B = \frac{1}{3}\int \mathrm{d}^3x\, q^\dagger q \quad , \tag{3.21}$$

where the factor of 1/3 is a normalization such that B can be interpreted as the baryon number. The $U(1)_V$ symmetry is always conserved in the theory (and no violation has been observed in nature). At this point, we can study the Dirac structure of the quark Lagrangian. With $\gamma_5^\dagger = \gamma_5$, $\{\gamma^\mu, \gamma_5\} = 0$ and $P^2_{L/R} = P_{L/R}$ we have

$$\begin{aligned}
\bar{q}\left(\mathrm{i}\not{D} - m\right) q &= q_L^\dagger \gamma^0 \left(\mathrm{i}\not{D} - m\right) q + q_R^\dagger \gamma^0 \left(\mathrm{i}\not{D} - m\right) q \\
&= q_L^\dagger P_L \gamma^0 \left(\mathrm{i}\not{D} - m\right) q + q_R^\dagger P_R \gamma^0 \left(\mathrm{i}\not{D} - m\right) q \\
&= q_L^\dagger \left(-\gamma^0 m\right) q_R + q_R^\dagger \left(-\gamma^0 m\right) q_L + q_L^\dagger \left(\gamma^0 \mathrm{i}\not{D}\right) q_L + q_R^\dagger \left(\gamma^0 \mathrm{i}\not{D}\right) q_R \quad .
\end{aligned} \tag{3.22}$$

It becomes obvious that the derivative term breaks neither of the remaining symmetries since it only couples left-handed quarks with left-handed quarks and right-handed quarks with right-handed quarks. A mass term, however, breaks $SU(N_f)_A$ and $U(1)_A$ since those transform right- and left-handed quarks oppositely. As long as m is proportional to unity in flavor space, $SU(N_f)_V$ stays conserved as left- and right-handed quarks are transformed equally. In the case of only two quark flavors, up and down, equal masses are a very good approximation and $SU(2)_V$ is just isospin symmetry. If m does not assign an equal mass to each quark flavor, the unitary transformation matrix does not generally commute with m anymore and $SU(N_f)_V$ is explicitly broken as well. The conserved currents and charges of $SU(N_f)_V$ and $SU(N_f)_A$ are

$$j^\mu_{V,a} = \bar{q}\gamma^\mu T_a q \quad , \quad Q^V_a = \int \mathrm{d}^3x\, q^\dagger T_a q \tag{3.23}$$

and

$$j^{\mu}_{A,a} = \bar{q}\gamma^{\mu}\gamma_5 T_a q \quad , \quad Q^A_a = \int \mathrm{d}^3x\, q^{\dagger} T_a \gamma_5 q \quad . \tag{3.24}$$

Even if the quarks are massless and the Lagrangian is chirally symmetric, $SU(N_f)_A$ can be broken in the vacuum state of the theory. In this context, chiral symmetry oftentimes exclusively refers to $SU(N_f)_A$ and one speaks of spontaneous chiral symmetry breaking. According to the Goldstone theorem, each spontaneously broken global symmetry means the existence of a massless boson, the Goldstone boson [36–38]. The vacuum of the theory becomes degenerate and the Goldstone bosons are thought of as particles that shift the vacuum state, mediated by the coserved charge operators of the broken symmetries. Looking at the conserved axial charges Q^A_a, it becomes clear that the $N_f^2 - 1$ Goldstone bosons that belong to broken $SU(N_f)_A$ should be pseudoscalar quark-antiquark bound states. Indeed, for the three lightest flavors u, d, s an octet of relatively light pseudoscalar mesons can be observed in nature. They are, however, not massless and the mesons with strange content are still considerably heavier than the pions which only have u, d content. Both of these effects can be attributed to the fact that chiral symmetry is only approximately realized in nature. Small u, d quark masses of order 3 MeV and a heavier strange quark mass of order 95 MeV explicitly break the symmetry [8]. An order parameter for the spontaneous breaking of chiral symmetry is the chiral condensate $\langle \bar{q}q \rangle = \langle \bar{q}_L q_R \rangle + \langle \bar{q}_R q_L \rangle$, cf. Eq. (3.22) [39]. A vacuum state of this form obviously breaks $SU(N_f)_A$, but also $U(1)_A$. The $U(1)_A$ symmetry is a special case in the sense that it is already anomalously broken due to quantum fluctuations (axial anomaly). Anomalous symmetry breaking specifies that a symmetry is conserved in the Lagrangian and thus in the classical theory, but not in the path integral measure of the corresponding quantum field theory (i.e. there exists no regularization that conserves it). As shown by 't Hooft, the axial anomaly gives rise to an instanton-induced effective interaction term of the form [40]

$$\kappa \left(\det \bar{q}_L q_R + \det \bar{q}_R q_L \right) \quad . \tag{3.25}$$

3.2 Asymptotic Freedom and Confinement

The coupling constant $\alpha_s = \frac{g^2}{4\pi}$ of quantum chromodynamics has the striking feature that its beta function is negative. A beta function measures the change in a coupling under a change of the renormalization scale. As depicted in Fig. 1, a negative beta function means that the coupling falls off for higher interaction energy scales. This feature has many important consequences. In quantum electrodynamics (QED), where the coupling is small for most interactions and diverges at high energies, perturbation theory works astonishingly well. In QCD, however, perturbation theory can only be applied at very high energies where the coupling becomes small. At these energy scales, QCD matter can be described as weakly interacting quarks and gluons. At very high energies, the theory becomes asymptotically free (non-interacting) [41, 42]. At low energies, the large coupling and the gluon self-interaction render the vacuum non-perturbative. The degrees of freedom in this regime do not have to be elemental quarks and gluons anymore. From experiment we know that only color-neutral bound states of quarks can be observed in large areas of the phase diagram. Such hadrons become effective degrees of freedom, which can ultimately also be seen in the well-known larger-scale world of protons and neutrons. This confinement of quark matter to composite

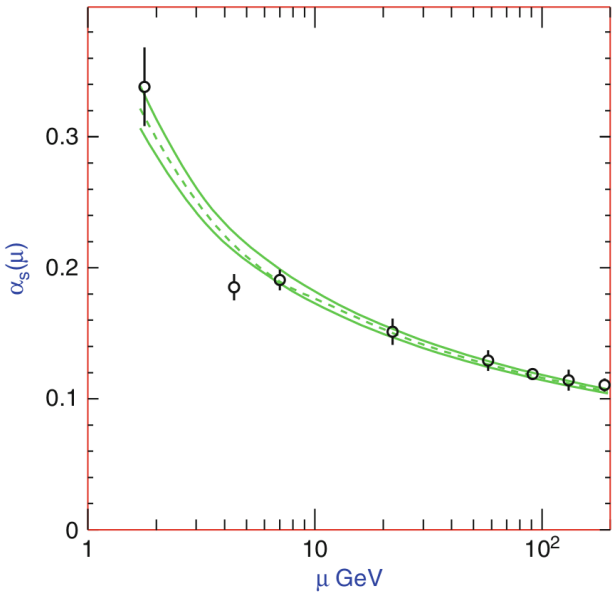

Figure 1: Running of the QCD coupling α_s with the interaction scale μ. Figure taken from Ref. [8].

objects has been observed both in experiments and in lattice QCD simulations [43], but it has not yet analytically been shown to be an actual feature of QCD.

3.3 Phase Diagram

The phase diagram of QCD is very rich in the sense that it exhibits various phases, which can be attributed to the non-perturbative nature of the theory and the resulting phenomena like confinement. As a consequence, calculations of QCD observables must also be conducted with non-perturbative methods. Among such methods, lattice QCD is a first principle approach that has successfully delivered many quantitative results like determining light hadron spectra and the running of the strong coupling [43]. The basic idea is to discretize the theory on a finite lattice in spacetime. Unfortunately, lattice QCD suffers from the famous sign problem that prohibits computations at non-vanishing real baryon chemical potentials to this day. At finite density, functional approaches like Dyson-Schwinger equations (DSE) [44–46] and the functional renormalization group (FRG) are employed [47–49]. Oftentimes such approaches are used in conjunction with effective theories such as the Nambu–Jona-Lasinio (NJL) model or the quark-meson model [50] which are believed to approximate QCD at low energies. Fig. 2 schematically depicts the phase diagram from a modern understanding. At low energies, i.e. low temperature and low chemical potential, chiral symmetry is broken and the vacuum consists of quark-antiquark bound states $\langle \bar{q}q \rangle$, the hadron resonance gas. Going along the temperature axis, a smooth deconfinement transition to a chirally symmetric quark-gluon plasma occurs at about $T \sim 150\,\mathrm{MeV}$. This is confirmed by lattice calculations and there is good agreement among DSE and FRG calculations as well [51–54]. Such calculations suggest the existence of a critical endpoint followed by a first-order transition line which is also seen under the inclusion of gluonic effective interactions in the form of an effective Polyakov loop potential [55–58]. Going to low

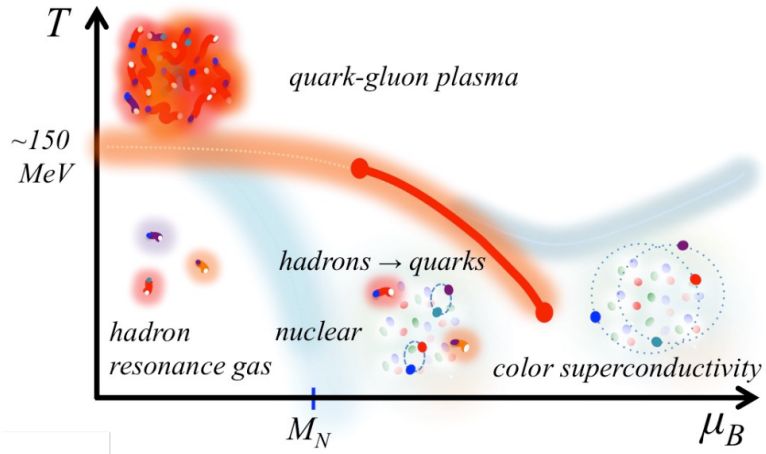

Figure 2: Schematic depiction of the phase diagram of quantum chromodynamics. The first axis shows the baryon chemical potential μ_B, the second axis denotes temperature T. Figure taken from Ref. [16].

temperatures and high densities, the phase diagram is still largely unknown. Along the baryon chemical potential axis, nucleons should become the relevant degrees of freedom up to the point where matter becomes so dense that quarks can directly interact. As already discussed, the point of emergence of quark matter and the role of strange quarks are of significant research interest at this time. Additionally, the existence of a diquark condensate that would lead to color superconductivity has been conjectured for high densities. The condensation of $\bar{q}q$ pairs becomes energetically expensive for high occupation numbers due to the high fermi level and low temperature. Diquark pairings near the fermi surface would become possible. The condensation energy of such diquarks would lower the energy density in this region, which is of significant importance for neutron stars [9, 22]. As shown in Fig. 2, the existence of a second critical point at low T after which the transition to color superconducting matter happens continuously is in discussion as well [16].

3.4 Effective Low-energy Description

In order to apply a functional renormalization group approach to QCD, we first have to develop an effective low-energy theory that allows us to neglect the complicated gauge sector. Note that from now on we work in Euclidean metric as described in App. A. The gauge terms can easily be brought into the Euclidean framework by following for the covarian derivate [Eq. (3.7)] that A_μ should transform like ∂_μ under Wick rotation:

$$A_t = \mathrm{i}A_\tau \quad . \tag{3.26}$$

From antisymmetry, we can follow for the field strength tensor

$$F_{\mu\nu}F^{\mu\nu} = -2F_{ti}F_{ti} + F_{ij}F_{ij} = 2F_{\tau i}F_{\tau i} + F_{ij}F_{ij} \quad . \tag{3.27}$$

Without explicitly denoting that the gamma matrices, A_μ, and $F_{\mu\nu}$ now transform in Euclidean space, the QCD Lagrangian reads

$$\mathcal{L}_{\mathrm{QCD}} = \bar{q}(\partial\!\!\!/_E + m)q + \frac{1}{4}F^a_{\mu\nu}F^{\mu\nu}_a - \mathrm{i}g\bar{q}\gamma^\mu A^a_\mu T_a q \quad . \tag{3.28}$$

The index positions have been left in a contracted form. Following the procedure in Ref. [59], the last term can be recast as a color current j^μ_a that the gluons couple to:

$$j^\mu_a := \bar{q}\gamma^\mu T_a q \quad , \quad -\mathrm{i}g\bar{q}\gamma^\mu A^a_\mu T_a q = -\mathrm{i}g A^a_\mu j^\mu_a \quad . \tag{3.29}$$

This allows us to write the QCD path integral in the form

$$\begin{aligned} Z_{\mathrm{QCD}} &= \int \mathcal{D}\bar{q}\mathcal{D}q\mathcal{D}A\, \mathrm{e}^{-\int \mathrm{d}^4x\, \mathcal{L}_{\mathrm{QCD}}} \\ &= \int \mathcal{D}\bar{q}\mathcal{D}q\, \mathrm{e}^{-\int \mathrm{d}^4x\, \bar{q}(\partial\!\!\!/_E+m)q} \int \mathcal{D}A\, \mathrm{e}^{-\int \mathrm{d}^4x \left[\frac{1}{4}F^a_{\mu\nu}F^{\mu\nu}_a - \mathrm{i}gA^a_\mu j^\mu_a\right]} \\ &= \int \mathcal{D}\bar{q}\mathcal{D}q\, \mathrm{e}^{-\left[\int \mathrm{d}^4x\, \bar{q}(\partial\!\!\!/_E+m)q + \Gamma_g[j]\right]} \end{aligned} \tag{3.30}$$

with

$$\Gamma_g[j] := -\ln \int \mathcal{D}A\, \mathrm{e}^{-\int \mathrm{d}^4x \left[\frac{1}{4}F^a_{\mu\nu}F^{\mu\nu}_a - \mathrm{i}gA^a_\mu j^\mu_a\right]} \quad . \tag{3.31}$$

Actually, a gauge fixing procedure must be performed to avoid integrating over gauge-invariant orbits multiple times. This would lead to Faddeev-Popov ghosts [60] in the Lagrangian. In this work, we will not take care of gauge fixing. For the quark interactions, Γ_g takes on the role of an effective action of the color currents that the gluons produce. Unlike the usual definition, the "external" field in the effective action is the current j that is dynamically produced for each configuration in the quark path integrals. For the gluon partition function, Γ_g is basically the generator of connected gluon correlation functions. Hence, a functional derivative of Γ_g with respect to j^μ_a evaluated at $j = 0$ is proportional (up to powers of g and the imaginary unit) to $\langle A^a_\mu \rangle$, the second derivative is proportional to the gluon propagator and so on. Note that for $j = 0$ there is no quark current interaction, thus the expectation values are those of pure Yang-Mills theory. If we assume a gauge that sets $\langle A^a_\mu \rangle = 0$ and expand Γ_g in powers of j around $j = 0$,

$$\Gamma_g[j] = -\sum_{n=0}^{\infty} \frac{(\mathrm{i}g)^n}{n!} \int \mathrm{d}^4x_1 \ldots \mathrm{d}^4x_n\, \Gamma^{(n)}_g(x_1, \ldots, x_n)^{a_1\ldots a_n}_{\mu_1\ldots\mu_n}\, j^{\mu_1}_{a_1}(x_1) \ldots j^{\mu_n}_{a_n}(x_n) \quad , \tag{3.32}$$

the first non-trivial and non-vanishing term stems from the second derivative. This expansion is comparable to a vertex expansion of the effective action in the quark picture into current interaction vertices. Only taking the gluon two-point function $\Gamma^{(2)}_g$ and dropping higher orders, we obtain

$$Z_{\mathrm{eff}} = \int \mathcal{D}\bar{q}\mathcal{D}q\, \mathrm{e}^{-\left[\int \mathrm{d}^4x\, \bar{q}(\partial\!\!\!/_E+m)q + \frac{g^2}{2}\int \mathrm{d}^4x\, \mathrm{d}^4y\, j^\mu_a(x)\Gamma^{(2)}_g(x,y)^{ab}_{\mu\nu} j^\nu_b(y)\right]} \quad . \tag{3.33}$$

This effective four-quark vertex is non-local, but for low energies or transferred momenta we can approximate it as point-like. Furthermore, we take the easiest choice for the color and Dirac indices

$$\Gamma^{(2)}_g(x,y)^{ab}_{\mu\nu} = \kappa\, \delta(x-y)\, \delta^{ab}\, g_{\mu\nu} \quad . \tag{3.34}$$

This yields

$$Z_{\text{eff}} = \int \mathcal{D}\bar{q}\mathcal{D}q \, \mathrm{e}^{-\int \mathrm{d}^4x \left[\bar{q}(\not{\partial}_E + m)q + \frac{g^2\kappa}{2} j_a^\mu j_\mu^a\right]} \quad . \tag{3.35}$$

While Eq. (3.34) can be understood as a low energy approximation, there is no conclusive argument that shows we can leave out higher orders in the expansion of Γ_g. Rather, investigations speak against this procedure [59]. Nevertheless, a field strength approach (FSA) as conducted in Ref. [59, 61–63] also results in an effective current-current interaction of this form. The idea of the FSA is to introduce an auxiliary field with the same tensor structure as the field strength tensor. This way, the gluon field can be put into Gaussian form and integrated out. The new dynamical field looks like the field strength tensor and couples to the quarks. To lowest order, the path integral over the field strength can be approximated by a stationary path. This returns the effective partition function given in Eq. (3.35) with the action

$$S_{\text{eff}}[\bar{q}, q] = \int \mathrm{d}^4x \left(\bar{q}(\not{\partial}_E + m)q + \frac{g^2\kappa}{2} j_a^\mu j_\mu^a\right) \quad . \tag{3.36}$$

The current-current interaction can be written out explicitly, taking into account flavor, color and Lorentz (or Euclidean) structure:

$$j_a^\mu j_\mu^a = (\bar{q}\gamma^\mu T_c^a \mathbb{1}_f q)\,(\bar{q}\gamma_\mu T_c^a \mathbb{1}_f q) \quad . \tag{3.37}$$

We will denote the $SU(N_c)$ generators for N_c quark colors T_c^a and the $U(N_f)$ generators T_f^a. Taking Dirac space as an example, we can also express the given vector channel interaction as a sum of scalar, pseudoscalar, vector and pseudovector interactions:

$$(\gamma^\mu)_{ij}(\gamma_\mu)_{kl} = \delta_{il}\delta_{kj} - (\gamma_5)_{il}(\gamma_5)_{kj} - \frac{1}{2}\left[(\gamma_\mu)_{il}(\gamma^\mu)_{kj} + (\gamma_\mu\gamma_5)_{il}(\gamma^\mu\gamma_5)_{kj}\right] \quad . \tag{3.38}$$

This procedure is called Fierz transformation. Note that there is also a tensor channel

$$\sigma_{\mu\nu} = \frac{\mathrm{i}}{2}[\gamma_\mu, \gamma_\nu] \tag{3.39}$$

such that in total the 16 basis elements of the Clifford algebra can be written [39]

$$\{\mathbb{1}, \gamma_\mu, \gamma_5, \mathrm{i}\gamma_\mu\gamma_5, \sigma_{\mu\nu}\} \quad . \tag{3.40}$$

However, the corresponding coefficients for the tensor channel in the Fierz transformation are zero. It is not produced from the given vector channel. Due to this transformation, one has to assume that such interactions that are not in the action in the first place are generated dynamically from fluctuations. One can not directly match a certain channel with an observation, e.g. a vector meson interaction, for this reason (Fierz ambiguity). Before we perform a Fierz transformation in Dirac space, however, we take care of the color current first. We see from the index structure in Eq. (3.38) that the new structure again couples $\bar{q}q$ currents, but in color space one obtains another index structure via a similar relation [64]:

$$(T_c^a)_{ij}(T_c^a)_{kl} = \frac{1}{2}\delta_{il}\delta_{jk} - \frac{1}{2N_c}\delta_{ij}\delta_{kl} \quad , \tag{3.41}$$

which can, under the use of the ε tensor identity

$$\varepsilon_{mik}\varepsilon_{mjl} = \delta_{ij}\delta_{kl} - \delta_{il}\delta_{kj} \quad , \tag{3.42}$$

be brought into the form

$$(T_c^a)_{ij}(T_c^a)_{kl} = \frac{1}{2}\left[\left(1-\frac{1}{N_c}\right)\delta_{il}\delta_{kj} - \frac{1}{N_c}\varepsilon_{mik}\varepsilon_{mjl}\right] \overset{(N_c=3)}{=} \frac{1}{3}\delta_{il}\delta_{kj} + \frac{1}{6}\varepsilon_{mik}\varepsilon_{mlj} \quad . \tag{3.43}$$

Comparing the indices, it becomes clear that the term with the deltas keeps a $(\bar{q}q)(\bar{q}q)$ type interaction, while the term with the epsilons couples $\bar{q}\bar{q}$ and qq. We call the first one meson channel, the second one diquark channel. It is noteworthy that the diquark channel is suppressed by a factor of $1/N_c$ (for high N_c) compared to the meson channel. At $N_c = 3$, however, this suppression is only a factor of $1/2$. We need to find suitable relations with the same index structure in Dirac and flavor space for each of the two channels individually. Eq. (3.38) already has the correct index structure for the mesons channel. With the definition $q^c := C\bar{q}^T$, $\bar{q}^c := q^T C$ where C is the charge conjugation matrix with the property $C\gamma^\mu C = (\gamma^\mu)^T$, the diquark channel relation is

$$\begin{aligned}(\gamma^\mu)_{ij}(\gamma_\mu)_{kl} &= (\gamma^\mu)_{ij}C_{lm}(\gamma_\mu)_{mn}C_{nk} \\ &= C_{ik}C_{lj} - (\gamma_5 C)_{ik}(C\gamma_5)_{lj} - \frac{1}{2}\left[(\gamma_\mu C)_{ik}(C\gamma^\mu)_{lj} + (\gamma_\mu\gamma_5 C)_{ik}(C\gamma^\mu\gamma_5)_{lj}\right] \quad .\end{aligned} \tag{3.44}$$

The flavor space relations are

$$\delta_{ij}\delta_{kl} = 2(T_f^a)_{il}(T_f^a)_{kj} \tag{3.45}$$

in the meson channel and

$$\delta_{ij}\delta_{kl} = \frac{1}{2}(\delta_{ij}\delta_{kl} - \delta_{il}\delta_{kj}) + \frac{1}{2}(\delta_{ij}\delta_{kl} + \delta_{il}\delta_{kj}) = -\frac{1}{2}\varepsilon_{mik}\varepsilon_{mlj} + s_{nik}s_{nlj} \tag{3.46}$$

in the diquark channel. s are the six symmetric basis matrices in three dimensions

$$s_1 = \begin{pmatrix}1&0&0\\0&0&0\\0&0&0\end{pmatrix} \quad , \quad s_2 = \begin{pmatrix}0&0&0\\0&1&0\\0&0&0\end{pmatrix} \quad , \quad s_3 = \begin{pmatrix}0&0&0\\0&0&0\\0&0&1\end{pmatrix} \quad , \tag{3.47}$$

$$s_4 = \frac{1}{\sqrt{2}}\begin{pmatrix}0&1&0\\1&0&0\\0&0&0\end{pmatrix} \quad , \quad s_5 = \frac{1}{\sqrt{2}}\begin{pmatrix}0&0&1\\0&0&0\\1&0&0\end{pmatrix} \quad , \quad s_6 = \frac{1}{\sqrt{2}}\begin{pmatrix}0&0&0\\0&0&1\\0&1&0\end{pmatrix} \quad . \tag{3.48}$$

The short-hand definitions

$$\Gamma := \left\{\mathbb{1}, \mathrm{i}\gamma_5, \frac{\mathrm{i}}{\sqrt{2}}\gamma_\mu, \frac{\mathrm{i}}{\sqrt{2}}\gamma_\mu\gamma_5\right\} \quad , \quad \tilde{T}_f := \left\{\frac{\mathrm{i}}{\sqrt{2}}\varepsilon_m, s_n\right\} \tag{3.49}$$

allow us to write

$$j_a^\mu j_\mu^a = -\frac{2}{3}\left(\bar{q}\Gamma^d\mathbb{1}_c T_f^a q\right)\left(\bar{q}\Gamma_d\mathbb{1}_c T_f^a q\right) + \frac{1}{6}\left(\bar{q}\Gamma^d\varepsilon_c^m\tilde{T}_f^a q^c\right)\left(\bar{q}^c\Gamma_d\varepsilon_c^m\tilde{T}_f^a q\right) \quad . \tag{3.50}$$

According to Ref. [16], the diquark channel with the strongest pairing interaction is the color-antisymmetric, flavor-antisymmetric, spin-singlet channel, i.e.

$$-\frac{1}{12}\left(\bar{q}\mathbb{1}_d\varepsilon_c^m\varepsilon_f^n q^c\right)\left(\bar{q}^c\mathbb{1}_d\varepsilon_c^m\varepsilon_f^n q\right) \quad . \tag{3.51}$$

3.5 Partial Bosonization

As discussed in Sec. 3.3, at low energies the meson channel dominates over the diquark channel and a diquark condensate is only expexted at high densities. By dropping the diquark channel, we arrive at the (Euclidean) Lagrangian of NJL-type models [39]:

$$\mathcal{L}_{\mathrm{NJL}}[\bar{q},q] = \bar{q}(\not{\partial}_E + m)q + \frac{\lambda}{2}\left[(\bar{q}T^a q)^2 - (\bar{q}T^a\gamma_5 q)^2 - \frac{1}{2}(\bar{q}T^a\gamma_\mu q)^2 - \frac{1}{2}(\bar{q}T^a\gamma_\mu\gamma_5 q)^2\right] \quad . \tag{3.52}$$

As we will break chiral symmetry explicitly via an effective potential later, we set the current quark masses m to zero. We focus on the scalar and pseudo-scalar channels, but note that the (pseudo-)vector channels might be obtained from the (pseudo-)scalar channels from a Fierz transformation as shown before. Thus our approach does not yield a Fierz complete effective action. A typical ansatz for the effective action of the NJL model entails point-like four-fermion interactions

$$\Gamma_{\mathrm{NJL}} = \int \mathrm{d}^4x \left\{\bar{q}\not{\partial}_E q + \frac{\lambda}{2}\left[(\bar{q}T^a q)^2 - (\bar{q}T^a\gamma_5 q)^2\right]\right\} \quad . \tag{3.53}$$

The problem with this approach is that the coupling diverges at the spontaneous chiral symmetry breaking scale [39]. This can be explained at hand of a bosonized version of the action. A bosonization procedure entails the use of a Hubbard-Stratonovich transformation [65, 66] that introduces auxiliary scalar fields in a Gaussian form

$$\mathcal{N}\int \mathcal{D}\sigma_a\mathcal{D}\pi_a\, \mathrm{e}^{-\frac{1}{2}\int \mathrm{d}^4x\left(m_\sigma^2\sigma_a^2 + m_\pi^2\pi_a^2\right)} = 1 \tag{3.54}$$

with the normalization $\mathcal{N}$ and flavor index a. The whole term is just identically multiplied with the partition function Z_{NJL}. Then the fields can be shifted [67]

$$\sigma_a \to \sigma_a + \frac{h_\sigma}{m_\sigma^2}(\bar{q}T^a q) \quad , \quad \pi_a \to \pi_a + \frac{h_\pi}{m_\pi^2}(\bar{q}\mathrm{i}\gamma_5 T^a q) \tag{3.55}$$

such that

$$\begin{aligned} -\frac{1}{2}(m_\sigma^2\sigma_a^2 + m_\pi^2\pi_a^2) \to -\frac{1}{2}(m_\sigma^2\sigma_a^2 + m_\pi^2\pi_a^2) - h_\sigma\sigma_a(\bar{q}T^a q) - h_\pi\pi_a(\bar{q}\mathrm{i}\gamma_5 T^a q) \\ - \frac{h_\sigma^2}{2m_\sigma^2}(\bar{q}T^a q)^2 + \frac{h_\pi^2}{2m_\pi^2}(\bar{q}\gamma_5 T^a q)^2 \quad . \end{aligned} \tag{3.56}$$

The choice

$$h_\sigma = h_\pi =: h_b \quad , \quad m_\sigma = m_\pi =: m_b \quad , \quad -\frac{h_b^2}{m_b^2} = \lambda \tag{3.57}$$

cancels the four-fermion vertex in the NJL action exactly. The remaining terms give

$$S_{\mathrm{bos.}}[\bar{q},q,\sigma,\pi] = \int \mathrm{d}^4x \left\{\bar{q}\left[\not{\partial}_E + h_b T^a\left(\sigma_a + \mathrm{i}\gamma_5\pi_a\right)\right]q + \frac{1}{2}m_b^2\left(\sigma_a^2 + \pi_a^2\right)\right\} \quad . \tag{3.58}$$

At this point, we can analyze the classical equations of motion:

$$\frac{\delta S_{\mathrm{bos.}}}{\delta\sigma_a} = h_b(\bar{q}T^a q) + m_b^2\sigma_a \overset{!}{=} 0 \quad , \quad \frac{\delta S_{\mathrm{bos.}}}{\delta\pi_a} = h_b(\bar{q}\mathrm{i}\gamma_5 T^a q) + m_b^2\pi_a \overset{!}{=} 0 \quad . \tag{3.59}$$

The classical solutions for σ_a and π_a correspond to the amount we shifted them in Eq. (3.55):

$$\sigma_a = -\frac{h_b}{m_b^2}\left(\bar{q}T^a q\right) \quad , \quad \pi_a = -\frac{h_b}{m_b^2}\left(\bar{q}\mathrm{i}\gamma_5 T^a q\right) \quad . \tag{3.60}$$

This allows the interpretation of the fields σ_a and π_a as scalar and pseudoscalar quark-antiquark bound states, respectively. For $N_f = 2$, the only state that is compatible with the vacuum $\langle\bar{q}q\rangle$ is σ_0 because $T^0 \sim \mathbb{1}$. Hence, we treat all other field vacuum expectation values as zero. With that in mind, the classical equation of motion for the quark Dirac spinor is

$$\frac{\delta S_{\text{bos.}}}{\delta\bar{q}} = \left(\partial\!\!\!/_E + h_b\langle\sigma_0\rangle\right) q \overset{!}{=} 0 \quad . \tag{3.61}$$

The mass-like term $m_q = h_b\langle\sigma_0\rangle$ signals that chiral symmetry must be broken for $\langle\sigma_0\rangle \neq 0$ which means that in this formulation we have easily found an order parameter for chiral symmetry breaking. On top of that, the problem with the diverging pointlike four-fermion coupling at symmetry breaking is solved. One could just add a kinetic term for the mesons. The four-fermion interaction is then transmitted via a meson field coupling to each quark-antiquark pair in form of a Yukawa type interaction. Basically, the formerly point-like vertex is now replaced by two Yukawa vertices and a meson propagator which allows for momentum dependence. Note that the bound state resonances m_{mes} can now be determined as well. The meson propagators $\sim \frac{1}{p^2 - m_{\text{mes}}^2}$ can be approximated as momentum independent for $m_{\text{mes}}^2 \gg p^2$ and the point-like approximation is revocered [39]. At symmetry breaking scale, however, massless Goldstone bosons emerge that push the $p = 0$ approximation of the propagator towards infinity. The correlation length diverges and point-like interactions are not a good approximation anymore. It shall be noted that the advantage we gain in the description of phase transitions comes at a trade-off. Firstly, the present action is derived from Fierz incomplete interactions. Secondly, effective four-fermion couplings are generated via meson exchange diagrams, thus the cancellation of the interaction only works at the UV scale of the theory and it has to be included in a complete ansatz for the effective action Γ. We will not do this and argue that the strength of this re-generated coupling is expected to be small compared to the rest [39]. A "dynamical hadronization" procedure could remedy both of these problems [68] and is considered for future works.

4 The Quark-meson Model

The quark-meson (QM) model is an effective theory that exhibits a first-order chiral phase transition with a critical endpoint [53]. It describes unconfined constituents quarks that couple to dynamical scalar and pseudoscalar meson degrees of freedom. The QM model takes the bosonized NJL action [Eq. (3.59)] and adds a kinetic term as well as a UV interaction potential U_Λ for the mesonic fields. With some renamed constants and the mesonic mass term absobed in U_Λ the Lagrangian reads

$$\mathcal{L}_{\mathrm{QM}} = \bar{q}\left[\partial\!\!\!/_E + gT_a\left(\sigma_a + \mathrm{i}\gamma_5\pi_a\right)\right]q + \frac{1}{2}(\partial_\mu\sigma_a)(\partial^\mu\sigma_a) + \frac{1}{2}(\partial_\mu\pi_a)(\partial^\mu\pi_a) + U_\Lambda \quad . \tag{4.1}$$

For finite quark densities, a chemical potential (which can also be flavor-dependent) is added:

$$-\bar{q}\gamma^0\mu q \quad . \tag{4.2}$$

The meson fields can be encoded in the $N_f \times N_f$ matrix

$$\Phi := T_a\phi_a = T_a(\sigma_a + \mathrm{i}\pi_a) \quad , \quad \Phi_5 := T_a(\sigma_a + \mathrm{i}\gamma_5\pi_a) \quad . \tag{4.3}$$

With Eq. (3.12) and

$$\mathrm{Tr}\left(\partial_\mu\Phi^\dagger\partial^\mu\Phi\right) = \partial_\mu\phi_a^*\partial^\mu\phi_b\mathrm{Tr}\left(T_aT_b\right) = \frac{1}{2}\partial_\mu\phi_a^*\partial^\mu\phi_a \tag{4.4}$$

the Lagrangian becomes

$$\mathcal{L}_{\mathrm{QM}} = \bar{q}\left[\partial\!\!\!/_E + g\Phi_5\right]q + \mathrm{Tr}\left(\partial_\mu\Phi^\dagger\partial^\mu\Phi\right) + U_\Lambda \quad . \tag{4.5}$$

Under chiral symmetry transformations, Φ has to transform like [69]

$$\Phi \longrightarrow U_R\Phi U_L^\dagger \quad . \tag{4.6}$$

for the quark interaction term to stay invariant. Of course, this is just conventional. We could also regard the subspace where $\Phi \to U_L\Phi U_R^\dagger$. Starting from a chirally invariant Lagrangian, U_Λ is in general a function of chiral invariants ρ_n. In total, N_f chiral invariants can be constructed the following way [50]:

$$\rho_n := \mathrm{Tr}\left[\left(\Phi^\dagger\Phi\right)^n\right] \quad , \quad n \in \{1, \ldots, N_f\} \quad . \tag{4.7}$$

Employing the cyclic invariance of the trace, it can easily be checked that ρ_n indeed stay invariant under transformation (4.6).

4.1 Explicit Symmetry Breaking

The experimentally observed differences in meson masses can be reproduced by adding explicit breaking terms to the theory. As we will see, terms linear in the fields do not change the evolution of the FRG flow and we can add

$$-\mathrm{Tr}\left[H\left(\Phi^\dagger + \Phi\right)\right] = -h_a\sigma_a \tag{4.8}$$

with $H := h_aT_a$. A chiral transformation

$$-h_a\mathrm{Tr}\left[T_a\left(U_\mathrm{L}\Phi^\dagger U_\mathrm{R}^\dagger + U_\mathrm{R}\Phi U_\mathrm{L}^\dagger\right)\right] \quad . \tag{4.9}$$

shows that any $h_a \neq 0$ generally breaks $SU(N_f)_A$ and $U(1)_A$. If h_0 is the only non-zero constant, $T_0 \sim \mathbb{1}$ implies that $SU(N_f)_V$ which rotates right- and left-handed flavors equally stays preserved. This is the analogon to equal masses for all quark flavors. Generally, only those h_a that correspond to diagonal generators can be non-zero because states that belong to non-diagonal generators are not flavor-neutral and must have vanishing vacuum expectation value (VEV). On top of the explicit breaking of chiral symmetry, the axial anomaly has influence on the meson masses. In particular, the mass difference between the heavy η meson and the η' meson can be correlated with the anomalous breaking of $U(1)_A$. The lowest order term that specifically breaks this symmetry is

$$- c \left[\mathrm{Det}\left(\Phi^\dagger\right) + \mathrm{Det}\left(\Phi\right)\right] \tag{4.10}$$

which encodes the instanton-induces determinant found by 't Hooft (cf Sec. 3.1). The behavior of this term under chiral symmetry transformations can be easily checked:

$$\begin{aligned} -c \left[\mathrm{Det}\left(U_\mathrm{L}\Phi^\dagger U_\mathrm{R}^\dagger\right) + \mathrm{Det}\left(U_\mathrm{R}\Phi U_\mathrm{L}^\dagger\right)\right] \\ = -c \left[\mathrm{Det}\left(U_\mathrm{L}\right)\mathrm{Det}\left(\Phi^\dagger\right)\mathrm{Det}\left(U_\mathrm{R}^\dagger\right) + \mathrm{Det}\left(U_\mathrm{R}\right)\mathrm{Det}\left(\Phi\right)\mathrm{Det}\left(U_\mathrm{L}^\dagger\right)\right] \\ = -c \left[\mathrm{e}^{\mathrm{i}(\alpha_\mathrm{L}-\alpha_\mathrm{R})}\mathrm{Det}\left(\Phi^\dagger\right) + \mathrm{e}^{\mathrm{i}(\alpha_\mathrm{R}-\alpha_\mathrm{L})}\mathrm{Det}\left(\Phi\right)\right] \quad . \end{aligned} \tag{4.11}$$

Pure $U(1)_V$ would rotate right- and left-handed particles by the same phase, $\alpha_L = \alpha_R$. Special unitary transformations have determinant 1 and also keep this term invariant. Hence, a $U(1)_A$ asymmetric phase is the only transformation that does not leave it invariant. In total, we can write the Lagrangian

$$\begin{aligned} \mathcal{L}(\bar{q}, q, \Phi) = \bar{q}\left(\partial\!\!\!/_E + gT_a\left(\sigma_a + \mathrm{i}\gamma_5\pi_a\right)\right)q + \mathrm{Tr}\left(\partial_\mu\Phi^\dagger\partial^\mu\Phi\right) + U_\Lambda(\rho_1, ..., \rho_{N_f}) \\ - c\left[\mathrm{Det}\left(\Phi^\dagger\right) + \mathrm{Det}\left(\Phi\right)\right] - \mathrm{Tr}\left[H\left(\Phi^\dagger + \Phi\right)\right] \quad . \end{aligned} \tag{4.12}$$

4.2 The Two-flavor QM Model

Due to their comparably very light and almost equal masses, u and d quarks determine most of the thermodynamic processes at low energies and allow an isospin-symmetric treatment. After all, particles that include strange or even heavier quarks are always instable in the vacuum. Therefore, the $N_f = 2$ QM model allows for some great simplifications and is expected to still deliver good first results. Here, T_a are the $U(2)$ generators

$$T_a = \frac{\tau_a}{2} \quad , \tag{4.13}$$

where $\tau_0 = \mathbb{1}$ and $\vec{\tau}$ are the Pauli matrices. The meson matrix Φ becomes

$$\Phi = \frac{1}{2}\begin{pmatrix} \sigma_0 + \sigma_3 & \sigma_1 - \mathrm{i}\sigma_2 \\ \sigma_1 + \mathrm{i}\sigma_2 & \sigma_0 - \sigma_3 \end{pmatrix} + \frac{\mathrm{i}}{2}\begin{pmatrix} \pi_0 + \pi_3 & \pi_1 - \mathrm{i}\pi_2 \\ \pi_1 + \mathrm{i}\pi_2 & \pi_0 - \pi_3 \end{pmatrix} \tag{4.14}$$

Since the only scalar mesons on the flavor diagonal are σ_0 and σ_3, the explicit symmetry breaking term condenses to $-h_0\sigma_0 - h_3\sigma_3$. σ_3 treats the u and d sector antisymmetrically and breaks $SU(2)_\mathrm{V}$ isospin symmetry. By setting $h_3 = 0$, we preserve this

symmetry which is only very mildly broken in nature and give u and d constituent quarks equal masses. The axial anomaly term also allows for a large simplification:

$$-c\left[\mathrm{Det}\left(\Phi^{\dagger}\right)+\mathrm{Det}\left(\Phi\right)\right]=-\frac{c}{2}\left(\sigma_0^2+\vec{\pi}^2-\pi_0^2-\vec{\sigma}^2\right) \quad . \tag{4.15}$$

A comparison with the mass term

$$\frac{m^2}{2}\left(\sigma_0^2+\vec{\sigma}^2+\pi_0^2+\vec{\pi}^2\right) \tag{4.16}$$

reveals that c must have the dimension of mass squared and adding up both terms yields

$$\frac{m^2-c}{2}\left(\sigma_0^2+\vec{\pi}^2\right)+\frac{m^2+c}{2}\left(\pi_0^2+\vec{\sigma}^2\right) \quad . \tag{4.17}$$

It is important that the determinant term has power N_f in the fields and only gives a mass contribution at $N_f = 2$. Here, the axial anomaly is actually responsible for a mass splitting between the flavor-neutral scalar meson and off-diagonal pseudoscalar mesons on the one hand and the diagonal pseudoscalar meson and the off-diagonal scalar mesons on the other hand. Because the description of heavier mesons would also require the consideration of strange quarks, it is instructive in this model to leave the heavier mesons out of the picture. This just corresponds to maximum axial symmetry breaking where one sends $m^2 + c \to \infty$ while keeping $m^2 - c$ finite. $m^2 - c$ can then be renamed to m^2. With infinite mass, the π_0 and $\vec{\sigma}$ decouple from – and do not contribute to – the thermodynamics, and only the σ_0 and $\vec{\pi}$ dynamics remain. One can now pull the remaining fields into a four-vector:

$$\varphi := (\sigma_0, \vec{\pi})^{\mathrm{T}} \quad . \tag{4.18}$$

Since $SU(2)$ transformations of Φ now just correspond to rotating the four fields, they correspond to $O(4)$ transformations of φ. Experimentally, the mesons are supposed to describe the light pions and the broad σ resonance. The $O(4)$ invariant Lagrangian is

$$\mathcal{L}_{2\mathrm{f}} = \bar{q}\left(\partial\!\!\!/_E + g\left(\sigma + \mathrm{i}\gamma_5\vec{\tau}\cdot\vec{\pi}\right)\right)q + \frac{1}{2}\left(\partial\vec{\varphi}\right)^2 + U_\Lambda(\vec{\varphi}^2) - h\sigma \quad , \tag{4.19}$$

where the index has been stripped from σ_0. The two chiral invariants are

$$\rho_1 = \frac{1}{2}\vec{\varphi}^2 \quad , \quad \rho_2 = \frac{1}{2}\rho_1^2 \quad . \tag{4.20}$$

The second chiral invariant is not independent from the first because half of the fields have been neglected as a consequence of maximum axial symmetry breaking. Taking fields up to fourth power, the UV potential reads

$$U_\Lambda(\vec{\varphi}^2) = \frac{m^2}{2}\vec{\varphi}^2 + \frac{\lambda}{4}\vec{\varphi}^4 \quad . \tag{4.21}$$

4.3 The 2+1-flavor QM Model

The influence of strangeness fluctuations close to the chiral phase transition is an interesting topic. At high temperatures and chemical potentials close to the transition, the heavier constituent strange quarks and strange hadrons should play a role. Thus, the inclusion of a third flavor is a sensible upgrade to the model. The isospin sub-symmetry

between the u and d quark is kept intact as a good approximation, hence the model is called 2+1-flavor QM model. We already introduced the $SU(3)$ generators that build upon the Gell-Mann matrices λ_a:

$$T_a = \frac{\lambda_a}{2}, \quad \lambda_0 = \sqrt{\frac{2}{3}}\mathbb{1} \quad . \tag{4.22}$$

The scalar and pseudoscalar meson nonets now feature 18 fields in total [69]:

$$T_a\sigma_a = \frac{1}{\sqrt{2}}\begin{pmatrix} \frac{1}{\sqrt{3}}\sigma_0 + \frac{1}{\sqrt{2}}\sigma_3 + \frac{1}{\sqrt{6}}\sigma_8 & \frac{1}{\sqrt{2}}(\sigma_1 - \mathrm{i}\sigma_2) & \frac{1}{\sqrt{2}}(\sigma_4 - \mathrm{i}\sigma_5) \\ \frac{1}{\sqrt{2}}(\sigma_1 + \mathrm{i}\sigma_2) & \frac{1}{\sqrt{3}}\sigma_0 - \frac{1}{\sqrt{2}}\sigma_3 + \frac{1}{\sqrt{6}}\sigma_8 & \frac{1}{\sqrt{2}}(\sigma_6 - \mathrm{i}\sigma_7) \\ \frac{1}{\sqrt{2}}(\sigma_4 + \mathrm{i}\sigma_5) & \frac{1}{\sqrt{2}}(\sigma_6 + \mathrm{i}\sigma_7) & \frac{1}{\sqrt{3}}\sigma_0 - \sqrt{\frac{2}{3}}\sigma_8 \end{pmatrix} , \tag{4.23}$$

$$T_a\pi_a = \frac{1}{\sqrt{2}}\begin{pmatrix} \frac{1}{\sqrt{3}}\pi_0 + \frac{1}{\sqrt{2}}\pi_3 + \frac{1}{\sqrt{6}}\pi_8 & \frac{1}{\sqrt{2}}(\pi_1 - \mathrm{i}\pi_2) & \frac{1}{\sqrt{2}}(\pi_4 - \mathrm{i}\pi_5) \\ \frac{1}{\sqrt{2}}(\pi_1 + \mathrm{i}\pi_2) & \frac{1}{\sqrt{3}}\pi_0 - \frac{1}{\sqrt{2}}\pi_3 + \frac{1}{\sqrt{6}}\pi_8 & \frac{1}{\sqrt{2}}(\pi_6 - \mathrm{i}\pi_7) \\ \frac{1}{\sqrt{2}}(\pi_4 + \mathrm{i}\pi_5) & \frac{1}{\sqrt{2}}(\pi_6 + \mathrm{i}\pi_7) & \frac{1}{\sqrt{3}}\pi_0 - \sqrt{\frac{2}{3}}\pi_8 \end{pmatrix} . \tag{4.24}$$

These matrices allow us to make some identification with experimentally measured resonances. The electrically neutral π^0 has quark content $\sim u\bar{u} - d\bar{d}$ and can thus be identified with π_3. π^+ has $u\bar{d}$ content and thus belongs to the entry $\frac{1}{\sqrt{2}}(\pi_1 + \mathrm{i}\pi_2)$ in the matrix, analog $\pi^- = \frac{1}{\sqrt{2}}(\pi_1 - \mathrm{i}\pi_2)$. The partners in the scalar meson nonet are $a_0^{0/+/-}$. The other off-diagonal elements can be identified with the Kaons $K^0, \bar{K}^0, K^+, K^-$ (pseudoscalar) and the κ resonances $\kappa^0, \bar{\kappa}^0, \kappa^+, \kappa^-$ (scalar). We set $\sigma_3 = 0$ at the VEV and $h_3 = 0$ in the explicit breaking term to preserve the isospin $SU(2)_\mathrm{V}$ (sub-)symmetry. σ_0, which is multiplied with the identity in flavor space, and σ_8, which is responsible for the mass splitting between light and strange quarks, are the only remaining scalar diagonal fields. Hence, only these can have a finite VEV. With the rotation [70]

$$\begin{pmatrix} \sigma_l \\ \sigma_s \end{pmatrix} = \frac{1}{\sqrt{3}}\begin{pmatrix} \sqrt{2} & 1 \\ 1 & -\sqrt{2} \end{pmatrix}\begin{pmatrix} \sigma_0 \\ \sigma_8 \end{pmatrix} \tag{4.25}$$

one can explicitly split the VEV into a light and a strange sector:

$$\langle\Phi\rangle = \mathrm{diag}\left(\frac{\langle\sigma_l\rangle}{2}, \frac{\langle\sigma_l\rangle}{2}, \frac{\langle\sigma_s\rangle}{\sqrt{2}}\right) \quad . \tag{4.26}$$

There are three independent chiral invariants. The terms are lengthy, but their VEVs reduce to

$$\begin{aligned} \langle\rho_1\rangle &= \frac{1}{2}\left(\langle\sigma_l\rangle^2 + \langle\sigma_s\rangle^2\right) \\ \langle\rho_2\rangle &= \frac{1}{8}\left(\langle\sigma_l\rangle^4 + 2\langle\sigma_s\rangle^4\right) \\ \langle\rho_3\rangle &= \frac{1}{32}\left(\langle\sigma_l\rangle^6 + 4\langle\sigma_s\rangle^6\right) \quad . \end{aligned} \tag{4.27}$$

Because ρ_3 already is of sixth power in the fields, its coupling is of negative mass dimension. We drop it and only consider relevant, traditionally renormalizable couplings to the UV potential [71]. Furthermore, at the VEV $\langle\rho_3\rangle$ can be expressed as a function

of $\langle\rho_1\rangle$ and $\langle\rho_2\rangle$ because all three depend on only two variables, $\langle\sigma_l\rangle$ and $\langle\sigma_s\rangle$. The UV potential becomes

$$U_\Lambda = U_\Lambda(\rho_1, \rho_2) = m^2\rho_1 + \lambda_1\rho_1^2 + \lambda_2\rho_2 \quad . \tag{4.28}$$

In $N_f = 3$, the axial anomaly term has fields to the power of three. Its expectation value can be calculated to be

$$-c\left[\mathrm{Det}\left(\langle\Phi\rangle^\dagger\right) + \mathrm{Det}\left(\langle\Phi\rangle\right)\right] = -\frac{c}{2\sqrt{2}}\langle\sigma_l\rangle^2\langle\sigma_s\rangle \quad . \tag{4.29}$$

5 Mean Field Approximation

A first idea about the behavior of a system can be inferred from a mean field approximation (MFA). As the name suggests, thermal and quantum fluctuations of the bosonic fields are neglected in this approach – they are treated as mean background fields the fermions couple to. Technically, the path integral over the meson fields is dropped and the only contribution to the partition function comes from the path $\Phi = \langle\Phi\rangle$ that will be the VEV. In N_f flavors, the partition function of the QM model is

$$Z = \int \mathcal{D}\bar{q}\mathcal{D}q\mathcal{D}\Phi\, \mathrm{e}^{-S[\bar{q},q,\Phi]} \tag{5.1}$$

with

$$\begin{aligned} S[\bar{q},q,\Phi] = \int_0^\beta \mathrm{d}\tau \int \mathrm{d}^3x \Big\{ &\bar{q}\left(\partial\!\!\!/_E + gT_a(\sigma_a + \mathrm{i}\gamma_5\pi_a)\right) q + \frac{(\partial\sigma_a)^2}{2} + \frac{(\partial\pi_a)^2}{2} \\ &+ U(\rho_1,\ldots,\rho_n) - c\left[\det\left(\Phi^\dagger\right) + \det\left(\Phi\right)\right] - h_a\sigma_a \Big\} \quad . \end{aligned} \tag{5.2}$$

At finite temperature, the integration of the Euclidean (imaginary) time is performed up to the inverse temperature β. Now the mesonic path integral is just left out and $\langle\Phi\rangle$ formally inserted:

$$\begin{aligned} Z_{\mathrm{mf}} &= \mathrm{e}^{-S_{\mathrm{mes}}[\langle\Phi\rangle]} \int \mathcal{D}\bar{q}\mathcal{D}q\, \mathrm{e}^{-\int_0^\beta \mathrm{d}\tau \int \mathrm{d}^3x\, \bar{q}(\partial\!\!\!/_E + \langle M\rangle)q} \\ &= \mathrm{e}^{-\int_0^\beta \mathrm{d}\tau \int \mathrm{d}^3x\, \Omega_{\mathrm{mes}}} \det\left(\partial\!\!\!/_E + \langle M\rangle\right) \quad . \end{aligned} \tag{5.3}$$

First of all, we have used that the thermodynamic grand canonical potential density is given by [72]

$$\Omega = -\frac{1}{\beta V}\ln Z \tag{5.4}$$

which allows the identification of the mesonic potential

$$\Omega_{\mathrm{mes}} := U(\langle\rho_1\rangle,\ldots,\langle\rho_n\rangle) - c\left[\det\left(\langle\Phi^\dagger\rangle\right) + \det\left(\langle\Phi\rangle\right)\right] - h_a\langle\sigma_a\rangle \quad . \tag{5.5}$$

Secondly, we have defined the matrix

$$M := gT_a(\sigma_a + \mathrm{i}\gamma_5\pi_a) \tag{5.6}$$

that encodes the interaction of the quarks with the static mesons. At $N_f = 2$, only $\langle\sigma_0\rangle$ is non-zero and

$$\langle M\rangle_{2f} = g\,\mathrm{diag}\left(\frac{\langle\sigma_0\rangle}{2}, \frac{\langle\sigma_0\rangle}{2}\right) \tag{5.7}$$

while for $N_f = 2+1$ only $\langle\sigma_0\rangle$ and $\langle\sigma_8\rangle$ are non-zero, which means the VEV simplifies to

$$\langle M\rangle_{2+1f} = g\,\mathrm{diag}\left(\frac{\langle\sigma_l\rangle}{2}, \frac{\langle\sigma_l\rangle}{2}, \frac{\langle\sigma_s\rangle}{\sqrt{2}}\right) \tag{5.8}$$

with the rotation into the light-strange sector given in Eq. (4.25). We see that at the expectation value M serves as an effective mass term for the constituent quarks. Lastly,

the Gaussian fermion term in Eq. (5.3) has been integrated out. It proves easier to write (omitting the index E for the Euclidean derivative)

$$\begin{aligned}
\det\left(\partial\!\!\!/ + \langle M\rangle\right) &= \left[\det\left(\partial\!\!\!/ + \langle M\rangle\right)\det\left(\partial\!\!\!/ + \langle M\rangle\right)\right]^{1/2} \\
&= \left[\det\left(\partial\!\!\!/ + \langle M\rangle\right)\det(\gamma_5)\det\left(\partial\!\!\!/ + \langle M\rangle\right)\det(\gamma_5)\right]^{1/2} \\
&= \left[\det\left(\partial\!\!\!/ + \langle M\rangle\right)\det\left(\gamma_5\left(\partial\!\!\!/ + \langle M\rangle\right)\gamma_5\right)\right]^{1/2} \\
&= \left[\det\left(\partial\!\!\!/ + \langle M\rangle\right)\det\left(-\partial\!\!\!/ + \langle M\rangle\right)\right]^{1/2} \\
&= \left[\det\left(-\partial\!\!\!/^2 + \langle M\rangle^2\right)\right]^{1/2} \\
&= \left[\det\left(\omega_n^2 + \boldsymbol{p}^2 + \langle M\rangle^2\right)\right]^{1/2}
\end{aligned} \tag{5.9}$$

The last line follows from the expression of the derivative operator in momentum space $\partial\!\!\!/^2 \to -p\!\!\!/^2$. Now we can use the identity $\ln\det A = \mathrm{Tr}\ln A$:

$$\begin{aligned}
\left[\det\left(\omega_n^2 + \boldsymbol{p}^2 + \langle M\rangle^2\right)\right]^{1/2} &= \exp\left\{\ln\left[\det\left(\omega_n^2 + \boldsymbol{p}^2 + \langle M\rangle^2\right)\right]^{1/2}\right\} \\
&= \exp\left\{\frac{1}{2}\mathrm{Tr}\ln\left(\omega_n^2 + \boldsymbol{p}^2 + \langle M\rangle^2\right)\right\} \quad .
\end{aligned} \tag{5.10}$$

The trace gives a factor of 4 from Dirac space, a factor of N_c from color space, a sum in flavor space and an integral over position and momentum space. In total, the thermodynamic potential is

$$\Omega = \Omega_{\mathrm{quark}} + \Omega_{\mathrm{mes}} = -\frac{1}{\beta V}\ln Z \tag{5.11}$$

which cancels the position space integral and yields (in the Matsubara formalism as defined in App. A)

$$\Omega_{\mathrm{quark}} = -2N_c\sum_f T\sum_n \int \frac{\mathrm{d}^3p}{(2\pi)^3}\ln\left(\omega_n^2 + \boldsymbol{p}^2 + m_f^2\right) \quad . \tag{5.12}$$

m_f^2 are just the N_f eigenvalues of $\langle M\rangle^2$ that can easily be read off of Eq. (5.7) or (5.8), respectively. In order to solve the Matsubara sum, we can make use of the identity

$$\ln\left(\omega_n^2 + \boldsymbol{p}^2 + m_f^2\right) = \int_0^{\boldsymbol{p}^2+m_f^2}\mathrm{d}\alpha^2\,\frac{1}{\omega_n^2+\alpha^2} + \ln(\omega_n^2) \quad . \tag{5.13}$$

The second term just gives a diverging constant that changes the potential equally at each point in meson field space (it does not depend on the quark masses) and hence has no physical relevance. We will only consider the first term. The Matsubara sum can be pulled into the integral and can be solved there. After adding a chemical potential

$$\omega_n \to \omega_n + \mathrm{i}\mu \tag{5.14}$$

the Matsubara sum can be solved with the residue theorem (cf. Ref. [73]) and yields

$$T\sum_n \frac{1}{(\omega_n + \mathrm{i}\mu)^2 + \alpha^2} = \frac{1}{4\alpha}\left[\tanh\left(\frac{\alpha-\mu}{2T}\right) + \tanh\left(\frac{\alpha+\mu}{2T}\right)\right] \tag{5.15}$$

for fermionic frequencies $\omega_n = (2n+1)\pi T$. The dummy integral can be solved analytically:

$$\begin{aligned}
&\int_0^{\boldsymbol{p}^2+m_f^2} \mathrm{d}\alpha^2 \, \frac{1}{4\alpha} \left[\tanh\left(\frac{\alpha-\mu}{2T}\right) + \tanh\left(\frac{\alpha+\mu}{2T}\right)\right] \\
&\qquad = \int_0^{E_f := \sqrt{\boldsymbol{p}^2+m_f^2}} \mathrm{d}\alpha \, \frac{1}{2} \left[\tanh\left(\frac{\alpha-\mu}{2T}\right) + \tanh\left(\frac{\alpha+\mu}{2T}\right)\right] \\
&\qquad = T \left[\ln\cosh\left(\frac{E_f-\mu}{2T}\right) - \ln\cosh\left(\frac{-\mu}{2T}\right) + (\mu \to -\mu)\right] \\
&\qquad = T \left[\ln\left(\mathrm{e}^{(E_f-\mu)/(2T)} + \mathrm{e}^{-(E_f-\mu)/(2T)}\right) + (\mu \to -\mu)\right] + \text{const.} \\
&\qquad = T \left[\frac{E_f}{2T} + \ln\left(1 + \mathrm{e}^{-(E_f-\mu)/T}\right) + (\mu \to -\mu)\right] + \text{const.} \\
&\qquad = E_f + T \left[-\ln\left(\frac{\mathrm{e}^{(E_f-\mu)/T}}{1+\mathrm{e}^{(E_f-\mu)/T}}\right) + (\mu \to -\mu)\right] + \text{const.} \\
&\qquad = E_f - T \left[\ln\left(1 - n_f(E_f,\mu,T)\right) + \ln\left(1 - n_f(E_f,-\mu,T)\right)\right] + \text{const.} \quad .
\end{aligned} \tag{5.16}$$

The symbol $(\mu \to -\mu)$ means that all other terms in the large bracket are to be summed up again, replacing μ with $-\mu$ this time.

$$n_f(E_f,\mu,T) := \frac{1}{1+\exp\left(\frac{E_f-\mu}{T}\right)} \tag{5.17}$$

is the Fermi-Dirac statistics and the expression "const." includes all terms that are independent of the meson fields and can be dropped. The same result can be obtained by using

$$\tanh\left(\frac{\alpha-\mu}{2T}\right) = 1 - 2\, n_f(\alpha,\mu,T) \quad . \tag{5.18}$$

The quark potential now reads

$$\begin{aligned}
\Omega_{\text{quark}} &= 2N_c \sum_f \int \frac{\mathrm{d}^3p}{(2\pi)^3} \left[-E_f + T\ln\left(1 - n_f(E_f,\mu,T)\right) + T\ln\left(1 - n_f(E_f,-\mu,T)\right)\right] \\
&= \frac{N_c}{\pi^2} \sum_f \int_0^\infty \mathrm{d}p\, p^2 \, \left[-E_f + T\ln\left(1 - n_f(E_f,\mu,T)\right) + T\ln\left(1 - n_f(E_f,-\mu,T)\right)\right] \\
&=: \Omega_{\text{vac}} + \Omega_q
\end{aligned} \tag{5.19}$$

with the vacuum term

$$\Omega_{\text{vac}} := -\frac{N_c}{\pi^2} \sum_f \int_0^\infty \mathrm{d}p\, p^2 \sqrt{p^2+m_f^2} \tag{5.20}$$

and the thermodynamic contribution

$$\Omega_q := \frac{N_c}{\pi^2} T \sum_f \int_0^\infty \mathrm{d}p\, p^2 \, \left[\ln\left(1 - n_f(E_f,\mu,T)\right) + \ln\left(1 - n_f(E_f,-\mu,T)\right)\right] \quad . \tag{5.21}$$

The vacuum term is divergent and would be obtained in a vacuum calculation in Minkowski space as well while the thermal fluctuations are finite additional contributions that vanish for $T \to 0$ [72]. In the standard mean field approximation (sMFA), the vacuum contribution is just ignored as it does not explicitly depend on T. However, the quark masses m_f are temperature dependent and give the vacuum term an implicit T-dependence which has an effect on the thermodynamics of the theory. We will employ both a sMFA and a mean field approach that follows from the functional renormalization group flow and includes the vacuum term in a fully renormalized fashion (see Sec. 6.4). The correct vacuum field configuration $\langle\sigma_0\rangle$ (analog $\langle\sigma_l\rangle, \langle\sigma_s\rangle$ in 2+1 flavors) can be found by minimizing Ω with respect to the fields.

6 Functional Renormalization Group Approach

The non-perturbative renormalization group goes back to the works of Kenneth Wilson in 1971 [74, 75]. In contrast to the formerly known perturbative renormalization group, the new idea is that a quantum field theory should not be understood as a fundamental theory that must hold at infinitely small distances, but rather as an effective description of the interactions at a given length scale. This can be derived from the path integral by a momentum shell transformation where all interactions of momenta that are higher than a given ultraviolet (UV) cutoff scale Λ are assumed to be already integrated out [76]. By successively including additional fluctuations in momentum shells, the effective couplings of the theory change. This change is given by the beta functions that are already known from perturbative calculations. However, the modern approach is not restricted to perturbative applications and also allows for a more general definition of renormalizability. A theory is renormalizable if only a finite number of RG-relevant couplings exists. RG-relevant couplings are those that are unstable at a given fixed point where the beta functions vanish. In this understanding, the renormalization group is the theory of scales and it allows for treatment of critical phenomena like continuous phase transitions [77]. The implementation of this framework in functional language is titled "functional renormalization group" (FRG). One usually obtains a flow equation that defines the change of some functional quantity under a change of the RG scale. This was first done by Polchinski who showed the connection between perturbative renormalizability and renormalizability according to Wilson's criterion [78]. In modern applications, the Wetterich equation [79–81], a flow equation for the effective action, is usually applied.

6.1 Wetterich Equation

The Wetterich equation introduces an RG-scale-dependent effective action Γ_k that interpolates between the classical action of a theory and the quantum effective action. Given a scalar field $\varphi(x)$, we denote its expectation value in the presence of a source term $J(x)$ as $\phi(x) = \langle\varphi(x)\rangle_J$ [49]. The classical action $S[\phi]$ does not include any fluctuations, while the full quantum effective action $\Gamma[\phi]$ includes all (thermodynamic and/or quantum) fluctuations. A scale dependence is introduced by means of an additional action term in the integrand of the partition function:

$$Z_k[J] := \int \mathcal{D}\varphi \, \mathrm{e}^{-S[\varphi]-\Delta S_k[\varphi]+\int J\varphi} \quad . \tag{6.1}$$

In order to follow Wilson's idea of successively including fluctuations, ΔS_k should look like a scale-dependent mass term that becomes infinitely large for $k = \Lambda$. The infinite mass suppresses all field dynamics around its expectation value and the classical equation of motion follows. At $k = 0$, ΔS_k must vanish to recover the original generating functional, $Z_{k=0}[J] = Z[J]$, which generates all quantum fluctuations. In momentum space the mass term of a scalar field has the form

$$\frac{1}{2}\int \frac{\mathrm{d}^4p}{(2\pi)^4}\, \tilde{\varphi}(-p)\, m^2\, \tilde{\varphi}(p) \quad , \tag{6.2}$$

hence ΔS_k is defined

$$\begin{aligned}\Delta S_k[\varphi] :&= \frac{1}{2}\int \frac{\mathrm{d}^4 p}{(2\pi)^4}\,\tilde{\varphi}(-p)\,R_k(p)\,\tilde{\varphi}(p)\\ &= \frac{1}{2}\int \mathrm{d}^4 x \int \mathrm{d}^4 y\,\varphi(x)\,R_k(x-y)\,\varphi(y) \quad .\end{aligned} \tag{6.3}$$

$R_k(p)$ is a dynamical regulator function that takes on the role (and dimensionality) of a squared mass and cuts off low-momentum fluctuations in a scale-dependent way. It has to fulfill several conditions that are given in Ref. [82]. Specifically, the regulator does not necessarily have to be sharp, i.e. it does not have to regulate all momenta $p^2 < k^2$ by an infinite mass term and include all fluctuations $p^2 > k^2$ without modifications. Some degree of smearing around the momentum shell is allowed as long as the respective conditions are fulfilled. The choice of regulator can be understood as a choice of path in theory space. While both the starting point with the given UV couplings and the end point with the physical interactions are fixed, the trajectory between these points is up to the regulator [49]. Note that the choice of regulator, even though the physical results should not depend on it, plays an important role in practice. The reason for this can be found in deviations from the exact flow. Such deviations always persist because of necessary truncations and approximations, but cutoff effects that arise e.g. when the temperature or chemical potential come too close to the UV scale Λ also play a role [83]. The impact of such errors depends on the chosen trajectory and gives rise to the requirement of a regulator with good convergence properties. An optimized regulator is given by the three-dimensional bosonic version of the Litim regulator [82]

$$R_k^B(\boldsymbol{p}) = (k^2 - \boldsymbol{p}^2)\,\theta\left(1 - \frac{\boldsymbol{p}^2}{k^2}\right) \tag{6.4}$$

that we will employ. From the modified partition function, we find the generator of connected diagrams in the usual way,

$$W_k[J] = \ln Z_k[J] \quad , \tag{6.5}$$

and with $\phi(x) = \delta W_k[J]/\delta J(x)$ the effective action is the modified Legendre transform

$$\Gamma_k[\phi] := \int J\phi - W_k[J] - \Delta S_k[\phi] \tag{6.6}$$

that can be shown to yield the classical action $S[\phi]$ at $k = \Lambda$ and the full quantum effective action $\Gamma[\phi]$ for $k = 0$. The strength of the approach is that the inclusion of quantum fluctuations which is commonly described by a path integral can now be expressed via a functional differential equation. The flow is evolved by infinitesimal steps in k. With the definition of the dimensionless "RG time" $t := \ln k/\Lambda$, the effective action can be worked out to change under a scale transformation like

$$\begin{aligned}\partial_t \Gamma_k[\phi] &= \frac{1}{2}\int_x \int_y \left(\Gamma_k^{(2)} + R_k\right)^{-1}(y-x)\,\partial_t R_k(x-y)\\ &= \frac{1}{2}\beta V \int_p \left(\Gamma_k^{(2)} + R_k\right)^{-1}(p)\,\partial_t R_k(p)\\ &= \frac{1}{2}\mathrm{Tr}\left[\left(\Gamma_k^{(2)} + R_k\right)^{-1}\,\partial_t R_k\right] \quad .\end{aligned} \tag{6.7}$$

The second line follows from a Fourier transformation to momentum space and the trace includes a sum over all subspaces of the field that have been left out in the notation. For the description of fermions, we define

$$Z_k[\chi,\bar{\chi}] := \int \mathcal{D}\bar{\Psi}\mathcal{D}\Psi\, \mathrm{e}^{-S[\bar{\Psi},\Psi]-\Delta S_k[\bar{\Psi},\Psi]+\int \bar{\chi}\Psi+\int \bar{\Psi}\chi} \tag{6.8}$$

with the regulator term

$$\Delta S_k[\bar{\Psi},\Psi] = \int \frac{\mathrm{d}^4 p}{(2\pi)^4}\, \bar{\Psi}(-p)R_k(p)\Psi(p) \quad . \tag{6.9}$$

Here, the regulator has to have the dimension of mass, not mass squared. We employ the fermionic three-dimensional Litim regulator

$$R_k^F(\boldsymbol{p}) = \boldsymbol{p}\cdot\boldsymbol{\gamma}\left(\sqrt{\frac{k^2}{\boldsymbol{p}^2}}-1\right)\theta\left(1-\frac{\boldsymbol{p}^2}{k^2}\right) \quad . \tag{6.10}$$

Working out the scale derivative of the fermionic modified effective action and taking care of the Grassmann nature of the fields, we find

$$\begin{aligned}\partial_t\Gamma_k[\bar{\psi},\psi] &= -\beta V\int_p \mathrm{tr}\left[\left(\Gamma_k^{(1,1)}+R_k\right)^{-1}(p)\,\partial_t R_k(p)\right]\\ &= -\mathrm{Tr}\left[\left(\Gamma_k^{(1,1)}+R_k\right)^{-1}\partial_t R_k\right]\end{aligned} \tag{6.11}$$

with the definition

$$\Gamma_k^{(1,1)}(x-y) := \left(\frac{\delta}{\delta\bar{\psi}(x)}\right)\left(-\frac{\delta}{\delta\psi(y)}\right)\Gamma_k[\bar{\psi},\psi] \tag{6.12}$$

where both derivatives act from the left. The general case of mixed scalar and spin-1/2-fields is then given by the full Wetterich equation

$$\partial_t\Gamma_k = \frac{1}{2}\mathrm{Tr}\left[\left(\Gamma_k^{(2)}+R_k^B\right)^{-1}\partial_t R_k^B\right] - \mathrm{Tr}\left[\left(\Gamma_k^{(1,1)}+R_k^F\right)^{-1}\partial_t R_k^F\right] \quad . \tag{6.13}$$

Because $(\Gamma_k^{(2)}+R_k)^{-1}$ is just the effective scale-dependent propagator, diagrammatic representations of the trace terms look like one-loop diagrams with insertions of $\partial_t R_k$. In contrast to a perturbative one-loop approximation, however, this propagator is not the bare propagator but the full effective version. Hence, the Wetterich equation is a functional partial differential equation that allows the successive integration of fluctuations in an exact way, given a theory that is defined at a UV momentum scale Λ.

6.2 Local Potential Approximation

Because of infinitely many possible field configurations, the solution of functional equations always requires a truncation that approximates the given functional. Here, the Wetterich equation has the advantage of being a flow equation for the quantum effective action. Already from its definition, the possibility of expanding Γ similarly to the

action of the theory comes to mind. The couplings in the vertex expansion are effective position-/momentum-space-dependent interaction vertices encoding all quantum fluctuations. As an example, the expansion for ϕ^4 theory in momentum space reads [32]

$$\Gamma[\phi] = \frac{1}{2}\int \frac{\mathrm{d}^4k}{(2\pi)^4}\,\tilde{\phi}(-k)(k^2+m^2)\tilde{\phi}(k) + \sum_{n=4}^{\infty}\frac{1}{n!}\int\frac{\mathrm{d}^4k_1}{(2\pi)^4}\cdots\int\frac{\mathrm{d}^4k_n}{(2\pi)^4} \\ (2\pi)^4\delta^4(k_1+\cdots+k_n)V_n(k_1,\ldots,k_n)\tilde{\phi}(k_1)\ldots\tilde{\phi}(k_n) \quad . \tag{6.14}$$

The first term is the inverse exact propagator (with m^2 denoting the physical mass in this case) and the V_n are the 1PI vertex functions. Another approximation of the effective action is the derivative expansion. The functional is summed in increasing order of derivative operators, e.g. for a real scalar field

$$\Gamma[\phi] = \int \mathrm{d}^4x\,\left[U(\phi) + \frac{1}{2}Z(\partial\phi)^2 + \mathcal{O}(\partial^4)\right] \quad . \tag{6.15}$$

$U(\phi)$ is the effective potential and Z, which couples to the kinetic term, is the wavefunction renormalization. Its advantage is that many relevant interactions are already encoded in the first term which becomes clear in the application to thermodynamics. To make this connection, we use the fact that in the Matsubara formalism the generating functional at vanishing external source is equal to the thermodynamic partition function: $Z[0] = Z$. The grand canonical potential density is then given by [72]

$$\Omega = -\frac{1}{\beta V}\ln Z = -\frac{1}{\beta V}W = \frac{1}{\beta V}\Gamma \tag{6.16}$$

where $\Gamma := \Gamma[\phi_0]$ and

$$\phi_0(x) := \left.\frac{\delta W[J]}{\delta J(x)}\right|_{J=0} \quad . \tag{6.17}$$

Given a constant, spacetime-independent field VEV ϕ_0 as it is expected for an isotropic thermodynamic ensemble, Eq. (6.15) becomes

$$\Gamma[\phi_0] = \beta V\,U(\phi_0) \quad . \tag{6.18}$$

This allows the identification

$$\Omega = U(\phi_0) \tag{6.19}$$

where ϕ_0 also minimizes the effective potential. In general, U is a function of the invariants of a given theory such that all fluctuations that respect its symmetries can be included. Of course, the derivative expansion can also be applied to the scale-dependent modified effective action Γ_k:

$$\Gamma_k[\phi] = \int \mathrm{d}^4x\,\left[U_k(\phi) + \frac{1}{2}Z_k(\partial\phi)^2 + \mathcal{O}(\partial^4)\right] \quad . \tag{6.20}$$

$U_k(\phi_0)$ then goes to Ω in the limit $k \to 0$. The local potential approximation (LPA) utilizes the derivative expansion, but only allows a scale-dependence in the lowest order term, the potential U_k. The running of the wavefunction renormalization is neglected and it is kept at the bare UV value $Z_k \equiv 1$. In this work we employ the local potential approximation and state that future investigations of the phase diagram at high densities beyond LPA are planned.

6.3 Application to Quark-meson Model

In our FRG approach towards high-density area of the QCD phase diagram, we proceed to calculate the flow equation for the quark-meson model in N_f flavors as given in Eq. (4.12). Therefore, we take the ansatz for the modified effective action in LPA:

$$\Gamma_k = \int \mathrm{d}^4x \left[\bar{q}\left(\partial\!\!\!/_E + gT_a\left(\sigma_a + \mathrm{i}\gamma_5\pi_a\right)\right)q + \frac{1}{2}(\partial\sigma_a)^2 + \frac{1}{2}(\partial\pi_a)^2 + \tilde{U}_k(\sigma_a,\pi_a)\right] \tag{6.21}$$

with

$$\tilde{U}_k(\sigma_a,\pi_a) = U_k(\rho_1,\ldots,\rho_{N_f}) - c\left[\mathrm{Det}\left(\Phi^\dagger\right) + \mathrm{Det}\left(\Phi\right)\right] - h_a\sigma_a \quad . \tag{6.22}$$

Note that now all fields are classical fields. Furthermore, in the fermionic sector the ansatz consists of a kinetic term with the Yukawa type coupling g from the Lagrangian which is taken to be scale-independent in LPA. The explicit symmetry breaking terms in $\tilde{U}_k$ have constant coefficients as well. The actual k-dependent effective potential U_k is, as mentioned in the last section, a function of the invariants of the theory. In the quark-meson model, those are the N_f chiral invariants which in turn depend on the meson fields σ_a and π_a. At the UV scale Λ, the effective potential U_k just becomes the initial potential U_Λ of the quark-meson model. Because the Wetterich equation gives the partial derivative $\partial_t\Gamma_k[\phi]$, we can evaluate the differential equation for a given field configuration $\phi(x)$ down to $k=0$. At the vacuum expectation value, we already know that all pseudoscalar meson condensates must vanish, as well as any scalar mesons that are non-diagonal in the generators. We denote the N_f diagonal generators T_d, $d \in \{1,\ldots,N_f\}$. In practice, this means that the second functional derivative has to be taken from the full effective action given in Eq. (6.21) and then evaluated at the VEV. In the fermionic sector, $\Gamma^{(1,1)}$ in momentum space becomes

$$\Gamma^{(1,1)}(p) = \mathrm{i}p\!\!\!/_E + gT_d\sigma_d \quad . \tag{6.23}$$

We use the fermionic regulator given in Eq. (6.10) and add it to the functional derivative. On top of that, we introduce a chemical potential in the same fashion as in the mean field approximation in Sec. 5:

$$\Gamma_k^{(1,1)} + R_k^F = \mathrm{i}(\omega_n + \mathrm{i}\mu)\gamma_0 + \mathrm{i}\boldsymbol{p}\cdot\boldsymbol{\gamma}\sqrt{\frac{k^2}{\boldsymbol{p}^2}}\,\theta\left(1-\frac{\boldsymbol{p}^2}{k^2}\right) + gT_d\sigma_d \quad . \tag{6.24}$$

The Dirac space inverse of this expression is given by

$$\left(\Gamma_k^{(1,1)} + R_k^F\right)^{-1} = \frac{-\mathrm{i}p_0\gamma_0 - \mathrm{i}\boldsymbol{p}\cdot\boldsymbol{\gamma}\sqrt{\frac{k^2}{\boldsymbol{p}^2}} + gT_d\sigma_d}{p_0^2 + k^2 + g^2(T_d\sigma_d)^2} \tag{6.25}$$

where $p_0 = \omega_n + \mathrm{i}\mu$. Note that the matrix expression $(T_d\sigma_d)^2$ in the denominator is not a problem because the T_d are diagonal in flavor space and thus the inverse is also diagonal. The θ-stepfunction has been omitted since it appears again in the scale derivative of the regulator in the Wetterich equation and cuts out all momenta higher than k, effectively rendering the θ-function in this expression equal to 1 in the area of interest. The regulator scale derivative reads

$$\begin{aligned}\partial_t R_k^F &= k\mathrm{i}\boldsymbol{p}\cdot\boldsymbol{\gamma}\left[\frac{1}{|\boldsymbol{p}|}\theta\left(1-\frac{\boldsymbol{p}^2}{k^2}\right) + \left(\frac{k}{|\boldsymbol{p}|}-1\right)\delta\left(1-\frac{\boldsymbol{p}^2}{k^2}\right)2\frac{\boldsymbol{p}^2}{k^3}\right] \\ &= \mathrm{i}\boldsymbol{p}\cdot\boldsymbol{\gamma}\left[\frac{k}{|\boldsymbol{p}|}\theta\left(1-\frac{\boldsymbol{p}^2}{k^2}\right) + \left(|\boldsymbol{p}| - \frac{\boldsymbol{p}^2}{k}\right)\delta(p-k)\right] \quad .\end{aligned} \tag{6.26}$$

The last term is always zero in the integral and hence does not contribute. We can make use of the trace identity

$$\mathrm{tr}\,(\gamma_\mu\gamma_\nu) = 4\delta_{\mu\nu} \tag{6.27}$$

and the fact that the trace over a product of an uneven number of gamma matrices is zero to see that the only contributing term in the product of the effective propagator [Eq. (6.25)] and the regulator derivative [Eq. (6.26)] is

$$\frac{k^2\theta\left(1-\frac{\boldsymbol{p}^2}{k^2}\right)}{p_0^2+k^2+g^2(T_d\sigma_d)^2} \quad . \tag{6.28}$$

The trace over color, flavor, Dirac, and phase space yields

$$\begin{aligned}\mathrm{Tr}\left[\left(\Gamma_k^{(1,1)}+R_k^F\right)^{-1}\partial_t R_k^F\right] &= 4N_c\sum_f\int \mathrm{d}^4x\,T\sum_n\int\frac{\mathrm{d}^3p}{(2\pi)^3}\frac{k^2\theta\left(1-\frac{\boldsymbol{p}^2}{k^2}\right)}{(\omega_n+\mathrm{i}\mu)^2+k^2+m_f^2}\\ &= \beta V\,\frac{2N_c}{12\pi^2}\sum_f\frac{k^5}{E_f}\left[\tanh\left(\frac{E_f-\mu}{2T}\right)+\tanh\left(\frac{E_f+\mu}{2T}\right)\right] \quad .\end{aligned} \tag{6.29}$$

The Matsubara sum is the same sum we encountered in the mean field approximation, c.f. Eq. (5.15). Furthermore, we have defined $E_f := \sqrt{k^2+m_f^2}$ where m_f^2 are the corresponding diagonal entries of the matrix $g^2(T_d\sigma_d)^2$. Continuing with the meson sector, the second functional derivative for each meson reads in momentum space

$$\Gamma_k^{(2)}(p) = p^2 + \tilde{U}_k^{(2)} \quad . \tag{6.30}$$

With the bosonic regulator given in Eq. (6.4) the sum becomes (setting the theta function to one)

$$\Gamma^{(2)} + R_k^B = p_0^2 + k^2 + \tilde{U}_k^{(2)} \tag{6.31}$$

and the non-vanishing part of the regulator derivative is

$$\partial_t R_k^B = 2k^2\theta\left(1-\frac{\boldsymbol{p}^2}{k^2}\right) \quad . \tag{6.32}$$

We use the notation $E_b := k^2+m_b^2$ and $m_b^2 := \tilde{U}_{k,bb}^{(2)}$, where the index b denotes the $2N_f^2$ meson fields and $\tilde{U}_{k,bb}^{(2)}$ is the second derivative with respect to the corresponding field. Due to the meson-meson interactions, the meson terms in the effective action are mixed. This means that the meson mass matrix $\tilde{U}_{k,ab}^{(2)}$ is not necessarily diagonal. The actual meson resonances are found by diagonalizing this matrix. Due to the cyclic invariance of the trace, this diagonalization does not change the evolution of the flow. Therefore, we proceed with m_b^2 now denoting the entries of the diagonalized mass matrix. Taking the trace in phase and meson space, the mesonic part of the Wetterich equation becomes

$$\begin{aligned}\frac{1}{2}\mathrm{Tr}\left[\left(\Gamma_k^{(2)}+R_k^B\right)^{-1}\partial_t R_k^B\right] &= \frac{1}{2}\int \mathrm{d}^4x\,T\sum_n\int\frac{\mathrm{d}^3p}{(2\pi)^3}\sum_b\frac{2k^2\theta\left(1-\frac{\boldsymbol{p}^2}{k^2}\right)}{\omega_n^2+k^2+m_b^2}\\ &= \beta V\frac{k^5}{12\pi^2}\sum_b\frac{1}{E_b}\coth\left(\frac{E_b}{2T}\right)\end{aligned} \tag{6.33}$$

with the solution of the Matsubara sum without chemical potential at bosonic frequencies $\omega_n = 2\pi n T$:

$$T \sum_n \frac{1}{\omega_n^2 + E^2} = \frac{1}{2E} \coth\left(\frac{E}{2T}\right) \quad . \tag{6.34}$$

Going back to Eq. (6.21) and inserting the vacuum expectation value of constant fields $\langle \sigma_d \rangle$, we see that

$$\partial_t \Gamma_k[\langle \sigma_d \rangle] = \int \mathrm{d}^4 x \, \partial_t U_k(\langle \rho_1 \rangle, \ldots, \langle \rho_{N_f} \rangle) = \beta V \, \partial_t U_k(\langle \rho_1 \rangle, \ldots, \langle \rho_{N_f} \rangle) \quad . \tag{6.35}$$

The volume factor βV cancels on both sides and the full flow equation for the effective potential U_k is

$$\begin{aligned} \partial_t U_k = \frac{k^5}{12\pi^2} \Bigg\{ & \sum_b \frac{1}{E_b} \coth\left(\frac{E_b}{2T}\right) \\ & - 2N_c \sum_f \frac{1}{E_f} \left[\tanh\left(\frac{E_f - \mu}{2T}\right) + \tanh\left(\frac{E_f + \mu}{2T}\right) \right] \Bigg\} \quad . \end{aligned} \tag{6.36}$$

It is worth pointing out that in this truncation all quantum fluctuations are dynamically encoded in the chirally symmetric meson potential U_k. Nevertheless, the derivation shows that the potential $\tilde{U}_k$ which additionally includes the explicit breaking terms determines the meson masses. However, since the so-called curvature masses $\tilde{U}^{(2)}_{k,bb}$ are the second derivatives with respect to the fields (while the physical pole masses are at the poles of the meson propagator), the linear chiral symmetry breaking term $-h_a \sigma_a$ does not contribute. Only the $U(1)_A$ breaking term modifies the meson masses on top of the potential U_k. For $k = 0$, the meson potential including the static symmetry breaking terms $\tilde{U} := \tilde{U}_{k=0}$ can be identified with Ω when evaluated at the vacuum configuration that minimizes $\tilde{U}$:

$$\Omega = \tilde{U}(\langle \sigma_d \rangle) \quad . \tag{6.37}$$

6.4 Renormalized Mean Field Approximation

In the derivation of the standard mean field approximation in Sec. 5 we dropped a divergent vacuum term with implicit dependence on temperature and chemical potential. Instead of regularizing and subsequently renormalizing this term by hand, one can just take the fermionic part of the given flow equation and drop the mesonic quantum fluctuations. Because of the exactness of the Wetterich equation, the vacuum term is included in fully renormalized form. It shall also be noted that due to the simple Gaussian structure in the fermionic Lagrangian in mean field approximation, the currently employed LPA treatment solves the fermionic path integral exactly and does not give an additional error. We take the ansatz

$$\Omega = \Omega_{\mathrm{mes}} + \Omega_q \tag{6.38}$$

for the grand canonic potential density with the meson potential defined in Eq. (5.5). The quark potential is equal to the effective fermion potential $U_{q,k}$ at scale $k = 0$ which can be written

$$\Omega_q = U_{q,k=0} = U_{q,k=\Lambda} - \int_0^\Lambda \mathrm{d}k \, \partial_k U_{q,k} \tag{6.39}$$

with $U_{q,k=\Lambda} = 0$ as the UV potential is given by the static meson potential and (with $\partial_t = k\partial_k$)

$$\partial_k U_{q,k} = -\frac{k^4 N_c}{6\pi^2} \sum_f \frac{1}{E_f} \left[\tanh\left(\frac{E_f - \mu}{2T}\right) + \tanh\left(\frac{E_f + \mu}{2T}\right) \right] \quad . \tag{6.40}$$

Unlike the meson masses, the fermion masses are static for a given vacuum configuration and do not depend on $U_{q,k}$ or its derivatives. Hence, the differential equation can just be integrated out as the integral sign suggests. Nevertheless, k is still the artificial RG scale and not necessarily equal to the momentum p found in the integral of the standard mean field approximation. We call this improved approach renormalized mean field approximation (rMFA).

7 Numerical Implementation

The given integrals and differential equations require a numerical solution. The greatest obstacle in that regard are the renormalization group flow equations. Even though we have reduced them from a functional partial differential equation (PDE) to a common PDE for each possible field configuration in U_k, solution techniques for such equations are still not very evolved. In particular, at a given field configuration a way must be found to determine the second derivative of $\tilde{U}_k$ with respect to the fields in order to determine the meson curvature masses m_b^2 in the equation. For the explicit symmetry breaking terms, this is not a problem as they can be calculated analytically beforehand, cf. App. C. The second derivatives of U_k, however, require a knowledge of the potential in an area around the given point. Among the solution techniques, various Taylor approximations either at (and moving with) the minimum of the potential (co-moving) or static expansions close to the expected minimum or even at two separate points [84] have been established. Furthermore, the flow can be discretized on a grid where each point stands for a possible field configuration [85, 86]. This approach is utilized here.

7.1 One- and Two-dimensional Grid

In Sec. 4 the possible non-zero meson fields at the expectation value have been reduced to a single field $\langle\sigma\rangle$ in the two-flavor case and the light and strange condensates $\langle\sigma_l\rangle$ and $\langle\sigma_s\rangle$ in the 2+1-flavor case. For $N_f = 2$, the potential is a function of one chiral invariant:

$$U_k = U_k(\rho) \quad . \tag{7.1}$$

This means that at the expectation value where $U_k = U_k(\langle\rho\rangle)$, the second derivative of U_k with respect to some field π_a is given

$$U^{(2)}_{k,\pi_a\pi_a} = \left[\frac{\partial U_k}{\partial\rho}\frac{\partial^2\rho}{\partial\pi_a^2} + \frac{\partial^2 U_k}{\partial\rho^2}\left(\frac{\partial\rho}{\partial\pi_a}\right)^2\right]\Bigg|_{\rho=\langle\rho\rangle} \quad . \tag{7.2}$$

In this case, $\langle\rho\rangle = \frac{1}{2}\langle\sigma\rangle^2$. This shows that the expectation values of the chiral invariants are in direct correspondence with the condensates (this is why we could write $U_k(\langle\sigma_d\rangle)$ before). The derivatives and second derivatives of the analytically known chiral invariants with respect to all meson fields can just be calculated and the expectation value inserted, which makes them known functions of the condensate. At this point, we use the fact that at $\rho = \langle\rho\rangle$, the derivative of U_k is analytically equivalent to

$$\frac{\partial U_k(\rho)}{\partial\rho}\bigg|_{\rho=\langle\rho\rangle} = \frac{\partial U_k(\langle\rho\rangle)}{\partial\langle\rho\rangle} = \frac{\partial U_k}{\partial\langle\sigma\rangle^2}\frac{\partial\langle\sigma\rangle^2}{\partial\langle\rho\rangle} = 2\frac{\partial U_k}{\partial\langle\sigma^2\rangle} =: 2U_k' \quad . \tag{7.3}$$

In this manner, all masses can be obtained as derivatives of U_k with respect to $\langle\sigma\rangle^2$ to first or second order. By putting U_k on a grid, one determines an array of N points

$$\{\langle\sigma\rangle_1^2, \ldots, \langle\sigma\rangle_N^2\} \tag{7.4}$$

where U_k is known and couples the points in a way that U_k can be determined as a continuous function of the variable $\langle\sigma\rangle^2$ which is differentiable up to second order at the grid points. In this work, we use a cubic spline interpolation which allows for an uncomplicated extraction of the first and second derivative directly at the N fixed

points. The derivatives at the outermost left and right points are determined by a finite difference formula. Note that at high chemical potential and $T = 0$, the fermionic threshold function becomes a theta function $\sim \theta(E_f - \mu)$ as shown in App. B. This sudden stop in the running of the potential at grid points that lie below this fermi surface (where the quark mass $m_f^2 \sim \sigma^2$ is so small that the energy $E_f = \sqrt{k^2 + m_f^2}$ drops below the chemical potential) means the first derivative U_k' gets a delta distribution peak $\sim \delta(E_f - \mu)$ at the respective point at the scale k where $E_f = \mu$. As laid out in App. B, such a delta distribution can be integrated out in an infinitesimal interval and adds a finite contribution to the potential derivative at the given grid point. This is of relevance in another grid coupling scheme given in Ref. [85] that uses Taylor expansions at the grid points has the first derivative U_k' running on the grid as well. At decreasing k, more and more derivatives experience a delta jump. On the one hand, it can be argued that this scheme is more accurate than a spline interpolation that washs out these jumps because the first derivative is only approximately determined from the function U_k itself. On the other hand, in the calculations for this work the approach given in Ref. [85] broke down exactly at the scale k where the onset of these phenomena was expected for the leftmost grid point. This can be associated to instabilities in the grid coupling that are especially vulnerable to fluctuations in the outermost derivatives. It can be argued that adding a hard contribution from a continuous theory like a delta distribution to a certain grid point while running a discretized, approximate system is not a reasonable choice. Hence, we use a spline interpolation in favor of higher stability and note that some non-analyticities might be washed out. It shall be mentioned that a coordinate transformation as given in Ref. [87] might circumvent this problem, but it only works for one chiral condensate in LPA so far. In order to attain comparable results, the approach taken here is extended to $N_f = 2 + 1$. Because we allow for two distinct condensates now, the grid must be set up in two dimensions. Instead of taking $\langle\sigma_l\rangle^2$ and $\langle\sigma_s\rangle^2$, the variables

$$x = \langle\sigma_l\rangle^2 \quad , \quad y = 2\langle\sigma_s\rangle^2 - \langle\sigma_l\rangle^2 \tag{7.5}$$

as employed in Ref. [71] are used. In this setup, the minimum of the potential will always be close to the starting value in y-direction. Furthermore, we modify the second chiral invariant such that

$$\tilde{\rho}_2 := \rho_2 - \frac{\rho_1}{3} \quad . \tag{7.6}$$

This yields the expectation values

$$\langle\rho_1\rangle = \frac{1}{4}(3x + y) \ , \ \langle\tilde{\rho}_2\rangle = \frac{1}{24}y^2 \quad \Longrightarrow \quad x = \frac{1}{3}\left(4\langle\rho_1\rangle - \sqrt{24\langle\tilde{\rho}_2\rangle}\right) \ , \ y = \sqrt{24\langle\tilde{\rho}_2\rangle} \quad . \tag{7.7}$$

Picking up the example of a meson field π_a, the second derivative of the chirally symmetric potential is

$$U^{(2)}_{k,\pi_a\pi_a} = \left[\frac{\partial U_k}{\partial\rho_1}\frac{\partial^2\rho_1}{\partial\pi_a^2} + \frac{\partial^2 U_k}{\partial\rho_1^2}\left(\frac{\partial\rho_1}{\partial\pi_a}\right)^2 + 2\frac{\partial^2 U_k}{\partial\rho_1\partial\tilde{\rho}_2}\frac{\partial\rho_1}{\partial\pi_a}\frac{\partial\tilde{\rho}_2}{\partial\pi_a} + \frac{\partial^2 U_k}{\partial\tilde{\rho}_2^2}\left(\frac{\partial\tilde{\rho}_2}{\partial\pi_a}\right)^2 + \frac{\partial U_k}{\partial\tilde{\rho}_2}\frac{\partial^2\tilde{\rho}_2}{\partial\pi_a^2}\right]\Bigg|_{\rho_1=\langle\rho_1\rangle\,,\,\tilde{\rho}_2=\langle\tilde{\rho}_2\rangle} \quad . \tag{7.8}$$

Again, the derivatives of the chiral invariants can be calculated and evaluated at the expectation value. The derivatives of the potential are determined in the following fashion:

$$\frac{\partial U_k}{\partial \langle \rho_1 \rangle} = \frac{\partial U_k}{\partial x} \frac{\partial x}{\partial \langle \rho_1 \rangle} + \frac{\partial U_k}{\partial y} \frac{\partial y}{\partial \langle \rho_1 \rangle} \quad , \tag{7.9}$$

similarly for the other derivatives. The grid now consists of two arrays of points, one with N_x points in x-direction and one with N_y points in y-direction. Each of the $N_x N_y$ grid points is thus given by a touple (x_i, y_j). The splines are set up the following way: for each constant y_c, there is a cubic spline interpolating over all N_x points (x_i, y_c) in x-direction. Similarly, for each value x_c, a cubic spline interpolates over the N_y points (x_c, y_j) in y-direction. This gives all first and second derivatives with respect to x and y at each grid point. Note that we also need a mixed derivative

$$\frac{\partial^2 U_k}{\partial x \partial y} \quad . \tag{7.10}$$

This is obtained from a finite difference three-point formula that interpolates the x-derivative in y-direction or vice versa. Concerning the stability of the approach, it has to be noted that the placement and spacing of grid points is of significant importance. For good accuracy, it is reasonable to place many grid points at low values of x because this is where the minimum will land in the chirally restored phase. Then again, there have to be enough points at high values of x and y such that the increase of the potential in that region stabilizes the second derivatives in the area of low condensates. This is due to the fact that some inverse meson energies that occur in the flow equation run very closely to the poles at $k^2 + \tilde{U}_k^{(2)} = 0$. For some of those mesons $\tilde{U}_k^{(2)}$ has non-vanishing contributions from the second derivatives with respect to x and y. Especially in the region of low T and high μ, the solution of the differential equation has been experienced as very unstable and only possible for certain grid point arrangements. The first configuration we use in this work entails

$$N_x = 35 \quad , \quad N_y = 20 \tag{7.11}$$

grid points, respectively, in a range $x_{\min} = 1\,\mathrm{MeV}^2$, $x_{\max} = (170)^2\,\mathrm{MeV}^2$ and $y_{\min} = (50)^2\,\mathrm{MeV}^2$, $y_{\max} = (180)^2\,\mathrm{MeV}^2$. Grid spacing is chosen linearly in $\sqrt{x}$ and linearly in y, respectively. The second configuration works with less points in the y-direction and reduces the numerical effort. It utilizes

$$N_x = 35 \quad , \quad N_y = 10 \quad , \tag{7.12}$$

in a range $x_{\min} = 1\,\mathrm{MeV}^2$, $x_{\max} = (170)^2\,\mathrm{MeV}^2$ and $y_{\min} = (75)^2\,\mathrm{MeV}^2$, $y_{\max} = (155)^2\,\mathrm{MeV}^2$ with the same spacing as before. For $N_f = 2$, the configuration $N = 40$, $\sigma^2_{\min} = 1\,\mathrm{MeV}^2$, $\sigma^2_{\max} = (170)^2\,\mathrm{MeV}^2$ has been chosen with a linear spacing in σ. Note that depending on the context we will denote the grid variable in $N_f = 2$ as σ, glossing over the fact that it is an expectation value. In this work, we use a UV cutoff of $\Lambda = 1\,\mathrm{GeV}$. Appropriate starting values are given in App. D. The solution of the coupled ordinary differential equations that are obtained from the grid ansatz is acquired with the help of a Dormand-Prince solver which is a Runge-Kutta type algorithm [88]. Furthermore, the flow equation is only evaluated up to an IR scale $k_{\mathrm{IR}} = 100\,\mathrm{MeV}$. At this point, the position of the minimum of the potential is expected to be static and independent of k such that further evaluation of the flow does not

change the physics. In sMFA, the integral is evaluated for the full range of possible momenta up to a point where the integrand falls under a predetermined numerical value [e.g. for values lower than $\exp(-30)$]. This is done with a Romberg integration routine. In rMFA, the computation is performed up to $k_{\mathrm{IR}} = 1\,\mathrm{MeV}$ with the same stepper used in the FRG flow. The minimum of the potential is determined by finding the roots of the derivatives of the potential which proofs to be more accurate than a direct minimization. The derivatives are either inferred from the derivatives at the grid points or, in mean field approximation, calculated directly from the integral equation via differentiation, see App. B.

7.2 Calculating the Equation of State

In order to compute the TOV equation, the equation of state (EoS) $p(\varepsilon)$ of matter at low temperature and high density must be known. In this work, we restrict ourselves to the determination of the EoS as generated from the quark-meson model. Despite the fact that it neither incorporates confinement (which gives rise to nucleonic degrees of freedom at finite chemical potential) nor gluon interactions (which should become important in the deconfined region), we believe that the effective interactions of constituent quarks and mesons yields qualitative results. From a phenomenological perspective, the applicability of the quark-meson model should be restricted to the description of quark matter in the inner core. Thus, a quantitative treatment entails the usage of a nucleonic model for the outer parts of the compact object as laid out in Sec. 2. With the study of a two-flavor as well as the 2+1-flavor model, we aim at gaining insights into the impact of the existence of strange quarks on the equation of state. Furthermore, a comparison of the mean field solution with the FRG solution that includes full meson dynamics can give helpful information on the influence of quantum fluctuations in dense matter. To extract the equation of state from the model, it suffices to regard the grand canonical potential density Ω that has been determined in all approximations. We use the thermodynamic relation [72]

$$\Omega = -\frac{1}{\beta V} \ln Z = -p \quad . \tag{7.13}$$

Note that in our approaches Ω is not normalized and can be shifted by a constant without changing the physics. In order to determine the correct pressure, we take into consideration that $\Omega = \Omega(T, \mu)$ is a function of temperature and chemical potential. Then we demand that the vacuum pressure at vanishing temperature and chemical potential p_{vac} is zero. This is done by the constant shift

$$p = \Omega(0,0) - \Omega(T,\mu) \quad . \tag{7.14}$$

On top of that, the definition of the grand canonic potential density is utilized:

$$\Omega(T,\mu) = \varepsilon - Ts - \mu n \quad . \tag{7.15}$$

s denotes the entropy density and n the particle density. In case of the quark-meson model, n is the asymmetric quark density. These two quantities can be inferred from

$$s = -\frac{\partial \Omega}{\partial T} \quad , \quad n = -\frac{\partial \Omega}{\partial \mu} \quad . \tag{7.16}$$

The inverted EoS is thus given by

$$\varepsilon(p) = -p + Ts + \mu n = -p - T\frac{\partial\Omega(T,\mu)}{\partial T} - \mu\frac{\partial\Omega(T,\mu)}{\partial\mu} \quad . \tag{7.17}$$

The derivatives of Ω can either be obtained numerically by slightly shifting T or μ, respectively, or analytically from the relation $\Omega = \tilde{U}(\langle\sigma_d\rangle)$ where $\langle\sigma_d\rangle$, $d \in \{1,\dots,N_f\}$, is the vacuum configuration that minimizes $\tilde{U}$. As a consequence, the derivative with respect to T or μ has to take into account the running minimum as well:

$$\frac{\partial\Omega}{\partial T} = \frac{\partial U(\langle\sigma_d\rangle)}{\partial T} + \sum_{a=1}^{N_f} \frac{\partial\tilde{U}(\sigma_d)}{\partial\sigma_a}\bigg|_{\sigma_d=\langle\sigma_d\rangle} \frac{\mathrm{d}\langle\sigma_a\rangle}{\mathrm{d}T} \quad . \tag{7.18}$$

Luckily, at the minimum the derivative of $\tilde{U}$ in each direction trivially vanishes:

$$\frac{\partial\tilde{U}(\sigma_d)}{\partial\sigma_a}\bigg|_{\sigma_d=\langle\sigma_d\rangle} = 0 \quad \forall a \in \{1,\dots,N_f\} \quad . \tag{7.19}$$

This means that only the explicit T- and μ-dependence of U has to be taken into account (the symmetry breaking terms do not depend on T or μ and vanish). In standard mean field approximation, this yields [cf. Eq. (5.21)]

$$\begin{aligned}\frac{\partial\Omega_q}{\partial T} = -\frac{N_c}{\pi^2}\sum_f \int_0^\infty \mathrm{d}p\, p^2 \{&\ln\left(1+\exp(-(E_f-\mu)/T)\right) + \ln\left(1+\exp(-(E_f+\mu)/T)\right) \\ &+ \frac{1}{T}\left(\frac{E_f-\mu}{1+\exp((E_f-\mu)/T)} + \frac{E_f+\mu}{1+\exp((E_f+\mu)/T)}\right)\} \quad .\end{aligned} \tag{7.20}$$

The derivative with respect to the chemical potential is

$$\frac{\partial\Omega_q}{\partial\mu} = -\frac{N_c}{\pi^2}\sum_f \int_0^\infty \mathrm{d}p\, p^2 \left(n_f - \bar{n}_f\right) \tag{7.21}$$

with $n_f := n_f(E_f,\mu,T)$ and $\bar{n}_f = n_f(E_f,-\mu,T)$ as defined in Eq. (5.17). Here the quark density is just proportional to the integral of quark occupation number minus antiquark occupation number over all spatial momenta. Similarly, the FRG flow equation follows

$$\partial_t\frac{\partial U_k}{\partial T} = \frac{\partial}{\partial T}\partial_t U_k \tag{7.22}$$

with

$$\frac{\partial\Omega}{\partial T} = \frac{\partial U_{k=0}}{\partial T} \tag{7.23}$$

evaluated at the configuration that minimizes $U_{k=0}$. Analog relations hold for the derivative with respect to the chemical potential. In the renormalized mean field approximation the integration of the flow yields for the temperature derivative of the quark potential

$$\frac{\partial\Omega_q}{\partial T} = -\frac{N_c}{6\pi^2}\sum_f \int_0^\Lambda \mathrm{d}k\, \frac{k^4}{2T^2E_f}\left[\frac{E_f-\mu}{\cosh^2\left(\frac{E_f-\mu}{2T}\right)} + \frac{E_f+\mu}{\cosh^2\left(\frac{E_f+\mu}{2T}\right)}\right] \tag{7.24}$$

and for the derivative with respect to μ:

$$\frac{\partial \Omega_q}{\partial \mu} = -\frac{N_c}{6\pi^2} \sum_f \int_0^\Lambda \mathrm{d}k \, \frac{k^4}{2TE_f} \left[\frac{1}{\cosh^2\left(\frac{E_f-\mu}{2T}\right)} - \frac{1}{\cosh^2\left(\frac{E_f+\mu}{2T}\right)} \right] \quad . \tag{7.25}$$

The meson potentials are static and independent of T and μ, hence the full entropy and particle density in mean field are the respective expressions multiplied by -1. The flow equations for the derivatives of the effective potential in the full functional renormalization group approach read

$$\partial_t \frac{\partial U_k}{\partial T} = \frac{k^5}{12\pi^2} \left\{ \sum_b \frac{1}{2T^2} \frac{1}{\sinh^2\left(\frac{E_b}{2T}\right)} - \left[\frac{1}{2T} \frac{1}{\sinh^2\left(\frac{E_b}{2T}\right)} + \frac{1}{E_b} \coth\left(\frac{E_b}{2T}\right) \right] \frac{1}{2E_b^2} \frac{\partial m_b^2}{\partial T} \right.$$
$$\left. + 2N_c \sum_f \frac{1}{2E_f T^2} \left[\frac{E_f - \mu}{\cosh^2\left(\frac{E_f-\mu}{2T}\right)} + \frac{E_f + \mu}{\cosh^2\left(\frac{E_f+\mu}{2T}\right)} \right] \right\} \tag{7.26}$$

and

$$\partial_t \frac{\partial U_k}{\partial \mu} = -\frac{k^5}{12\pi^2} \left\{ \sum_b \left[\frac{1}{E_b} \coth\left(\frac{E_b}{2T}\right) + \frac{1}{2T} \frac{1}{\sinh^2\left(\frac{E_b}{2T}\right)} \right] \frac{1}{2E_b^2} \frac{\partial m_b^2}{\partial \mu} \right.$$
$$\left. + 2N_c \sum_f \frac{1}{2TE_f} \left[-\frac{1}{\coth^2\left(\frac{E_f-\mu}{2T}\right)} + \frac{1}{\coth^2\left(\frac{E_f+\mu}{2T}\right)} \right] \right\} \quad . \tag{7.27}$$

Because of the meson sector that introduces back-coupling via the second derivatives of U_k in the meson masses m_b^2, the dependence of those masses on T and μ must be taken into account, e.g. via

$$\frac{\partial m_b^2}{\partial T} = \frac{\partial \tilde{U}^{(2)}_{k,bb}}{\partial T} = \left(\frac{\partial U_k}{\partial T} \right)^{(2)}_{bb} \quad . \tag{7.28}$$

The last step follows since the partial derivative does not touch the fields and the explicit breaking terms in $\tilde{U}_k$ do not run with T or μ. As explained in App. C and the previous section, the second derivatives with respect to the fields are determined directly from the potential U_k in the numerical setup, in which case this is equivalent to

$$\frac{\partial m_b^2}{\partial T} = \frac{\partial m_b^2}{\partial U_k} \frac{\partial U_k}{\partial T} \quad . \tag{7.29}$$

Many of the given expressions do not have a trivial limit for $T \to 0$. Nevertheless, smooth limits must exist for observable quantities and thermodynamic potentials. Especially, the entropy density should go to zero at vanishing temperature. All analytic limits of the given (and some additional) expressions can be found in App. B. In the FRG approach, the additional flow equations for s and n given here are numerically solved simultaneously with the flow equation for the potential (as they require the derivatives of the potential at each grid point as well and therefore couple to the original flow equation). In other words, there are now three ordinary differential equations per grid point, i.e. $3N$ equations for $N_f = 2$ and $3N_xN_y$ coupled equations for $N_f = 2 + 1$.

7.3 Solving the Tolman-Oppenheimer-Volkoff Equation

The TOV equation setup consists of the two coupled ordinary differential equations given in Eq. (2.28). The equation of state in its inverted form, $\varepsilon(p)$, is given discretely through the computation in the quark-meson model as described in the previous section. Both ε and p are calculated for a series of chemical potentials and the discrete points are connected via a linear interpolation. Note that one could just as well use a smooth cubic spline interpolation, but the great number of computed points should allow a connection of the points by straight lines. This also has the advantage that the first order chiral phase transition, which is signified by a jump in energy density, is not washed out as much. The differential equations are then solved by the Dormand-Prince stepper for various central pressures p_0 with $m(0) = 0$. In order to obtain physical results, we restore factors of c^2 such that the TOV equation reads

$$\begin{aligned} \frac{\mathrm{d}p(r)}{\mathrm{d}r} &= -\frac{G}{c^2}\frac{(\varepsilon(r)+p(r))\left[m(r)+4\pi r^3 p(r)/c^2\right]}{r\left[r-2Gm(r)/c^2\right]} \quad , \\ \frac{\mathrm{d}m(r)}{\mathrm{d}r} &= 4\pi r^2 \varepsilon(r)/c^2 \quad . \end{aligned} \tag{7.30}$$

We work in cgs units

$$[G] = \frac{\mathrm{cm}^3}{\mathrm{g}\cdot\mathrm{s}^2} \quad , \quad [c] = \frac{\mathrm{cm}}{\mathrm{s}} \quad . \tag{7.31}$$

r is inserted in cm, m in g, ε and p are inserted in erg/cm^3 where

$$1\,\mathrm{erg} = 1\,\frac{\mathrm{g}\cdot\mathrm{cm}^2}{\mathrm{s}^2} \quad . \tag{7.32}$$

From the calculation of the equation of state in natural units, pressure and energy density are given in MeV^4 which can be converted (by multiplying factors of $\bar{h}$ and c) with

$$1\,\mathrm{MeV}^4 \mathrel{\widehat{=}} 2.085\times 10^{26}\,\frac{\mathrm{erg}}{\mathrm{cm}^3} \quad . \tag{7.33}$$

In this setup, the three constants in use are

$$G = 6.6732\times 10^{-8}\,\frac{\mathrm{cm}^3}{\mathrm{g}\cdot\mathrm{s}^2} \quad , \quad c = 2.9979\times 10^{10}\,\frac{\mathrm{cm}}{\mathrm{s}} \quad , \quad M_\odot = 1.987\times 10^{33}\,\mathrm{g} \quad . \tag{7.34}$$

The results are then converted to suitable units, e.g. km for radii and MeV/fm^3 for pressures and energy densities. The TOV equation is evaluated until p hits a small minimum pressure p_{min}. On the one hand, this small absolute value helps to constrain neutron star radii as the pressure usually tends to decay very slowly and never completely hits the $p = 0$ line. On the other hand, it could be observed from the equations of state of the quark-meson model that the calculated pressure first dips into negative values, after which it increases with increasing ε. This very small regime of negative pressures which occurs close to the first-order phase transition could be a numerical error or a peculiarity of the model. Nevertheless, the absolute value of the negative pressure stays of order $\lesssim 0.1\,\mathrm{MeV/fm}^3$. Consequently, we choose $p_{\mathrm{min}} = 0.1\,\mathrm{MeV/fm}^3$ in order to always deal with positive pressures at a level above the order of uncertainty. This choice also limits the central pressures to values of $10\,\mathrm{MeV/fm}^3$ and above such that the pressure at which the evaluation of the TOV equation is stopped is always less than 1% of p_0 and the compact object can be assumed to be largely integrated out.

8 Numerical Results

With the necessary tools at hand, the dynamics of the quark-meson model can now be studied numerically. Specifically, the impact of mesonic quantum fluctuations becomes evident from a comparison between mean field and FRG results. Furthermore, the role of strangeness in the thermodynamics of the theory can be inferred since both $N_f = 2$ and $N_f = 2 + 1$ calculations are presented. After an initial study of the order parameters of the model, we focus on fluctuations at low T and high μ. The equation of state in that regime of the phase diagram is utilized in the TOV equation to yield mass-radius relationships for neutron stars.

8.1 Chiral Condensates

As shown in the previous sections, non-vanishing vacuum meson condensates correspond to a non-trivial minimum of the effective potential which breaks chiral symmetry and renders the constituent quarks massive. Therefore, they are order parameters for chiral symmetry breaking. At vanishing temperature and chemical potential, chiral symmetry is spontaneously broken and the parameters of the theory have been fixed to yield physical values for σ_l and σ_s, cf. App. D. As shown in Fig. 3, at increasing temperature the condensates decay and chiral symmetry is restored. This behavior is most prominent in the light sector, while the strange condensate only decays slowly. Due to explicit symmetry breaking, the condensates do not vanish at finite T but asymptotically go to zero. In mean field as well as FRG calculations, the phase transition is a smooth crossover. Without explicit symmetry breaking (chiral limit), this would become a second-order phase transition.

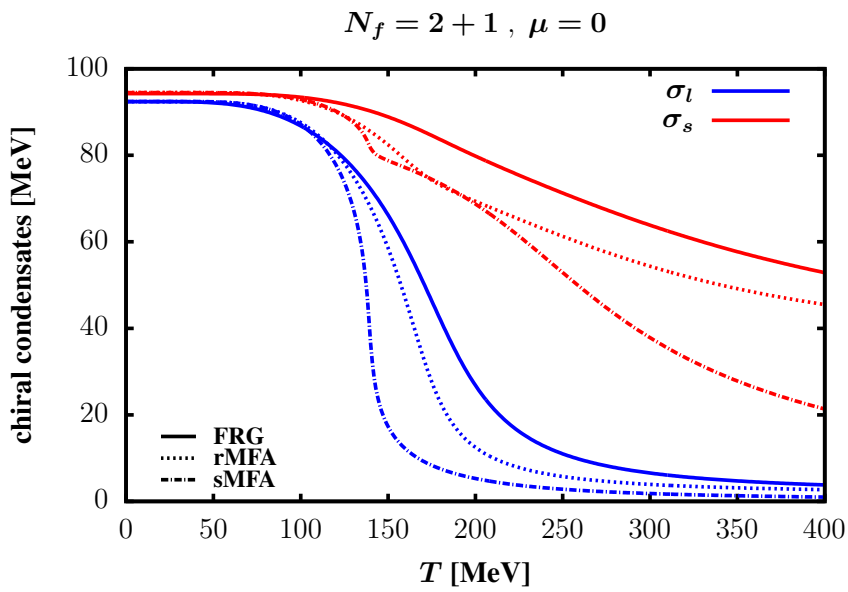

Figure 3: Light and strange condensates in 2+1 flavors at vanishing chemical potential.

While the qualitative behavior is similar for all solution schemes employed in this work, there are significant quantitative differences between standard mean field, renormalized mean field, and FRG solutions. The difference between the sMFA and rMFA approach

can generally be attributed to the inclusion of the vacuum term in rMFA, in this case its implicit temperature dependence. This holds up to the point where UV cutoff effects play a role in rMFA. This happens because we defined the rMFA approach based on the fermionic part of the FRG flow. This flow equation comes with a UV cutoff Λ and as soon as T or μ come close to the cutoff in order of magnitude, the UV potential should become dependent on T or μ. Neglecting this dependence causes regulator-dependent cutoff effects at the IR scale [83] and both rMFA and FRG are expected to suffer from this phenomenon, especially since this work considers chemical potentials up to $\mu = 500\,\text{MeV}$ with a UV cutoff of only $1\,\text{GeV}$. Since in the LPA truncation the fermionic part of the effective actions does not have a running coupling and all quantum fluctuations are encoded in the meson potential, it should be expected that one can relate the FRG scale k to the momentum variable p in the sMFA integral [cf. Eq. (5.21)] and safely push the rMFA UV cutoff to higher values. Taking the same cutoff as the FRG approach, however, allows us to directly attribute any differences between rMFA and FRG solutions to mesonic fluctuations which are neglected in the mean field approximation.

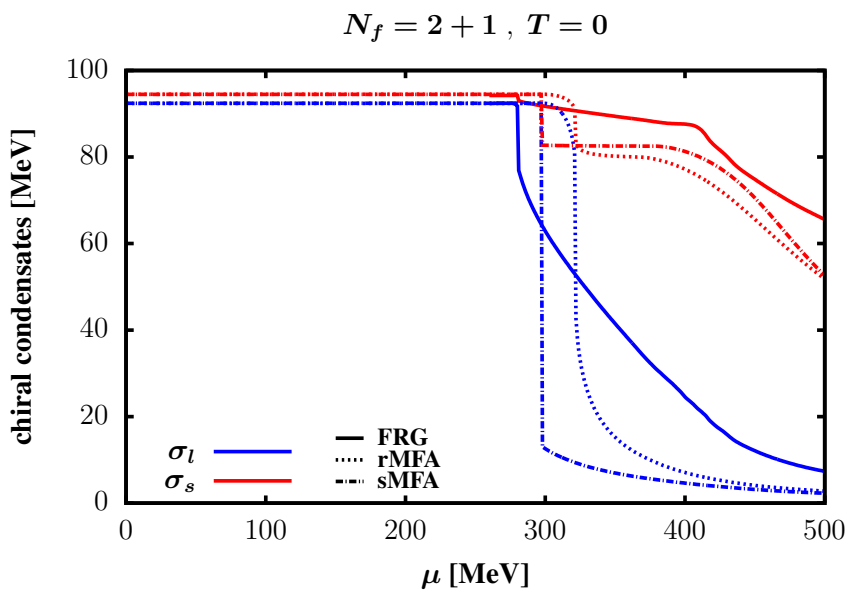

Figure 4: Light and strange condensates in 2+1 flavors at vanishing temperature.

Fig. 4 depicts the light and strange condensates at vanishing temperature up to a chemical potential of 500 MeV. As expected, the condensates stay constant until the chemical potential hits the order of the light quark mass of $m_l = 300\,\text{MeV}$. Note that the Silver Blaze rule forbids a smooth change in the vacuum of the theory until μ hits m_l, thus only a sudden first-order transition (to a new vacuum) is possible for $\mu < m_l$. Hence, only the rMFA solution where the transition happens at $\mu > m_l$ exhibits a smooth decay of the condensate before the first order jump. Since all approaches show a clear first-order transition at vanishing T, but a crossover transition at vanishing μ, the existence of a critical endpoint in the phase diagram is always implied. The exact position of this endpoint has been found to depend on the fitted sigma mass in mean field approximation [70]. The proximity of the critical endpoint (CEP) to the $T = 0$ line in the phase diagram is usually related to the magnitude of the first-order jump

and the critical chemical potential thereby depends on it as well. Specifically, the very large jump in the light condensate in sMFA indicates that the transition is still far from a crossover transition and the CEP is at high T, while the small jump in the FRG solution suggests a CEP at low T. It can also be observed in Fig. 4 that the first order transition in the light chiral condensate also slightly modifies the strange condensate, after which the latter stays on an almost constant plateau in all solution schemes. At $\mu \sim 400\,\text{MeV}$, the strange condensate starts dropping off smoothly which can be interpreted as a second, smooth (chiral) phase transition in the strange sector. This also shows in a comparison of the light condensate in 2+1 flavors with the only condensate of the two-flavor model as depicted in Fig. 5. In the FRG solution, the 2+1-flavor light condensate starts deviating from the two-flavor condensate at the exact same scale of above $\sim 400\,\text{MeV}$ where the strange condensate begins to undergo a smooth decay. This might be the case in the rMFA and sMFA solutions, too, but the light condensate is already too low to display that kind of behavior.

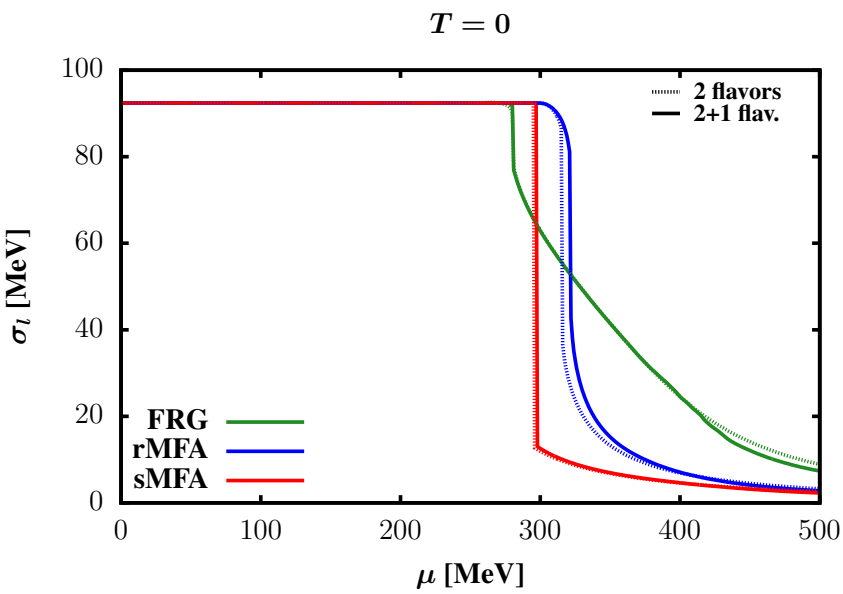

Figure 5: Light condensate in two and 2+1 flavors at vanishing temperature.

8.2 Meson Masses

Since the (inverse) meson energies give essential contributions to the FRG flow equation, it makes sense to study the meson masses in the thermodynamic regime of interest, i.e. at $T = 0$ and high chemical potential. Fig. 6 displays all non-degenerate meson masses at $N_f = 2 + 1$. Again, the qualitative behavior is already captured by the mean field solutions concerning e.g. the jumps in the meson masses at the first-order transition. The most interesting masses are those of the scalar flavor-diagonal mesons σ and f_0. Note that there is light-strange flavor mixing both in the diagonal scalar and pseudoscalar sector. Furthermore, the scalar flavor-diagonal masses are the only ones that generally depend on the second and mixed derivatives with respect to the grid variables, because they are a mixture of the only mesons that do not vanish at the VEV, σ_l and σ_s (c.f. App. C). During the evolution of the FRG flow, σ and f_0

are experienced to render the meson energies very close to zero at some points on the grid for high μ (in contrast to the pion poles that also occur at high T) . They vastly contribute to the instability of the flow equation at low T and high μ. This can be observed in the oscillatory behavior of the f_0 mass when it dips to lower values around $\mu \sim 400\,\text{MeV}$. Interestingly, the mean field solutions experience a sudden drop in the f_0 mass, too, but well before the chemical potential where the strange condensate starts melting down. Another peculiar feature of sMFA is that the σ and f_0 meson seem to switch places at $\mu \approx 430\,\text{MeV}$. The σ meson mass continues the original path of the f_0 meson mass and the f_0 meson mass extends the path of the original σ meson mass.

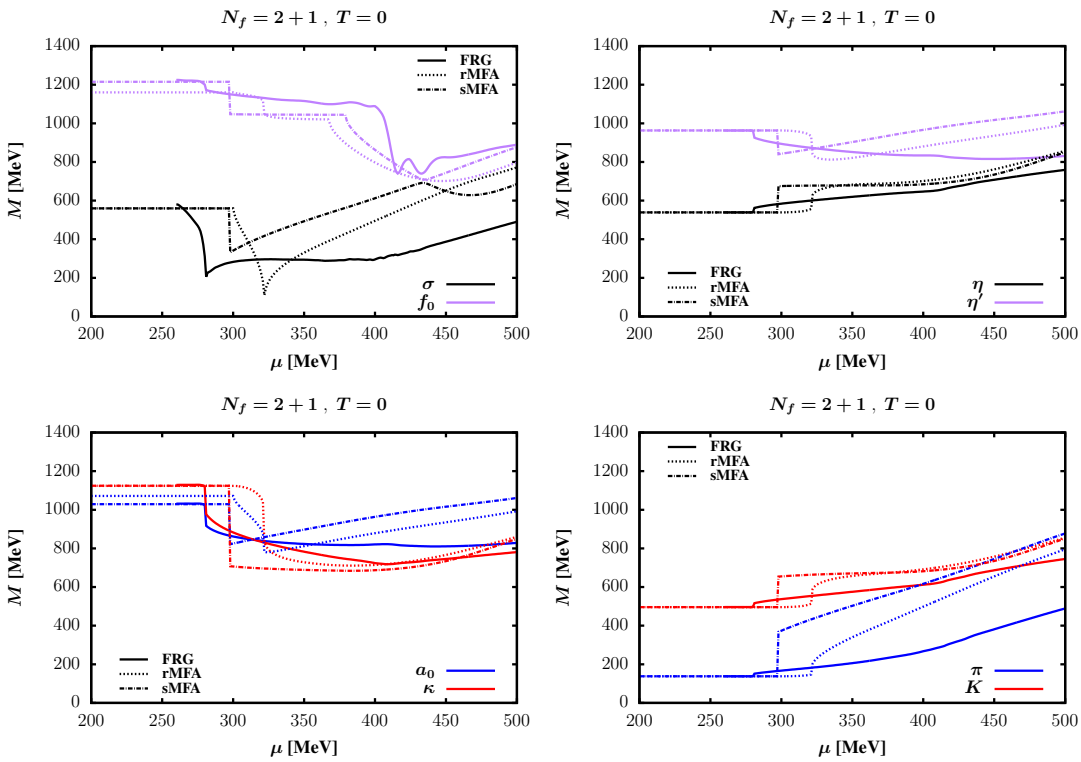

Figure 6: 2+1 flavor meson masses as a function of μ at $T = 0$. Top left: scalar singlets σ, f_0. Top right: pseudoscalar singlets η, η'. Bottom left: scalar flavor off-diagonal states a_0, κ. Bottom right: pseudoscalar states π, K.

This idea is confirmed by Fig. 7 which compares the sigma and pion masses of the two-flavor and 2+1-flavor models. The sMFA solution experiences a sudden strong deviation of the sigma mass in 2+1 flavors from the two-flavor mass at the chemical potential mentioned before. Aside from this, all calculations show a slight deviation of the masses in both models beginning at some chemical potential above 400 MeV, respectively. This can probably be attributed to the second chiral phase transition in the strange sector which already shifted the condensates at that scale. The deviations in the sigma and pion masses in rMFA at the first-order transition should be related to the shift of the first-order line from two to 2+1 flavors which can be observed in Fig. 5. In the FRG case, Fig. 7 shows a different oscillatory behavior for the sigma mass when comparing the two- and 2+1-flavor results close to the first-order jump. In both $N_f = 2$ and $N_f = 2+1$, the sigma mass first increases before dipping to $M_\sigma \approx 200\,\text{MeV}$. This initial increase before the first-order transition is unphysical and can be explained

with the grid setup. Because at $T = 0$ the threshold function of the fermionic sector of the flow equation becomes a theta function, cf. App. B, the fermionic flow becomes zero for $\sqrt{k^2 + m_l^2} < \mu$ or $\sqrt{k^2 + m_s^2} < \mu$, respectively. Of course, for a fixed μ this happens at higher k for grid points at low values of σ_l and σ_s (as m_l and m_s are proportional to the condensates). Hence, the potential already changes its shape "left" of the vacuum configuration at increasing μ (as more and more points stop running at some k) while the minimum still lies stable at the constant vacuum condensate. The spline interpolation now takes into account all grid points, also those with lower masses than the the vacuum configuration, and yields a different second derivative at e.g. $\mu = 250\,\text{MeV}$ than at $\mu = 0$ while the minimum is still in the right place. The second derivative, however, influences the sigma mass and already modifies it before the first-order transition. In other words, this effect is an artifact of the spline interpolation because contributions of a local analytic cutoff from the theta function are smeared out by an interpolation on a finite number of points. The difference between the two-flavor and 2+1-flavor oscillations then lies in the different grid setups, i.e. $N = 40$ grid points are used in two flavors while $N_x = 35$ grid points in the light direction are utilized in the 2+1-flavor case.

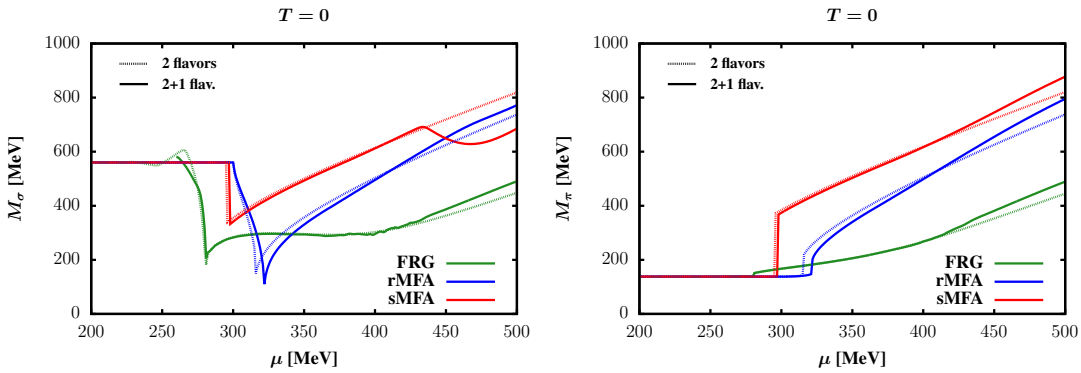

Figure 7: Light meson masses as a function of μ at $T = 0$ for $N_f = 2$ and $N_f = 2 + 1$. Left panel: σ meson. Right panel: π.

8.3 Influence of Grid Configuration

While we can assume that the small overshooting of the sigma mass at μ close to the first-order phase transition only has a negligible effect and the 35 and 40 grid points, respectively, give a good interpolation of the potential, the situation looks different for the f_0 mass in 2+1 flavors. As the heavier meson, it has the higher portion of strangeness. The strange condensate is encoded in the y-direction on the grid, consequently one might expect a dependence of the f_0 mass on the number of grid points in y-direction N_y. Indeed, Fig. 8 shows that from the point where the strange condensate begins to melt, $\mu \gtrsim 400\,\text{MeV}$, there is also a strong oscillatory behavior in the f_0 mass that heavily depends on N_y. The single sharp dip the f_0 mass exhibits in the $N_y = 10$ configuration is reminiscent of the behavior of the sigma mass at the light chiral phase transition and one might tend to give that configuration more credit. However, a study of both configurations at higher temperatures seems to indicate that the $N_y = 20$ configuration with two equal minima is closer to the truth. On top of that, more grid

points should lead to better accuracy (at least with the low number of points given here) and the $N_y = 20$ curve gives a more stable impression. Unfortunately, numerical difficulties are encountered at chemical potentials close to the first-order transition in this configuration as soon as the T- and μ-derivatives of the effective potential are put onto the grid as well. Due to the high numerical effort in this case, the $N_y = 10$ configuration had to be utilized for all computations that include entropy and particle density. Concerning the influence of the grid configuration on the physical results, we will see that the meltdown of the strange condensate significantly reduces the stiffness of the equation of state in the 2+1-flavor FRG approach. Hence, stable neutron stars lie at $\mu \lesssim 400\,\text{MeV}$ where both grid configurations yield stable results.

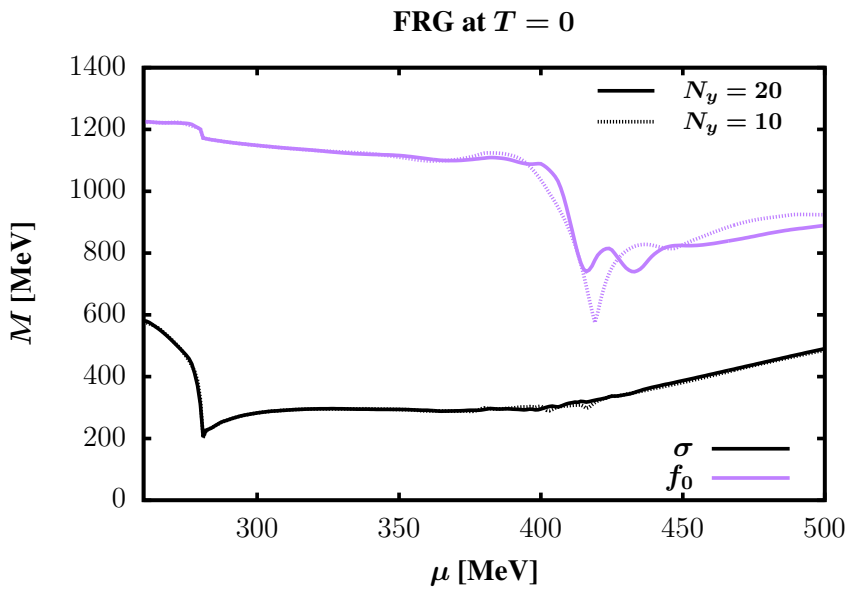

Figure 8: Flavor diagonal scalar mesons σ, f_0 in FRG as a function of μ at $T = 0$. Shown are two different grid configurations with $N_y = 10$ and $N_y = 20$, where N_y denotes the number of grid points in y-direction.

8.4 Phase Diagram

The quark-meson model exhibits two phases, a phase of spontaneously broken chiral symmetry at low energies and a chirally restored phase at high energies. The transition lines are depicted in the phase diagram, Fig. 9. The given phase diagram of the two-flavor model shows that both mean field and FRG calculations feature a smooth crossover transition at low chemical potential and high temperature. This result is in agreement with lattice QCD calculations as mentioned in Sec. 3. At low temperature and high chemical potential, mean field and FRG results agree on a first-order transition to chirally symmetric matter. The end of the first-order line is marked by a critical endpoint. As discussed before, the existence and position of such a point in the phase diagram of quantum chromodynamics is still under investigation. Note that the crossover line is determined by the inflation point of the light condensate of the explicitly broken model. This point is not as strongly determined as the first-order jump, i.e. the exact trajectory of the crossover line depends on the direction in the

T-μ-plane that is taken in the computation of the diagram. In this work, we determined the inflation point by going radially outwards from the origin of the T-μ-plane. The phase diagram can be used to give us a better idea of the role of quantum fluctuations on the thermodynamics of the theory. In sMFA, the first order region is very large, in rMFA the CEP is significantly closer to the $T = 0$ axis. In FRG, the CEP goes to even lower temperatures, which agrees with our findings from the magnitude of the first-order jump in Fig. 4. The vacuum fluctuations already significantly modify the phase diagram, while the meson fluctuations give another important contribution. On top of the new position of the CEP, we see in Fig. 9 that the FRG curve exhibits a back-bending behavior at low T, whereas the mean field results show a curve that hits the μ axis at a 90 degree angle as expected. This back-bending behavior is actually unphysical, as it implies a negative entropy density (for positive particle density) via the Clausius-Clapeyron relation [89]

$$\frac{\mathrm{d}T_c}{\mathrm{d}\mu_c} = -\frac{\Delta n}{\Delta s} \quad . \tag{8.1}$$

The observation of negative entropy densities will be explicitly confirmed and discussed in the next section.

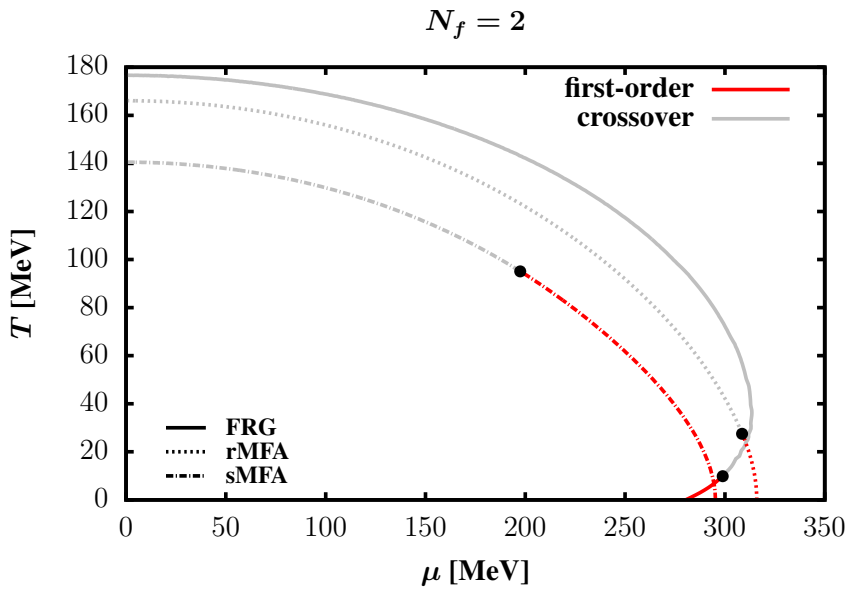

Figure 9: Phase diagram of the two-flavor quark-meson model. Shown are the FRG, rMFA, and sMFA solution which each exhibit a first-order and a crossover region. The critical endpoints (CEPs) are marked with black dots.

As this work also studies the role of strangeness at high densities, next to the impact of mesonic and vacuum fluctuations, we compare the FRG transition lines of the two-flavor and the 2+1-flavor model in Fig. 10. On the one hand, including strange mesons results in a crossover line that bends more strongly to lower temperatures. On the other hand, the position of the critical endpoint and the first-order line stays fixed. Thus, strange quarks and mesons do not have an impact on the position of the phase transition at low T and high μ. This, however, does not mean that they do not have an impact on the equation of state. After all, the strange mesons are additional summands

in the flow equation that directly determines the pressure of the system and, via its T and μ derivatives, the entropy and quark density as well.

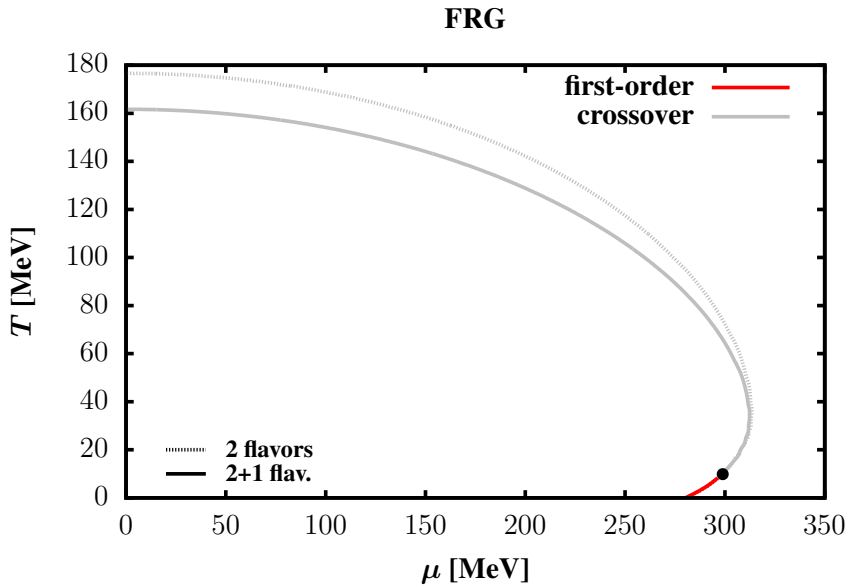

Figure 10: Phase diagram of the two-flavor and the 2+1-flavor quark-meson model in FRG. The (common) critical endpoint is marked with a black dot.

8.5 Thermodynamic Properties

In order to determine the influence of (strangeness) fluctuations on the equation of state, we calculate the pressure, energy density, entropy density, and particle density as laid out in Sec. 7.2. The entropy and particle density are determined from their analytic flow equations which are solved on the grid simultaneously to the solution of the effective potential. For $N_f = 2$ and vanishing temperature, all quantities are given (in scaled form) in Fig. 11. Due to vanishing temperature, the entropy density is always zero. The thermodynamic relation for the energy density degenerates to

$$\varepsilon = \mu n - p \quad . \tag{8.2}$$

This is reflected in Fig. 11 where the scaled pressure matches the gap between the scaled energy and particle density. Up to the first-order transition, all properties are those of the $T = 0$, $\mu = 0$ vacuum which can be understood in the way that the chemical potential is smaller than the light quark mass of the respective vacuum state and no net quark density can be achieved. After the transition, the particle density in standard mean field approximation immediately exhibits constant scaling $n \sim \mu^3$. In renormalized mean field approximation, n also quickly converges to the same scaling behavior and even displays the same scaling constant. This is no surprise because at $T = 0$ the expressions for the particle density in rMFA and sMFA both degenerate to the same term as shown in Eq. (B.13) and (B.12). From the given expression, an asymptotic scaling factor of $2/\pi^2 \approx 0.2$ for $N_f = 2$ immediately follows. In the FRG approach, n seems to asymptotically converge to the $\sim \mu^3$ scaling behavior as well. This should be expected for high μ from dimensional analysis, but for the given range

of chemical potentials in this work we observe significant differences as compared to the mean field solutions. These differences are due to meson fluctuations which means those contributions are expected to have an impact on the properties of compact objects.

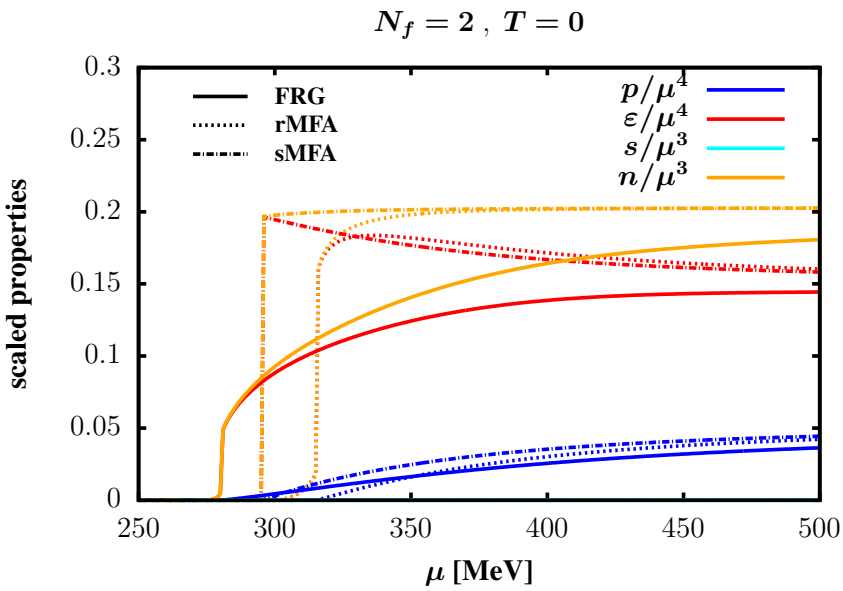

Figure 11: Pressure p, energy density ε, entropy density s, and particle density n of the two-flavor QM model at $T = 0$, scaled by powers of μ to make them dimensionless. Solutions are given for FRG, rMFA, and sMFA.

Contributions from non-zero entropy can only be observed at finite temperature. Consequently, we repeat the analysis at a constant, low temperature. All scaled properties for $N_f = 2$ and $T = 5\,\text{MeV}$ are displayed in Fig. 12. In terms of pressure, energy density, and particle density, there are no significant differences to the $T = 0$ case, as expected. While in sMFA and rMFA, a small positive entropy density emerges, we find a large negative entropy density in the full FRG solution. We have already followed a negative entropy density from the back-bending behavior of the FRG transition line in the phase diagram. We can now observe that s stays negative up to high chemical potentials, while it seems to asymptotically vanish. Unfortunately, it has not been possible to go to much higher μ due to numerical difficulties, but at a UV cutoff of 1 GeV cutoff effects should dominate the behavior at some point in any case. This unphysical peculiarity of the low-temperature dynamics of the quark-meson model has only recently been described in Ref. [89]. Multiple reasons for the negative entropy density are currently under discussion. Reminding ourselves that in the derivation of an effective low-energy description of QCD (cf. Sec. 3) we dropped the diquark interaction terms, it could well be that Cooper pairs that lead to color superconductivity should form already from the fermion interactions at the Fermi surface in the quark-meson model [89]. Disallowing a diquark condensate thus pushes the theory into the wrong vacuum state. Another possibility is the emergence of inhomogeneous phases. Again, we only allow for a certain vacuum configuration, i.e. a spatially homogeneous chiral condensate. Removing the condition of spatial homogeneity would allow the formation of complex structures at high density and low temperature, but requires new solution techniques and high numerical effort [89]. Next to the possibility of an unphysical vac-

uum, the errors that are induced by the lowest order truncation (LPA) of the derivative expansion of the effective action (cf. Sec. 6) could also play a role.

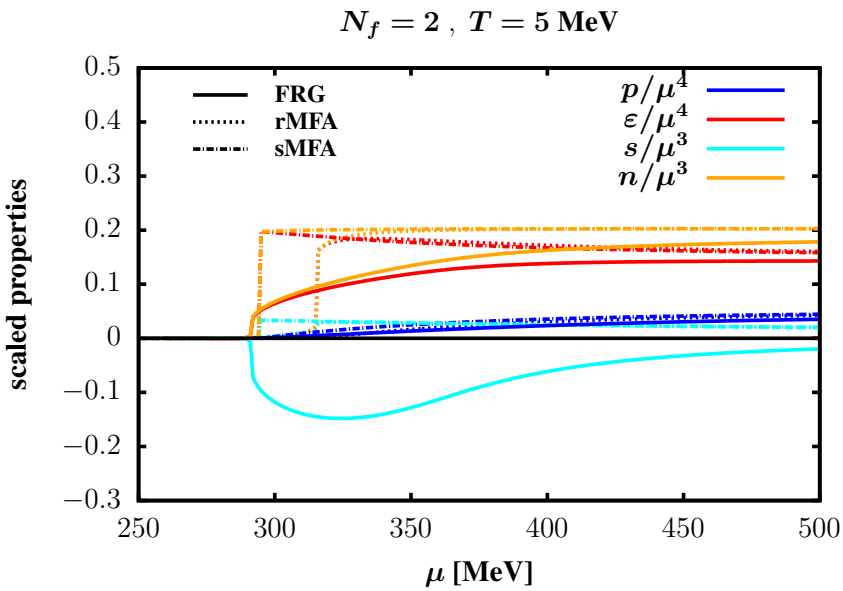

Figure 12: Pressure p, energy density ε, entropy density s, and particle density n of the two-flavor QM model at $T = 5\,\text{MeV}$, scaled by powers of μ to make them dimensionless. Solutions are given for FRG, rMFA, and sMFA.

To study the effects of the inclusion of strange quarks and the behavior of the entropy at different temperatures at the same time, we plot the scaled versions of p, ε, s, and n at $T = 1\,\text{MeV}$ for $N_f = 2 + 1$ in Fig. 13. In mean field approximation, the particle density again rises to the constant scaling with a factor of ≈ 0.2 up to a chemical potential of about 400 MeV. Then it slowly increases and will eventually scale with the $N_f = 3$ factor of $3/\pi^2 \approx 0.3$. Because the strange condensate melts down much more slowly, however, m_s stays finite even for high μ and the scaling factor is not reached in the given range of chemical potentials. In the FRG solution, the picture is slightly different. Here, the onset of the meltdown of the strange condensate is more sudden and causes a kink in the curves for s, n, and ε. Interestingly, this happens at $\mu \approx 420\,\text{MeV}$. In the vacuum, the mass of the strange constituent quarks is fixed to

$$m_s = \frac{g\langle\sigma_s\rangle}{\sqrt{2}} \approx 430\,\text{MeV} \tag{8.3}$$

with the parameters given in App. D. The difference of about 10 MeV between the onset of the phase transition in the strange sector and the vacuum mass of the strange quarks is explained by Fig. 4. At the first-order transition of the light condensate, the strange condensate already jumps to a slightly lower value. Hence, the onset of a second, smooth chiral transition happens at the scale of the strange quark mass. Concerning the entropy density in Fig. 13, it assumes a very small positive value in sMFA and rMFA, which is expected at $T = 1\,\text{MeV}$. The absolute value of the negative entropy of the FRG solution has increased compared to the solution at $T = 5\,\text{MeV}$. Note that before the kink, the two-flavor and 2+1-flavor models should allow for this comparison. After the onset of the effects of strangeness, the entropy density does not fall off smoothly as it does in Fig. 12.

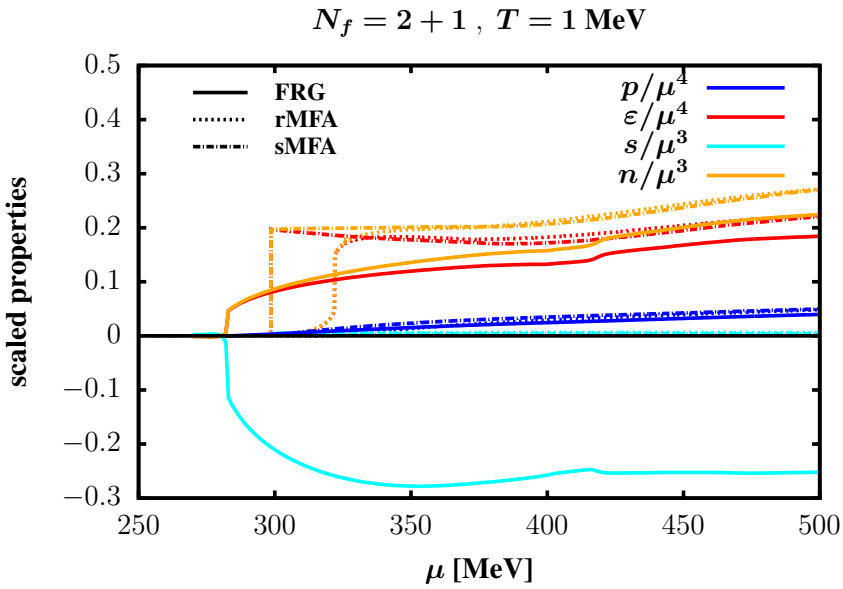

Figure 13: Pressure p, energy density ε, entropy density s, and particle density n of the 2+1-flavor QM model at $T = 1\,\text{MeV}$, scaled by powers of μ to make them dimensionless. Solutions are given for FRG, rMFA, and sMFA.

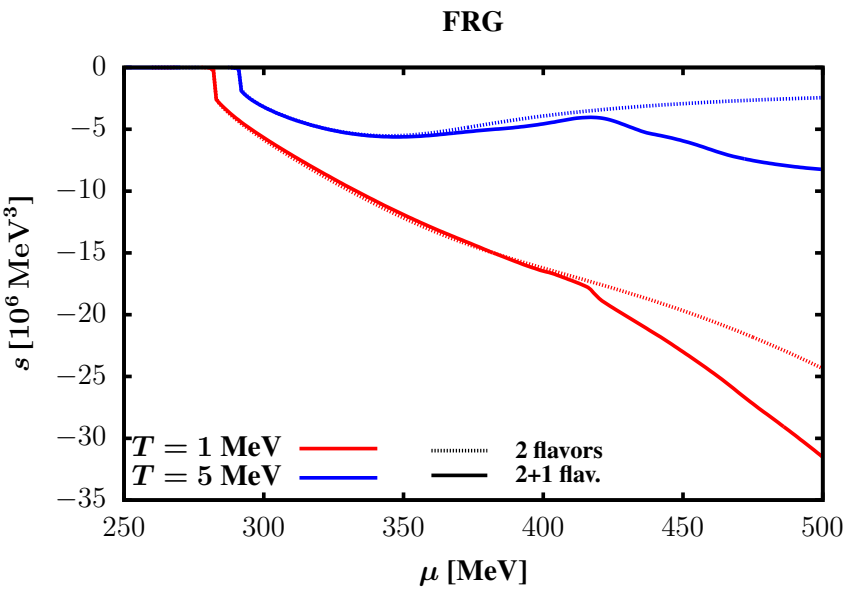

Figure 14: Entropy density as a function of μ in units of $10^6\,\text{MeV}^3$. Shown are $T = 1\,\text{MeV}$ and $T = 5\,\text{MeV}$ results in two and 2+1 flavors.

A more direct comparison of s in two and 2+1 flavors at $T = 1\,\text{MeV}$ and $T = 5\,\text{MeV}$ is given in Fig. 14. Here, it becomes clear that at very low temperatures the absolute value of the entropy density does not decrease, but even increases with higher chemical potentials. This also occurs in the two-flavor model that shows a slowly vanishing s at $T = 5\,\text{MeV}$. In total, this suggests that in the phase diagram at low T the region

of negative entropy is not bounded from the right. Furthermore, the meltdown of the strange condensate and the consequential emergence of additional light (strange) mesons significantly push the entropy to even more negative values. Note that the contribution of the entropy to the equation of state is very small at these temperatures, because s goes in multiplied by T, whereas n is multiplied by the much larger chemical potential. Thus, the unphysical negative entropy contributions to the equation of state of compact objects at almost zero temperature are expected to be negligible.

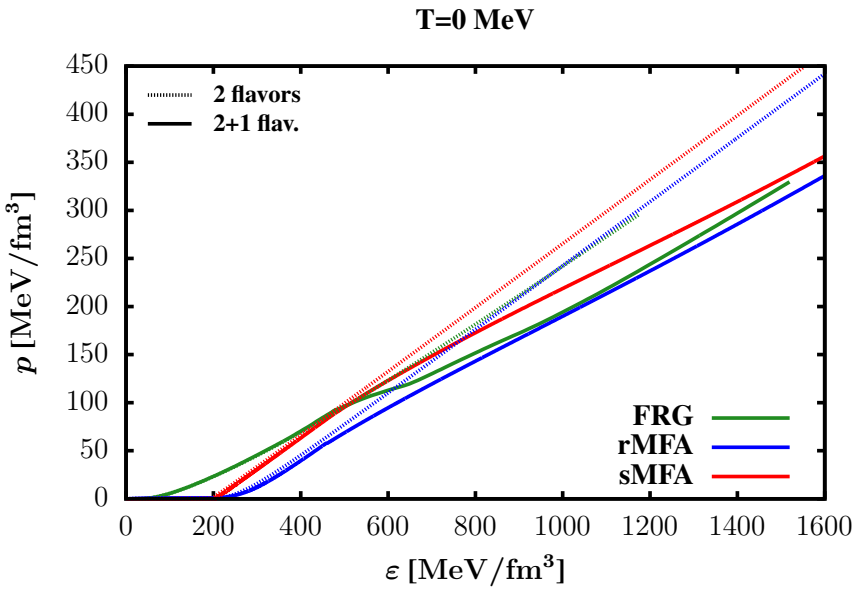

Figure 15: Equations of state of the two- and 2+1-flavor QM models at $T = 0$ in FRG, rMFA, and sMFA.

With the particle and entropy density as well as the pressure at hand, the energy density ε can be calculated according to Eq. (7.17). Taking the pressure as a function of ε, we have found the equation of state. For $T = 0$, it is shown for all solution schemes in Fig. 15. In general, it can be observed that for high ε the two-flavor and the 2+1-flavor EoS split up. The two-flavor equations keep up their original slope while the effective theory with strange degrees of freedom assumes a lower slope. While this happens gradually in sMFA and rMFA, the 2+1-flavor FRG curve stays on top of the two-flavor curve up to pressures $p \lesssim 100\,\mathrm{MeV/fm^3}$. Then, the 2+1-flavor curve deviates and becomes quite flat, after which it assumes a slope comparable to the mean field 2+1-flavor equations of state. Clearly, this behavior can be associated with the onset of effects from the second phase transition and meltdown of the strange condensate which has previously been observed to happen more gradually in mean field calculations and more rapidly in FRG calculations. Regarding the low pressure region, is is found that the sMFA curve hits the $p = 0$ axis in a straight line whereas the rMFA curve features a more gradual onset of pressure. This is directly related to the fact that in sMFA the light condensate immediately jumps to a new vacuum state in a strong first-order transition, cf. Fig. 4. Hence, there are no non-zero data points from the chirally broken regime and after the transition the vacuum state only weakly shifts to lower σ_l at increasing μ. In rMFA, the condensate first continuously melts down and yields data points with low values for p and ε before the first-order phase transition occurs. In the EoS, such a phase transition

manifests itself by a jump in energy density at constant pressure. Note that this jump is not visible in Fig. 15 because it happens at very low pressures. The more gradual onset that is visible is rather related to the smooth decay of the light condensate in the chirally symmetric regime after the first-order transition. As the phase transition is not as strong as the on in sMFA, it leaves σ_l at a higher value (which initially yields lower pressures at a given ε as compared to sMFA results) and the condensate decays more slowly. Of course, the first-order transition is even weaker in FRG, which is why its equation of state features a very early and gradual onset of pressure. Up to the scale where the strange condensate begins to melt, $p \approx 100\,\mathrm{MeV/fm^3}$, the FRG curve is dominated by the almost constant decay rate of the light condensate after the chiral phase transition as displayed in Fig. 5. Regarding the stiffness of the equations of state, it is clear that in mean field approximation the 2+1-flavor curves are less stiff than the two-flavor EoS. Furthermore, the rMFA curve is less stiff than the sMFA curve even though at high energies, they attain the same slope which is very well visible in parallel two-flavor curves. In the functional renormalization group approach, the 2+1-flavor curve only loses stiffness at $p \gtrsim 100\,\mathrm{MeV/fm^3}$. Hence, it can be expected that the maximum neutron star mass that can be obtained at $N_f = 2+1$ stems from a central pressure of less than this value.

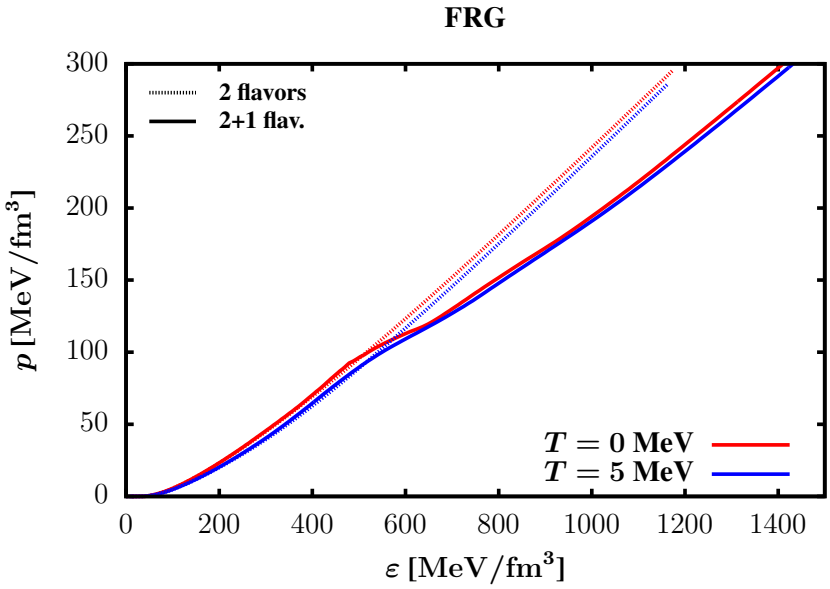

Figure 16: Equations of state of the two- and 2+1-flavor QM model FRG solutions at $T = 0$ and $T = 5\,\mathrm{MeV}$.

To summarize our results to this point, we have seen that in mean field approximation both the inclusion of vacuum fluctuations as well as the consideration of strange degrees of freedom reduce the stiffness of the equation of state. The inclusion of meson fluctuations in the full FRG approach, however, significantly modifies the equation of state and yields finite pressures already at low energy densities. On top of that, it allows for a regime up to a certain pressure where the equation of state is insensitive to strangeness and a reduction of stiffness does not occur. In order to determine the influence of temperature fluctuations, we compare the EoS in FRG at $T = 5\,\mathrm{MeV}$ with the $T = 0$ results as depicted in Fig. 16. It becomes clear that higher temperatures also

result in lower pressures at a given energy density and therefore reduce the stiffness of the equation of state. Concerning the restrictions we imposed on possible equations of state in Sec. 2, we e.g. in Fig. 11 that

$$\frac{\partial n}{\partial \mu} > 0 \tag{8.4}$$

is always the case. From Fig. 15 it is evident that the causality condition

$$\frac{\partial p}{\partial \varepsilon} < 1 \tag{8.5}$$

is fulfilled at each point as well.

8.6 Application to Neutron Stars

In order to obtain the mass-radius relationships for compact objects, the Tolman-Oppenheimer-Volkoff equation (7.30) is solved for a variety of central pressures p_0. The functions of the TOV equation depend on the radial coordinate r. They are the pressure $p(r)$ and the mass $m(r)$ that is enclosed within the sphere of radius r. When the pressure reaches zero (or a small numerical value, cf. Sec. 7.3), the evaluation of the differential equation is stopped and the neutron star radius is determined as $R = r(p = 0)$ and the mass is given by $M = m(R)$. For an exemplary central pressure of $p_0 = 50\,\mathrm{MeV/fm^3}$, the pressure and enclosed mass are depicted as functions of r in Fig. 17.

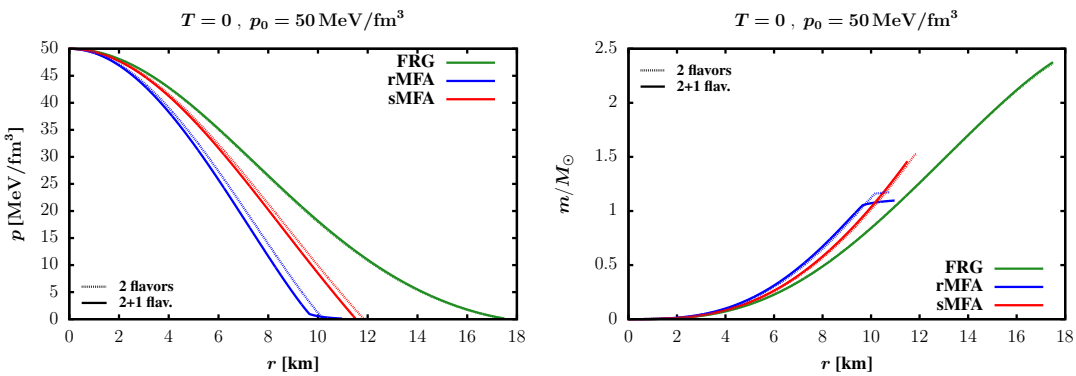

Figure 17: Neutron star pressure $p(r)$ and enclosed mass $m(r)$ as functions of the radial coordinate r in two-flavor and 2+1-flavor FRG, rMFA, and sMFA for an exemplary central pressure of $p_0 = 50\,\mathrm{MeV/fm^3}$.

With physical equations of state that include nucleonic degrees of freedom, one usually finds that the pressure has an inflation point after which it gradually goes to zero, while similarly the mass slowly saturates at increasing r. This is partly visible in the FRG solution whereas the standard mean field approximation does not exhibit this behavior at all. That can be explained by the sharp onset of finite pressures with constant slope in the sMFA equation of state when the FRG equation of state displays a gradual increase in slope. In rMFA, a sudden kink is visible in the $p(r)$ curve at low p as well as in the $m(r)$ curve at the corresponding r. After this kink, the pressure only slowly decays and the mass saturates. An explanation of this effect is given by our previous observation that at increasing μ the light condensate first smoothly melts down a few

MeV until the first-order jump occurs. The evolution after the kinks in Fig. 17 is based on data points from the chirally broken regime (before the first order transition). Hence, the first-order chiral transition actually directly influences the low-pressure behavior of the star in our model.

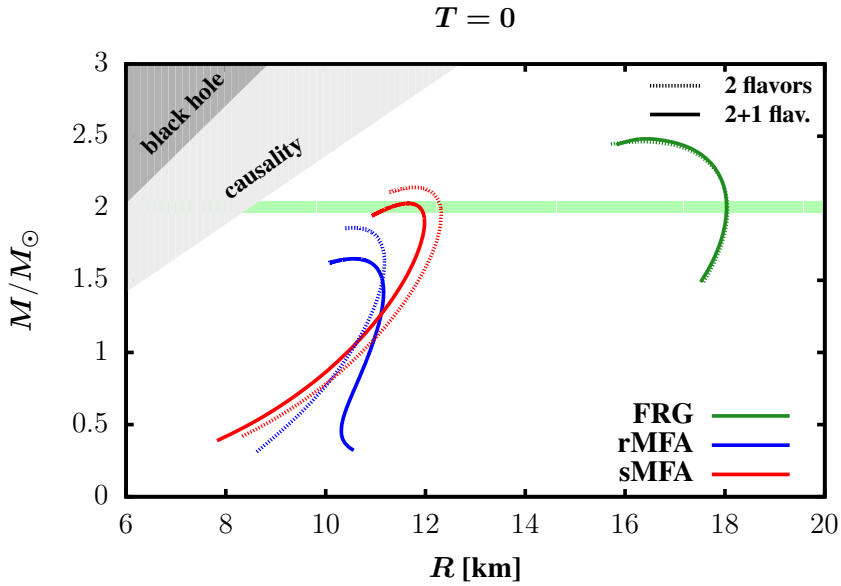

Figure 18: Mass-radius relationships for 2-flavor and 2+1-flavor FRG, rMFA, and sMFA equations of state at $T = 0$. The green band is the mass $2.01(4)\,M_\odot$ of the pulsar J0348+0432 [10]. The black hole area encloses all $R \leq 2GM/c^2$, causality violation is assumed for $R \leq 2.87GM/c^2$, cf. Sec. 2.4.

The computed neutron star M-R-relationships are displayed in Fig. 18. In sMFA, both the two-flavor and the 2+1-flavor graph manage to achieve a maximum mass of more than $2M_\odot$. As expected, the inclusion of strange matter reduces the maximum possible mass both in sMFA and rMFA. Apparently, vacuum fluctuations account for a significant reduction in stiffness of the equation of state such that two solar masses cannot be achieved in rMFA. The 2+1-flavor curve is found to bend towards higher radii at low masses. This makes sense since the data points from the chirally broken regime significantly flatten the $p(r)$ line as shown in Fig. 17. At low central pressures, that regime makes up larger parts of the neutron star and the radius where the pressure hits (almost) zero increases. At increasing central pressures, one moves upwards in the curves towards higher masses. As soon as the masses start decreasing for increasing p_0, the stability criterion defined in Sec. 2 is violated. Hence, the downwards bends at the top of the given curves belong to unstable stars. It shall also be noted that since a minimum central pressure of $10\,\mathrm{MeV/fm^3}$ is employed as explained in Sec. 7.3, the lower parts of the curve are not shown. Already at this minimum central pressure, shifts in the low mass regimes of the given curves can be observed upon e.g. manipulating the minimum pressure at which the evolution of the TOV equation is stopped. The high mass regimes of the curves, however, are found to be stable under slight variations of such parameters. After all, we can only provide a qualitative analysis at this point because the given equation of state does not include nucleonic degrees of freedom and can not serve as a realistic model going to low pressures and densities. Nevertheless,

it is a very interesting result that the two-flavor and 2+1-flavor curves are nearly identical in the FRG solution. This means that the part of the equation of state that is insensitive to strangeness, at $p \lesssim 100\,\mathrm{MeV/fm}^3$, is the only relevant part already at $N_f = 2$. Consequently, the emergence of strangeness does not have the dreaded effect of reducing the stiffness of the EoS as found in the mean field studies. Hence, in our model compact stars live in a phase of partially restored chiral symmetry in the light sector, whereas the strange sector still exhibits heavy constituent quarks and mesons. With a pure QM model equation of state, the full FRG mass-radius curve yields up to $M \approx 2.5\,M_\odot$, but lies at radii of $R \approx 17\,\mathrm{km}$ which is about 1.5 times the radius obtained in typical calculations.

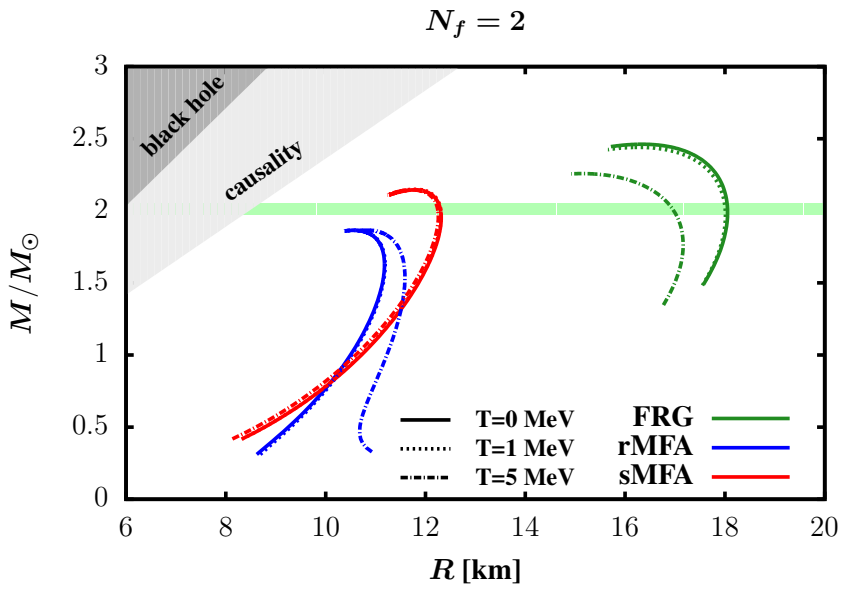

Figure 19: Mass-radius relationships for the 2-flavor FRG, rMFA, and sMFA solutions as depicted in Fig. 18, for $T = 0$, $T = 1\,\mathrm{MeV}$, and $T = 5\,\mathrm{MeV}$.

At temperatures below 1 MeV [16], neutron stars are cold objects in the context of the strong interaction. Thus, it is expected that the $T = 0$ data gives a very good approximation to the dynamics at the actual temperature of a given neutron star. To confirm this expectation, the mass-radius relationships at $N_f = 2$ and multiple temperatures are compared in Fig. 19. Almost no difference can be observed between $T = 0$ and $T = 1\,\mathrm{MeV}$ results which gives confirmation. However, at $T = 5\,\mathrm{MeV}$ already significant effects can be found in rMFA and FRG calculations. In sMFA, temperature variations in this regime do not seem to have a large impact on the solution of the TOV equation.

8.7 Influence of Infrared Cutoff

Due to the high demands on computation power of the two-dimensional grid and the increasingly low step sizes of the Runge-Kutta type ordinary differential equation solver at low values of k, we have employed an infrared cutoff of 100 MeV throughout this work. In order to test the reliability of the calculated data, the influence of the IR cutoff on the results shall be examined. Therefore, the $N_f = 2$ FRG starting parameters have

been slightly amended (with the differential evolution algorithm, cf. App. D) such that they yield the same physical vacuum observables at an IR scale of 90 MeV as they did for $k_{\mathrm{IR}} = 100\,\mathrm{MeV}$. With the new parameters, the $T = 0$ $M(R)$ curve has been recalculated and a comparison is shown in Fig. 20. While there is a slight variation in the low-mass regime of the graph, both solutions follow the same qualitative behavior. While a cutoff of 90 MeV or lower should prove to be better suited for a quantitative study, IR cutoff effects can be rated as insignificant for the purpose of this work.

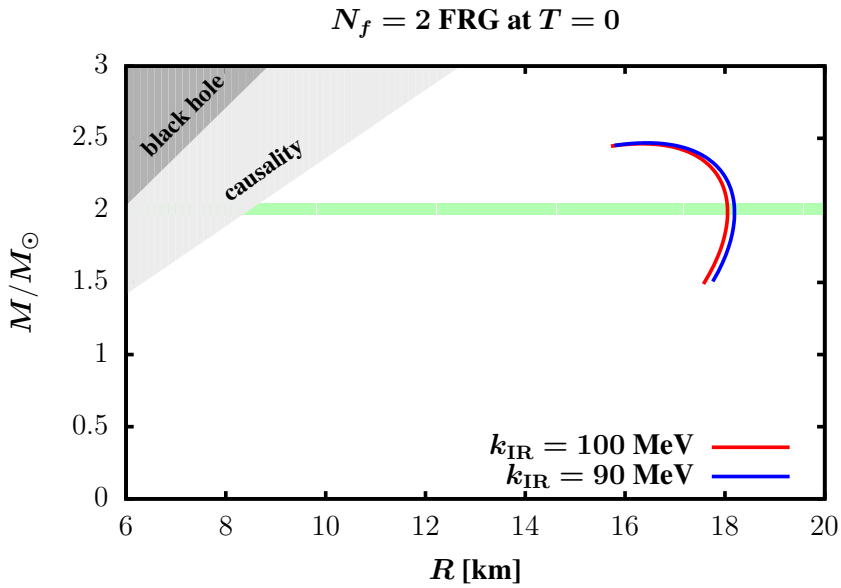

Figure 20: Mass-radius relationships for the two-flavor FRG solution as depicted in Fig. 18 for two different IR cutoffs $k_{\mathrm{IR}} = 100\,\mathrm{MeV}$ and $k_{\mathrm{IR}} = 90\,\mathrm{MeV}$.

9 Summary and Outlook

In this work, the role of high density fluctuations in compact stellar objects has been studied. Therefore, the equation of state of cold and dense strongly interacting matter is required. Because there are no first principle calculations of QCD in that regime to this day, the quark-meson model, an effective theory that incorporates the low-energy degrees of freedom of QCD, is utilized. It exhibits spontaneous chiral symmetry breaking in the vacuum and a phase transition to chirally symmetric matter at increasing T and μ. In order to study the influence of quantum fluctuations, the quark-meson model has been solved both in mean field approximation and in an FRG approach featuring the LPA (local potential approximation) truncation. The mean field study has been further split into a standard mean field approximation (sMFA) which neglects the vacuum contribution to the grand canonical potential and a renormalized mean field approximation (rMFA) that includes the vacuum term in renormalized form. Additionally, the QM model has been studied with only two degenerate light quark flavors and under the inclusion of heavier strange quarks. In both cases, an explicit symmetry breaking term has been added to account for finite current quark mass effects like non-zero pion masses. An axial symmetry breaking term in $N_f = 2 + 1$ allows for a realistic meson spectrum.

It has been found that at low temperatures, both mean field solutions as well as the FRG calculation display a first-order chiral phase transition. The 2+1-flavor model shows that this phase transition predominantly occurs in the light chiral condensate and that the strange condensate remains largely intact. Only at chemical potentials of the order of the strange constituent quark mass, the condensate of strange quarks begins to slowly melt down. This effect could be observed in mean field approximation as well as FRG. Other than the fact that the transition line in rMFA is slightly shifted in 2+1 flavors compared to the two-flavor version, the inclusion of strange degrees of freedom has been found to have negligible impact on the thermodynamics of the theory up to the scale of the onset of the meltdown of the strange condensate. At this scale, the f_0 scalar meson mass has been observed to exhibit a similar behavior to that of the sigma mass at the first-order transition. That can be interpreted as another hint to the fact that the gradual meltdown of the strange condensate should be treated as a second, washed-out crossover phase transition. Furthermore, the effects of the second phase transition significantly weaken the equation of state which could be inferred from a comparison to two-flavor results. In our findings, the inclusion of vacuum fluctuations also weakens the EoS, as do higher temperatures. Concerning finite temperatures, negative entropy densities have been found at low, non-zero T in the FRG solution. Possible explanations of this unphysical behavior are still under discussion and may be investigated in the future. One of the possibility to remedy this effect is the allowance for a diquark condensate. This can be done in form of a quark-meson-diquark model as proposed in Ref. [90, 91]. After the determination of the equation of state, the Tolman-Oppenheimer-Volkoff (TOV) equation has been solved and neutron star mass-radius relationships have been determined. While the onset of strangeness effects at high chemical potentials is more gradual in mean field approxmation, the FRG solutions shows identical two-flavor and 2+1-flavor equations of state up to a sudden onset of said strangeness effects. It is found that in FRG, stable neutron stars live at pressures where these effects do not play a role, hence both two-flavor and 2+1-flavor

curves display identical mass-radius relationships. Neutron star radii are determined to be higher that typical calculations suggest, but neutron star masses of up to $2.5\,M_\odot$ can be achieved. In mean field approximation, both sMFA and rMFA solution show that strange quarks lead to lower maximal neutron star masses. Thus, we can conclude that the inclusion of quantum fluctuations, specifically meson fluctuations in our model, plays a significant role both for neutron star masses and radii as well as the effects of strangeness on compact objects. This result is especially interesting regarding the hyperon puzzle as most models predict a weakening of the equation of state due to strangeness effects. It also stands in contrast to the recent result given in Ref. [92]. In this publication, the effects of quantum fluctuations are determined to be only at the 5% level in a similar one-flavor model.

Regarding future works, a more quantitative treatment could be performed. To this end, the given EoS of the QM model must be combined with the EoS of a well-understood nucleonic model. Of course, further questions in relation to the QM model EoS have to be answered as well. One of them is the influence of ultraviolet (UV) cutoff effects on the solution. This could be achieved by varying the UV cutoff of the FRG solution and comparing several results. That question is of significance because e.g. in rMFA we have observed that the position of the critical endpoint is sensitive to the UV cutoff. Specifically, at $\Lambda = 5\,\mathrm{GeV}$ the transition line has been found to be a pure crossover line without a critical endpoint. Another question is the impact of truncation effects. Going to better truncations than the LPA in the FRG approach is planned for future works, as well as the incorporation of dynamical hadronization. Finally, it shall be mentioned that the quark-meson model misses important degrees of freedom of QCD at high densities and low temperatures. As already mentioned, baryonic degrees of freedom definitely play an important role and even gluonic degrees of freedom should emerge at some point. Thus, even though this study gives a first impression of the importance of mesonic fluctuations and the role of strangeness in a setup of interacting quarks and mesons, a solution of the pending question of the QCD phase diagram in the regime of compact objects will require the inclusion of all relevant effects.

A Matsubara Formalism

The Matsubara formalism makes a connection of quantum field theory to statistical mechanics and therefore allows the study of QFT at finite temperature as a functional field theory in Euclidean space with compactified (imaginary) time. This formalism is convenient as long as no real-time observables must be computed, in which case some application of a real-time formalism [93, 94] comes into place. To make the connection, we remember that the partition function of statistical mechanics is defined as

$$Z_{\text{stat}} = \operatorname{Tr} \mathrm{e}^{-\beta H} = \sum_{\alpha} \langle \alpha | \mathrm{e}^{-\beta H} | \alpha \rangle \quad . \tag{A.1}$$

For time independent Hamiltonians H and $\beta := \mathrm{i}\Delta t$ the definition of the quantum mechanical path integral reveals that

$$Z_{\text{stat}} = \int_{\alpha(0)=\alpha(-\mathrm{i}\beta)} \mathcal{D}\alpha \, \mathrm{e}^{\mathrm{i}\int_0^{-\mathrm{i}\beta} \mathrm{d}t \, L} = \int_{\alpha(\tau=0)=\alpha(\tau=\beta)} \mathcal{D}\alpha \, \mathrm{e}^{\int_0^{\beta} \mathrm{d}\tau \, L} \quad . \tag{A.2}$$

The temperature takes on the role as an imaginary time with $\tau := \mathrm{i}t$ (Wick rotation). The trace demands the state $|\alpha\rangle$ to be reached periodically after the imaginary time interval β. It also has to be pointed out that the path integral now includes all *physical* paths featuring periodic boundary conditions with periodicity β from *all* starting points due to the sum in the trace, not just one specific state. A dimension that does not stretch from $-\infty$ to ∞ but is finite and periodic is called compact. Going back to a field formalism, one has (writing Z for Z_{stat} from now on) [72]

$$Z = \oint \mathcal{D}\varphi \, \mathrm{e}^{\int_0^{\beta} \mathrm{d}\tau \int \mathrm{d}^3x \mathcal{L}} \quad . \tag{A.3}$$

The loop integral sign stands for the periodic boundary conditions in the path integral. It will be omitted from now on. Of course, the Lagrangian density also has to be adjusted to the rotation in the complex plane of the x^0 component. For a free scalar field this is

$$\begin{aligned} \mathcal{L} = \frac{1}{2}\left(\frac{\partial\varphi}{\partial t}\right)^2 - \frac{1}{2}(\nabla\varphi)^2 - \frac{1}{2}m^2\varphi^2 &= -\left[\frac{1}{2}\left(\frac{\partial\varphi}{\partial\tau}\right)^2 + \frac{1}{2}(\nabla\varphi)^2 + \frac{1}{2}m^2\varphi^2\right] \\ &= -\left[\frac{1}{2}(\partial_E\varphi)^2 + \frac{1}{2}m^2\varphi^2\right] =: -\mathcal{L}_E \end{aligned} \tag{A.4}$$

where the index E hints at the now Euclidean metric in the derivative term. In total, we have

$$Z = \int \mathcal{D}\varphi \, \mathrm{e}^{-\int_0^{\beta} \mathrm{d}\tau \int \mathrm{d}^3x \mathcal{L}_E} =: \int \mathcal{D}\varphi \, \mathrm{e}^{-S_E} \quad . \tag{A.5}$$

For fermions, the same procedure can be done [72]. The Lagrangian density

$$\mathcal{L} = \bar{\psi}\left(\mathrm{i}\partial\!\!\!/ - m\right)\psi = \bar{\psi}\left(\mathrm{i}\partial_\mu\gamma^\mu - m\right)\psi = \bar{\psi}\left(\mathrm{i}\partial_t\gamma_0 - \mathrm{i}\partial_i\gamma_i - m\right)\psi \tag{A.6}$$

becomes

$$-\mathcal{L}_E = \bar{\psi}\left(-\partial_\tau\gamma_0 - \mathrm{i}\partial_i\gamma_i - m\right)\psi = -\bar{\psi}\left(\partial_\mu\tilde{\gamma}_\mu + m\right)\psi = -\bar{\psi}\left(\partial\!\!\!/_E + m\right)\psi \tag{A.7}$$

where

$$\tilde{\gamma}_\mu := (\gamma_0, \mathrm{i}\boldsymbol{\gamma}) \tag{A.8}$$

and $\partial_0 := \partial_\tau$. Using $\tilde{\gamma}_\mu$ additionally has the advantage of Euclidean anticommutation relations:

$$\{\tilde{\gamma}_\mu, \tilde{\gamma}_\nu\} = 2\delta_{\mu\nu}\mathbb{1} \quad . \tag{A.9}$$

In this work, we will exclusively utilize Euclidean field theory. Note that the Lagrangian now has a structure that would resemble $T + V$ in classical mechanics. Reintroducing a source term, the partition function acts as the generating functional

$$Z[J] = \int \mathcal{D}\varphi \, \mathrm{e}^{-S+\int_0^\beta \mathrm{d}\tau \int \mathrm{d}^3x \, J(\tau,\boldsymbol{x})\varphi(\tau,\boldsymbol{x})} =: \int \mathcal{D}\varphi \, \mathrm{e}^{-S+\int J\varphi} \quad . \tag{A.10}$$

The generating functional for connected diagrams in Euclidean field theory is defined

$$W[J] := \ln Z[J] \quad . \tag{A.11}$$

Furthermore, there is one major difference between bosons and fermions in this formalism due to periodicity. It can be shown from the anticommutation relations of the fermion field operators in the propagator that

$$\psi(0, \boldsymbol{x}) = -\psi(\beta, \boldsymbol{x}) \quad . \tag{A.12}$$

The anti-periodicity of $\psi(x)$ has consequences that become apparent under a Fourier transformation to momentum space. For a scalar field where $\varphi(x)$ is periodic in τ, the Fourier integral becomes a sum divided by the period length:

$$\varphi(\tau, \boldsymbol{x}) = \frac{1}{\beta} \sum_{n=-\infty}^{\infty} \int \frac{\mathrm{d}^3k}{(2\pi)^3} \, \mathrm{e}^{\mathrm{i}(\boldsymbol{k}\cdot\boldsymbol{x}+\omega_n\tau)} \varphi_n(\boldsymbol{k}) = T \sum_{n=-\infty}^{\infty} \int \frac{\mathrm{d}^3k}{(2\pi)^3} \, \mathrm{e}^{\mathrm{i}k\cdot x} \varphi(\omega_n, \boldsymbol{k}) \tag{A.13}$$

where $\omega_n = (2\pi/\beta)n = 2\pi T n$. The anti-periodicity can be understood as adding an additional phase shift π/β that gives a half rotation π in the complex plane, which is just a minus sign, under $\tau \to \tau + \beta$. Therefore it suffices to have $\omega_n = (2n+1)\pi T$ and fermion fields can be Fourier transformed just like above. For the purpose of encoding all fluctuations in an effective action, the quantum effective (or average) action $\Gamma[\phi]$ can be defined as the functional Legendre transform of $W[J]$:

$$\Gamma[\phi] := -W[J] + \int \mathrm{d}^4x \, J(x)\phi(x) \quad . \tag{A.14}$$

Taking into consideration that the derivative of $W[J]$ with respect to the source J gives the field expectation value $\langle\varphi\rangle_J$ and the natural variable of the Legendre transform is exactly the derivative of the original function, we can make the identification $\phi = \langle\varphi\rangle_J$.

B Analytic Limits

In this appendix, the derivatives of the effective potential with respect to the fields in mean field approximation are determined. Furthermore, analytic limits $T \to 0$ are given for the expressions found in Sec 5, 6, and 7.2. In mean field approximation, the derivative of the total potential with respect to a field consists of the derivative of the meson potential Ω_{mes} plus the contribution of the quark flow. The shape of the meson potential in $N_f = 2$ and $N_f = 2+1$ is given in App. D. The quark contribution follows from the differentiation of the quark potential integral. In sMFA, it reads

$$\frac{\partial \Omega_q}{\partial \sigma_i} = \frac{N_c}{2\pi^2} g^2 \sigma_i \int_0^\infty \mathrm{d}p \, \frac{p^2}{E_i} \left(n_f(E_i, \mu, T) + \bar{n}_f(E_i, -\mu, T) \right) \quad i \in \{l, s\} \tag{B.1}$$

with σ_i the possible condensates in N_f flavors. In the limit of vanishing temperature, the fermi statistics only gives a contribution for $\mu > m_i$ which is

$$\left.\frac{\partial \Omega_q}{\partial \sigma_i}\right|_{T=0} \overset{\mu > m_i}{=} \frac{N_c}{4\pi^2} g^2 \sigma_i \left[\mu \sqrt{\mu^2 - m_i^2} - m_i^2 \ln \left(\frac{\sqrt{\mu^2 - m_i^2} + \mu}{m_i} \right) \right] \quad . \tag{B.2}$$

In rMFA, the derivative of the quark potential is

$$\begin{aligned} \frac{\partial \Omega_q}{\partial \sigma_i} = \frac{N_c}{6\pi^2} g^2 \sigma_i \int_{k_{\text{IR}}}^{\Lambda} \mathrm{d}k \, k^4 \Bigg(& -\frac{1}{2E_f^3} \left[\tanh\left(\frac{E_f - \mu}{2T} \right) + \tanh\left(\frac{E_f + \mu}{2T} \right) \right] \\ & + \frac{1}{4TE_f^2} \left[\frac{1}{\cosh^2\left(\frac{E_f - \mu}{2T}\right)} + \frac{1}{\cosh^2\left(\frac{E_f + \mu}{2T}\right)} \right] \Bigg) \quad . \end{aligned} \tag{B.3}$$

Note that in the limit of vanishing temperature the last part produces a delta distribution

$$\frac{1}{4T \cosh^2\left(\frac{E_f - \mu}{2T}\right)} \overset{T \to 0}{\longrightarrow} \delta(E_f - \mu) \overset{\mu > m_f}{=} \frac{E_f}{k} \delta(k - \sqrt{\mu^2 - m_f^2}) \quad . \tag{B.4}$$

Therefore, the limit can be evaluated to be

$$\left.\frac{\partial \Omega_q}{\partial \sigma_i}\right|_{T=0} = \frac{N_c}{6\pi^2} g^2 \sigma_i \left(\mathcal{I}_1 + \begin{Bmatrix} \frac{(\mu^2 - m_f^2)^{3/2}}{\mu} & \mu > E_{\text{end}} \\ 0 & \text{else} \end{Bmatrix} \right) \tag{B.5}$$

with

$$\begin{aligned} \mathcal{I}_1 :&= -\int_{x_2}^{x_1} \mathrm{d}k \, \frac{k^4}{E_f^3} \\ &= -\frac{1}{2} \left[\frac{3m_f^2 x_1 + x_1^3}{\sqrt{x_1^2 + m_f^2}} - \frac{3m_f^2 x_2 + x_2^3}{\sqrt{x_2^2 + m_f^2}} - 3m_f^2 \ln \left(\frac{x_1 + \sqrt{x_1^2 + m_f^2}}{x_2 + \sqrt{x_2^2 + m_f^2}} \right) \right] \quad . \end{aligned} \tag{B.6}$$

Here, $x_1 = \Lambda$ and

$$x_2 = \begin{cases} k_{\text{IR}} & \mu < m_f \\ \max\left(k_{\text{IR}}, \sqrt{\mu^2 - m_f^2} \right) & \text{else} \quad . \end{cases} \tag{B.7}$$

The analytic limits of the equations given in the thesis are listed below.

- Eq. (5.21):

$$\begin{aligned}\Omega_q|_{T=0} &= \frac{N_c}{\pi^2}\sum_f \int_0^\infty \mathrm{d}p\, p^2\,(E_f-\mu)\,\theta(\mu-E_f) \\ &= \frac{N_c}{\pi^2}\sum_f \begin{cases} 0 & \mu \le m_f \\ \int_0^{\sqrt{\mu^2-m_f^2}} \mathrm{d}p\, p^2\,(E_f-\mu) & \mu > m_f \end{cases}\end{aligned} \tag{B.8}$$

with

$$\begin{aligned}&\int_0^{\sqrt{\mu^2-m_f^2}} \mathrm{d}p\, p^2\,(E_f-\mu) \\ &\qquad = \frac{1}{24}\left(\mu\sqrt{\mu^2-m_f^2}(5m_f^2-2\mu^2) - 3m_f^4 \ln\left(\frac{\sqrt{\mu^2-m_f^2}+\mu}{m_f}\right)\right) \quad .\end{aligned} \tag{B.9}$$

- Eq. (6.36):

$$\partial_t U_k|_{T=0} = \frac{k^5}{12\pi^2}\left[\sum_b \frac{1}{E_b} - 4N_c\sum_f \frac{1}{E_f}\theta(E_f-\mu)\right] \quad . \tag{B.10}$$

- Eq. (6.40):

$$\begin{aligned}\Omega_q|_{T=0} &= \frac{N_c}{6\pi^2}\sum_f \int_{x_2}^{x_1} \mathrm{d}k\, \frac{k^4}{E_f} \\ &= \frac{N_c}{6\pi^2}\frac{1}{4}\sum_f \{\sqrt{x_1^2+m_f^2}(2x_1^3-3m_f^2x_1) - \sqrt{x_2^2+m_f^2}(2x_2^3-3m_f^2x_2) \\ &\qquad + 3m_f^4 \ln\left(\frac{x_1+\sqrt{x_1^2+m_f^2}}{x_2+\sqrt{x_2^2+m_f^2}}\right)\} \quad .\end{aligned} \tag{B.11}$$

with the definitions of x_1 and x_2 as given above.

- Eq. (7.21):

$$\left.\frac{\partial\Omega_q}{\partial\mu}\right|_{T=0} = -\frac{N_c}{3\pi^2}\sum_f \begin{cases} 0 & \mu \le m_f \\ (\mu^2-m_f^2)^{3/2} & \mu > m_f \end{cases} \quad . \tag{B.12}$$

- Eq. (7.25):

$$\left.\frac{\partial\Omega_q}{\partial\mu}\right|_{T=0} = -\frac{N_c}{3\pi^2}\sum_f \begin{cases} (\mu^2-m_f^2)^{3/2} & \mu > E_{\mathrm{IR}} \\ 0 & \text{else} \end{cases} \quad . \tag{B.13}$$

This is the same contribution that is given in the standard mean field case just above, only corrected for a finite value of k_{IR}.

- Eq. (7.26):

$$\partial_t \frac{\partial U_k}{\partial T}\bigg|_{T=0} = -\frac{k^5}{12\pi^2} \sum_b \frac{1}{2E_b^3} \frac{\partial m_b^2}{\partial T}\bigg|_{T=0} \quad . \tag{B.14}$$

- Eq. (7.27):

$$\partial_t \frac{\partial U_k}{\partial \mu}\bigg|_{T=0} = -\frac{k^5}{12\pi^2} \left\{ \sum_b \frac{1}{2E_b^3} \frac{\partial m_b^2}{\partial \mu}\bigg|_{T=0} - 2N_c \sum_f \frac{2}{k} \delta\left(k - \sqrt{\mu^2 - m_f^2}\right) \right\} \quad , \tag{B.15}$$

In sMFA and rMFA, the temperature derivatives can both be shown to vanish in the limit $T \to 0$. This corresponds to vanishing entropy as expected. Note that Eq. (B.14) suggests that this is also the case for the FRG approach if the starting values are $\partial U_k/\partial T = 0$ at each point. Of course, the UV potential is inserted as temperature independent and renders vanishing entropy. If this was not the case, a finite entropy would be produced. Hence, this starting value looks like a (possibly unstable) fixed point of the differential equation which could explain the negative entropies at $T \to 0$ while still rendering vanishing entropy at $T = 0$, cf. Sec. 8. Concerning Eq. (B.15), it has to be noted that the delta distribution gives a contribution to the flow. For each grid point, the flow is halted at the relevant value of k and a finite contribution that stems from integrating the delta distribution out in an infinitesimal interval is added. This contribution is exactly the complete contribution of the mean field approaches, given in Eq. (B.13).

C Meson Masses

Under meson masses we understand the *curvature masses* $\tilde{U}^{(2)}_{bb}$ where $\tilde{U}$ is the effective potential including explicit breaking terms. The derivatives have to be evaluated at the VEV.

C.1 Mean Field Approximation

In mean field approximation, we get a contribution from the static meson potential Ω_{mes} and the fermionic integral. The meson potential derivatives read in two flavors

$$\left\langle \frac{\partial^2 \Omega_{\text{mes}}}{\partial \sigma^2} \right\rangle = m^2 + 3\lambda\sigma^2 \quad , \quad \left\langle \frac{\partial^2 \Omega_{\text{mes}}}{\partial \pi_i^2} \right\rangle = m^2 + \lambda\sigma^2 \quad . \tag{C.1}$$

where the meson potential is equal to the UV potential given in Eq. (4.21). In 2+1 flavors, the potential given in Eq. (4.28) (with the axial symmetry breaking term added) renders

$$\begin{aligned}
\left\langle \frac{\partial^2 \Omega_{\text{mes}}}{\partial \sigma_0^2} \right\rangle &= m^2 + \frac{\lambda_1}{3}(7\sigma_l^2 + 4\sqrt{2}\sigma_l\sigma_s + 5\sigma_s^2) + \lambda_2(\sigma_l^2 + \sigma_s^2) - \frac{c}{3}(2\sigma_l + \sqrt{2}\sigma_s) \\
\left\langle \frac{\partial^2 \Omega_{\text{mes}}}{\partial \sigma_8^2} \right\rangle &= m^2 + \frac{\lambda_1}{3}(5\sigma_l^2 - 4\sqrt{2}\sigma_2\sigma_s + 7\sigma_s^2) + \frac{\lambda_2}{2}(\sigma_l^2 + 4\sigma_s^2) + \frac{c}{6}(4\sigma_l - \sqrt{2}\sigma_s) \\
\left\langle \frac{\partial^2 \Omega_{\text{mes}}}{\partial \sigma_0 \partial \sigma_8} \right\rangle &= \frac{2\lambda_1}{3}(\sqrt{2}\sigma_l^2 - \sigma_l\sigma_s - \sqrt{2}\sigma_s^2) + \frac{\lambda_2}{\sqrt{2}}(\sigma_l^2 - 2\sigma_s^2) + \frac{c}{6}(\sqrt{2}\sigma_l - 2\sigma_s) \\
\left\langle \frac{\partial^2 \Omega_{\text{mes}}}{\partial \sigma_1^2} \right\rangle &= m^2 + \lambda_1(\sigma_l^2 + \sigma_s^2) + \frac{3\lambda_2}{2}\sigma_l^2 + \frac{c}{\sqrt{2}}\sigma_s \\
\left\langle \frac{\partial^2 \Omega_{\text{mes}}}{\partial \sigma_4^2} \right\rangle &= m^2 + \lambda_1(\sigma_l^2 + \sigma_s^2) + \frac{\lambda_2}{2}(\sigma_l^2 + \sqrt{2}\sigma_l\sigma_s + 2\sigma_s^2) + \frac{c}{2}\sigma_l \\
\left\langle \frac{\partial^2 \Omega_{\text{mes}}}{\partial \pi_0^2} \right\rangle &= m^2 + \lambda_1(\sigma_l^2 + \sigma_s^2) + \frac{\lambda_2}{3}(\sigma_l^2 + \sigma_s^2) + \frac{c}{3}(2\sigma_l + \sqrt{2}\sigma_s) \\
\left\langle \frac{\partial^2 \Omega_{\text{mes}}}{\partial \pi_8^2} \right\rangle &= m^2 + \lambda_1(\sigma_l^2 + \sigma_s^2) + \frac{\lambda_2}{6}(\sigma_l^2 + 4\sigma_s^2) + \frac{c}{6}(-4\sigma_l + \sqrt{2}\sigma_s) \\
\left\langle \frac{\partial^2 \Omega_{\text{mes}}}{\partial \pi_0 \partial \pi_8} \right\rangle &= \frac{\lambda_2}{3\sqrt{2}}(\sigma_l^2 - 2\sigma_s^2) + \frac{c}{6}(-\sqrt{2}\sigma_l + 2\sigma_s) \\
\left\langle \frac{\partial^2 \Omega_{\text{mes}}}{\partial \pi_1^2} \right\rangle &= m^2 + \lambda_1(\sigma_l^2 + \sigma_s^2) + \frac{\lambda_2}{2}\sigma_l^2 - \frac{c}{\sqrt{2}}\sigma_s \\
\left\langle \frac{\partial^2 \Omega_{\text{mes}}}{\partial \pi_4^2} \right\rangle &= m^2 + \lambda_1(\sigma_l^2 + \sigma_s^2) + \frac{\lambda_2}{2}(\sigma_l^2 - \sqrt{2}\sigma_l\sigma_s + 2\sigma_s^2) - \frac{c}{2}\sigma_l \quad .
\end{aligned} \tag{C.2}$$

Note that all mixed second derivatives but the ones in the $0-8$-sector (scalar as well as pseudo-scalar) vanish at the VEV. For the quark contribution, we have to consider the field dependence of the eigenvalues m_f^2 of the quark mass matrix $M_q^2 := g^2\Phi^\dagger\Phi$ and

take the derivatives from Eq. (5.21). In sMFA we conclude [70]

$$\left\langle \frac{\partial^2 \Omega_q}{\partial \phi_a \partial \phi_b} \right\rangle = \frac{N_c}{\pi^2} \sum_{f=u,d,s} \int_0^\infty \mathrm{d}p\, p^2 \frac{1}{2E_f} \left[(n_f + \bar{n}_f) \left(m_{f,ab}^2 - \frac{m_{f,a}^2 m_{f,b}^2}{2E_f^2} \right) - (b_f + \bar{b}_f) \frac{m_{f,a}^2 m_{f,b}^2}{2E_f T} \right] \tag{C.3}$$

where $n_f := n_f(E_f, \mu, T)$, $\bar{n}_f := n_f(E_f, -\mu, T)$, $b_f := n_f(1 - n_f)$, $\bar{b}_f := \bar{n}_f(1 - \bar{n}_f)$, $m_{f,ab}^2 := \frac{\partial^2 m_f^2}{\partial \phi_a \phi_b}$, and $m_{f,a}^2 := \frac{\partial m_f^2}{\partial \phi_a}$, all mass eigenvalue derivatives are evaluated at the expectation value. For $T = 0$ the integral vanishes for $\mu < m_f$. We get the limit

$$\left\langle \frac{\partial^2 \Omega_q}{\partial \phi_a \partial \phi_b} \right\rangle \Bigg|_{T=0} = \frac{N_c}{4\pi^2} \sum_{\substack{f \\ \mu > m_f}} \{ m_{f,ab}^2 \left[\mu \sqrt{\mu^2 - m_f^2} - m_f^2 \ln \left(\frac{\mu + \sqrt{\mu^2 - m_f^2}}{m_f} \right) \right] - m_{f,a}^2 m_{f,b}^2 \ln \left(\frac{\mu + \sqrt{\mu^2 - m_f^2}}{m_f} \right) \} \quad . \tag{C.4}$$

In rMFA, the corresponding integral at finite temperature is

$$\begin{aligned} \left\langle \frac{\partial^2 \Omega_q}{\partial \phi_a \partial \phi_b} \right\rangle = \frac{N_c}{6\pi^2} \sum_f \int_{k_{\mathrm{IR}}}^{\Lambda} \mathrm{d}k\, k^4 \, \{ & \\ & \left(\frac{3 m_{f,a}^2 m_{f,b}^2}{4E_f^5} - \frac{m_{f,ab}^2}{2E_f^3} \right) \left[\tanh\left(\frac{E_f - \mu}{2T} \right) + \tanh\left(\frac{E_f + \mu}{2T} \right) \right] \\ & + \left(\frac{m_{f,ab}^2}{4TE_f^2} - \frac{3 m_{f,a}^2 m_{f,b}^2}{8TE_f^4} \right) \left[\frac{1}{\cosh^2\left(\frac{E_f - \mu}{2T}\right)} + \frac{1}{\cosh^2\left(\frac{E_f + \mu}{2T}\right)} \right] \\ & - \frac{m_{f,a}^2 m_{f,b}^2}{8T^2 E_f^3} \left[\frac{\tanh\left(\frac{E_f - \mu}{2T}\right)}{\cosh^2\left(\frac{E_f - \mu}{2T}\right)} + \frac{\tanh\left(\frac{E_f + \mu}{2T}\right)}{\cosh^2\left(\frac{E_f + \mu}{2T}\right)} \right] \} \quad . \end{aligned} \tag{C.5}$$

At $T = 0$, the last term behaves like the derivative of a delta distribution and we have to partially integrate to obtain

$$\begin{aligned} \left\langle \frac{\partial^2 \Omega_q}{\partial \phi_a \partial \phi_b} \right\rangle \Bigg|_{T=0} = \frac{N_c}{6\pi^2} \sum_f \Bigg[& m_{f,ab}^2 \mathcal{I}_1 + \frac{3 m_{f,a}^2 m_{f,b}^2}{2} \mathcal{I}_2 \\ & + \begin{cases} m_{f,ab}^2 \frac{(\mu^2 - m_f^2)^{3/2}}{\mu} - m_{f,a}^2 m_{f,b}^2 \left(\frac{1}{2} \frac{(\mu^2 - m_f^2)^{3/2}}{\mu^3} + \frac{3}{2} \frac{\sqrt{\mu^2 - m_f^2}}{\mu} \right) & \mu > E_{\mathrm{IR}} \\ 0 & \text{else} \end{cases} \Bigg] \end{aligned} \tag{C.6}$$

with the conventions from App. B, $\mathcal{I}_1$ from Eq. (B.6) and

$$\mathcal{I}_2 := \int_{x_2}^{x_1} \mathrm{d}k \, \frac{k^4}{E_f^5} = -\frac{1}{3}\left[\frac{x_1(3m_f^2+4x_1^2)}{(m_f^2+x_1^2)^{3/2}} - \frac{x_2(3m_f^2+4x_2^2)}{(m_f^2+x_2^2)^{3/2}} \right. \\ \left. -3\ln\left(\frac{x_1+\sqrt{x_1^2+m_f^2}}{x_2+\sqrt{x_2^2+m_f^2}}\right)\right] \quad . \tag{C.7}$$

For $N_f = 2$, the derivatives of the isospin symmetric quark mass m_q^2 can easily be evaluated with the definition of Φ given in Eq. (4.14):

$$m_{q,\sigma}^2 = \frac{1}{2}g^2\sigma \quad , \quad m_{q,\sigma\sigma}^2 = \frac{1}{2}g^2 \quad , \quad m_{q,\pi_i}^2 = 0 \quad , \quad m_{q,\pi_i\pi_i}^2 = \frac{1}{2}g^2 \quad . \tag{C.8}$$

The VEV of the mass is $\langle m_q^2\rangle = g^2\langle\sigma\rangle^2/4$ and all mixed derivatives vanish. For $N_f = 2+1$, the eigenvalue derivatives are more complicated to obtain. One can e.g. use an algorithm for the derivatives of the eigenvalues with respect to a parameter as given in Ref. [95]. This algorithm only requires a diagonalization to be known at the point of derivative, i.e. at the VEV where the matrix is already diagonal:

$$\langle M_q^2\rangle = \begin{pmatrix} m_l^2 & 0 & 0 \\ 0 & m_l^2 & 0 \\ 0 & 0 & m_s^2 \end{pmatrix} \quad . \tag{C.9}$$

Special care has to be taken for the first two degenerate eigenvalues because any linear combination of eigenvectors gives another eigenvector and hence the actual eigenvector basis (for general values of fields, not necessarily at the VEV) is not known. The necessary procedure is outlined in Ref. [95] as well. For the light and strange mass VEVs we here find [cf. Eq. (5.8)]:

$$\langle m_l^2\rangle = g^2\frac{\langle\sigma_l\rangle^2}{4} \quad , \quad \langle m_s^2\rangle = g^2\frac{\langle\sigma_s\rangle^2}{2} \quad . \tag{C.10}$$

The non-zero eigenvalue derivatives are tabulated in Tab. 1 and agree with Ref. [70]. In order to connect the derivatives to meson masses in the 2+1-flavor case, we have to find a base where all mixed derivatives vanish. The fields we then obtain represent the physical meson states. We only have non-vanishing mixed derivatives in the $0-8$-sector (or light-strange sector under rotation) because here we have quark-antiquark states with vacuum quantum numbers and the mixing of the two scalar and two pseudoscalar mesons in terms of light and strange content is not uniquely determined. We define the scalar and pseudoscalar mixing angles θ_S and θ_P as the field rotation angles for diagonalization:

$$\begin{pmatrix} f_0 \\ \sigma \end{pmatrix} = \begin{pmatrix} \cos\theta_S & -\sin\theta_S \\ \sin\theta_S & \cos\theta_S \end{pmatrix}\begin{pmatrix} \sigma_0 \\ \sigma_8 \end{pmatrix} \quad , \quad \begin{pmatrix} \eta \\ \eta' \end{pmatrix} = \begin{pmatrix} \cos\theta_P & -\sin\theta_P \\ \sin\theta_P & \cos\theta_P \end{pmatrix}\begin{pmatrix} \pi_0 \\ \pi_8 \end{pmatrix} \quad . \tag{C.11}$$

Define $\langle\partial^2\tilde{U}/\partial\phi_i\partial\phi_j\rangle := m_{\phi_i\phi_j}^2$. A simple use of chain rule and diagonalization conditions delivers the formulas for the mixing angle,

$$\tan 2\theta_S = \frac{2m_{\sigma_0\sigma_8}^2}{m_{\sigma_0\sigma_0}^2 - m_{\sigma_8\sigma_8}^2} \quad , \quad \tan 2\theta_P = \frac{2m_{\pi_0\pi_8}^2}{m_{\pi_0\pi_0}^2 - m_{\pi_8\pi_8}^2} \quad , \tag{C.12}$$

and the diagonalized masses [70]:

$$m_\sigma^2 = \frac{1}{2}(m_{\sigma_0\sigma_0}^2 + m_{\sigma_8\sigma_8}^2 + \Delta_S) \quad , \quad m_{f_0}^2 = \frac{1}{2}(m_{\sigma_0\sigma_0}^2 + m_{\sigma_8\sigma_8}^2 - \Delta_S) \tag{C.13}$$

$$m_{\eta'}^2 = \frac{1}{2}(m_{\pi_0\pi_0}^2 + m_{\pi_8\pi_8}^2 + \Delta_P) \quad , \quad m_\eta^2 = \frac{1}{2}(m_{\pi_0\pi_8}^2 + m_{\sigma_s\sigma_s}^2 - \Delta_P) \tag{C.14}$$

with

$$\Delta_S := \sqrt{(m_{\sigma_0\sigma_0}^2 - m_{\sigma_8\sigma_8}^2)^2 + 4m_{\sigma_0\sigma_8}^4} \quad , \quad \Delta_P := \sqrt{(m_{\pi_0\pi_0}^2 - m_{\pi_8\pi_8}^2)^2 + 4m_{\pi_0\pi_8}^4} \quad . \tag{C.15}$$

		$2m_{l,\alpha}^2 m_{l,\beta}^2/g^4$	$2m_{l,\alpha\beta}^2/g^2$	$m_{s,\alpha}^2 m_{s,\beta}^2/g^4$	$m_{s,\alpha\beta}^2/g^2$
σ_0	σ_0	$\frac{1}{3}\sigma_l^2$	$\frac{2}{3}$	$\frac{1}{3}\sigma_s^2$	$\frac{1}{3}$
σ_1	σ_1	$\frac{1}{2}\sigma_l^2$	1	0	0
σ_4	σ_4	0	$\frac{\sigma_l}{\sigma_l-\sqrt{2}\sigma_s}$	0	$\frac{\sqrt{2}\sigma_s}{\sqrt{2}\sigma_s-\sigma_l}$
σ_8	σ_8	$\frac{1}{6}\sigma_l^2$	$\frac{1}{3}$	$\frac{2}{3}\sigma_s^2$	$\frac{2}{3}$
σ_0	σ_8	$\frac{\sqrt{2}}{6}\sigma_l^2$	$\frac{\sqrt{2}}{3}$	$-\frac{\sqrt{2}}{3}\sigma_s^2$	$-\frac{\sqrt{2}}{3}$
π_0	π_0	0	$\frac{2}{3}$	0	$\frac{1}{3}$
π_1	π_1	0	1	0	0
π_4	π_4	0	$\frac{\sigma_l}{\sigma_l+\sqrt{2}\sigma_s}$	0	$\frac{\sqrt{2}\sigma_s}{\sigma_l+\sqrt{2}\sigma_s}$
π_8	π_8	0	$\frac{1}{3}$	0	$\frac{2}{3}$
π_0	π_8	0	$\frac{\sqrt{2}}{3}$	0	$-\frac{\sqrt{2}}{3}$

Table 1: Quark mass derivatives in $N_f = 2+1$ evaluated at the expectation value. The light sector is multiplied by two due to the up-down-degeneracy.

C.2 Functional Renormalization Group

In the full FRG flow, the meson fluctuations are included in the flow, thus there is no static contribution from the meson sector. The derivatives of $\tilde{U}_k$ are obtained from the spline-interpolation on the grid. For $N_f = 2$, the grid is one-dimensional and the grid variable is $\langle\sigma^2\rangle$ [cf. Sec. 7]. The masses are therefore

$$\left.\frac{\partial^2 U}{\partial\sigma^2}\right|_{\langle\sigma\rangle} = \left.\frac{\partial}{\partial\sigma}\frac{\partial U}{\partial\rho}\frac{\partial\rho}{\partial\sigma}\right|_{\langle\sigma\rangle} = \left.\left[\frac{\partial U}{\partial\rho}\frac{\partial^2\rho}{\partial\sigma^2} + \frac{\partial^2 U}{\partial\rho^2}\left(\frac{\partial\rho}{\partial\sigma}\right)^2\right]\right|_{\langle\sigma\rangle} = 2U' + 4\sigma^2 U'' \tag{C.16}$$

and

$$\left.\frac{\partial^2 U}{\partial\pi^2}\right|_{\langle\sigma\rangle} = \left.\frac{\partial}{\partial\pi}\frac{\partial U}{\partial\rho}\frac{\partial\rho}{\partial\pi}\right|_{\langle\sigma\rangle} = \left.\left[\frac{\partial U}{\partial\rho}\frac{\partial^2\rho}{\partial\pi^2} + \frac{\partial^2 U}{\partial\rho^2}\left(\frac{\partial\rho}{\partial\pi}\right)^2\right]\right|_{\langle\sigma\rangle} = 2U' \tag{C.17}$$

where the primes denote a derivative with respect to the grid variable $\langle\sigma^2\rangle$. For $N_f = 2+1$, however, the two-dimensional grid is set up in the variables x and y as outlined in Sec. 7. In short, we pick up the definition

$$\tilde{U} := U(\rho_1, \tilde{\rho}_2) - c\xi - h_l\sigma_l - h_s\sigma_s \tag{C.18}$$

with

$$\xi := \det\left(\Phi^\dagger\right) + \det\left(\Phi\right) \quad . \tag{C.19}$$

The linear terms at the end will not contribute to the second derivatives and are dropped here. Then the chain rule yields e.g. for the first derivative (implicitly assuming the expression to be evaluated at the VEV in the end)

$$\begin{aligned}\frac{\partial \tilde{U}}{\partial \phi_i} &= \frac{\partial U}{\partial \rho_1}\frac{\partial \rho_1}{\partial \phi_i} + \frac{\partial U}{\partial \tilde{\rho}_2}\frac{\partial \tilde{\rho}_2}{\partial \phi_i} - c\frac{\partial \xi}{\partial \phi_i} \\ &= \frac{\partial U}{\partial x}\left(\frac{\partial x}{\partial \rho_1}\frac{\partial \rho_1}{\partial \phi_i} + \frac{\partial x}{\partial \tilde{\rho}_2}\frac{\partial \tilde{\rho}_2}{\partial \phi_i}\right) + \frac{\partial U}{\partial y}\left(\frac{\partial y}{\partial \rho_1}\frac{\partial \rho_1}{\partial \phi_i} + \frac{\partial y}{\partial \tilde{\rho}_2}\frac{\partial \tilde{\rho}_2}{\partial \phi_i}\right) - c\frac{\partial \xi}{\partial \phi_i} \quad .\end{aligned} \tag{C.20}$$

This is worked out more precisely in Sec. 7. For the derivatives of x and y with respect to ρ_1 and $\tilde{\rho}_2$ (again, implicitly at the VEV) we follow from Eq. (7.7)

$$\frac{\partial x}{\partial \rho_1} = \frac{4}{3} \quad , \quad \frac{\partial x}{\partial \tilde{\rho}_2} = -\frac{4}{y} \quad , \quad \frac{\partial y}{\partial \rho_1} = 0 \quad , \quad \frac{\partial y}{\partial \tilde{\rho}_2} = \frac{12}{y} \quad . \tag{C.21}$$

Calculating the derivatives of the chiral invariants and the axial breaking term at the minimum, we get in total:

$$\begin{aligned}\frac{\partial^2 \tilde{U}}{\partial \sigma_l^2} &= 2U_x - 2U_y + 4xU_{xx} + 4xU_{yy} - 8xU_{xy} - \frac{c}{2}\sqrt{x+y} \\ \frac{\partial^2 \tilde{U}}{\partial \sigma_s^2} &= 4U_y + 8(x+y)U_{yy} \\ \frac{\partial^2 \tilde{U}}{\partial \sigma_l \partial \sigma_s} &= 4\sqrt{2x(x+y)}(-U_{yy} + U_{xy}) - \frac{c}{\sqrt{2}}\sqrt{x} \\ \frac{\partial^2 \tilde{U}}{\partial \sigma_1^2} &= \left(2 - 4\frac{x}{y}\right)U_x + \left(12\frac{x}{y} - 2\right)U_y + \frac{c}{2}\sqrt{x+y} \\ \frac{\partial^2 \tilde{U}}{\partial \sigma_4^2} &= -2\frac{x + \sqrt{x(x+y)}}{y}U_x + \left(4 + 6\frac{x + \sqrt{x(x+y)}}{y}\right)U_y + \frac{c}{2}\sqrt{x} \\ \frac{\partial^2 \tilde{U}}{\partial \pi_0^2} &= \frac{4}{3}U_x + \frac{c}{3}(2\sqrt{x} + \sqrt{x+y}) \\ \frac{\partial^2 \tilde{U}}{\partial \pi_8^2} &= \frac{2}{3}U_x + 2U_y + \frac{c}{6}(\sqrt{x+y} - 4\sqrt{x}) \\ \frac{\partial^2 \tilde{U}}{\partial \pi_0 \partial \pi_8} &= \frac{2\sqrt{2}}{3}U_x - 2\sqrt{2}U_y + \frac{c}{3\sqrt{2}}(\sqrt{x+y} - \sqrt{x}) \\ \frac{\partial^2 \tilde{U}}{\partial \pi_1^2} &= 2U_x - 2U_y - \frac{c}{2}\sqrt{x+y} \\ \frac{\partial^2 \tilde{U}}{\partial \pi_4^2} &= 2\frac{\sqrt{x(x+y)} - x}{y}U_x + \left(4 + 6\frac{x - \sqrt{x(x+y)}}{y}\right)U_y - \frac{c}{2}\sqrt{x}\end{aligned} \tag{C.22}$$

with

$$U_a := \frac{\partial U}{\partial a} \quad , \quad U_{ab} := \frac{\partial^2 U}{\partial a \partial b} \quad a, b \in \{x, y\} \quad . \tag{C.23}$$

D Parameter Fixing

The input parameters of the UV potential $\tilde{U}_\Lambda$ as well as the Yukawa coupling of the quark-meson model have to be fixed in the vacuum at $T = 0$, $\mu = 0$. Fixing those values to physical observables allows us to predict the behavior of the theory at finite temperature and chemical potential. Therefore, we remember that in 2+1 flavors we use a potential of the form

$$\tilde{U}_\Lambda = U_\Lambda(\rho_1, \rho_2) - c\xi - h_l\sigma_l - h_s\sigma_s \tag{D.1}$$

where in mean field approximation

$$U_\Lambda(\rho_1, \rho_2) = m^2\rho_1 + \lambda_1\rho_1^2 + \lambda_2\rho_2 \quad . \tag{D.2}$$

In the FRG formalism we define the UV couplings

$$U_\Lambda(\rho_1, \tilde{\rho}_2) = a_{10}\rho_1 + \frac{a_{20}}{2}\rho_1^2 + a_{01}\tilde{\rho}_2 \tag{D.3}$$

with the modified second chiral invariant defined in Eq. (7.6). For mean field approximations, the meson potential is static (no fluctuations are included). The quark-potential has to be added to obtain the full potential. Note that for the sMFA the quark contribution to the vacuum is zero, while it becomes finite in the rMFA(FRG) case (as the vacuum term is included). Hence, the parameters have to differ in order to render the same physical results. Including the full FRG flow, there are also vacuum contributions from the mesons. Thus, the FRG UV couplings turn into starting values for the FRG flow that renders the physical couplings for $k = 0$. The gap equations

$$\left.\frac{\partial\tilde{U}}{\partial\sigma_l}\right|_{\sigma_l=\langle\sigma_l\rangle,\sigma_s=\langle\sigma_s\rangle} = 0 \quad , \quad \left.\frac{\partial\tilde{U}}{\partial\sigma_s}\right|_{\sigma_l=\langle\sigma_l\rangle,\sigma_s=\langle\sigma_s\rangle} = 0 \tag{D.4}$$

render h_l and h_s, respectively:

$$h_l = \left.\frac{\partial U(\rho_1, \tilde{\rho}_2) - c\xi}{\partial\sigma_l}\right|_{\langle\sigma_l\rangle,\langle\sigma_s\rangle} \quad , \quad h_s = \left.\frac{\partial U(\rho_1, \tilde{\rho}_2) - c\xi}{\partial\sigma_s}\right|_{\langle\sigma_l\rangle,\langle\sigma_s\rangle} \quad . \tag{D.5}$$

The derivatives can be directly translated into physical observables (cf. Ref. [70, 69], and App. C):

$$h_l = f_\pi m_\pi^2 \quad , \quad h_s = \sqrt{2}f_K m_K^2 - \frac{1}{\sqrt{2}}f_\pi m_\pi^2 \quad . \tag{D.6}$$

The pion mass is taken to be $m_\pi = 138\,\text{MeV}$, the Kaon mass $m_K = 496\,\text{MeV}$, the decay constants are $f_\pi = 92.4\,\text{MeV}$ and $f_K = 113\,\text{MeV}$. This gives $h_l = (120.73\,\text{MeV})^3$ and $h_s = (336.41\,\text{MeV})^3$. It has also been used that (PCAC relations)

$$\langle\sigma_l\rangle = f_\pi = 92.4\,\text{MeV} \quad , \quad \langle\sigma_s\rangle = \frac{1}{\sqrt{2}}(2f_K - f_\pi) = 94.5\,\text{MeV} \quad . \tag{D.7}$$

In sMFA, $c = 4807.84\,\text{MeV}$ can be determined analytically by fixing the sum of the squared masses of η and η' [70], but the same value will be used for rMFA and full FRG as well [71]. In the case of rMFA and full FRG, the chosen UV cutoff is $\Lambda = 1\,\text{GeV}$. In the FRG flow, we use $k_{\text{IR}} = 100\,\text{MeV}$ and in rMFA we integrate down to $k_{\text{IR}} = 1\,\text{MeV}$.

Furthermore, we use the Yukawa coupling strength $g = 6.5$ which gives constituent quark masses of

$$m_l = \frac{g}{2}\langle\sigma_l\rangle \approx 300\,\text{MeV} \quad , \quad m_s = \frac{g}{\sqrt{2}}\langle\sigma_s\rangle \approx 434\,\text{MeV} \quad . \tag{D.8}$$

The sigma meson mass has been set to 560 MeV in this work. There is still no clarity from the experimental side on the exact value of the sigma resonance. Consequently, many figures seen in literature include results that are fitted to various sigma masses of the possible spectrum. The corresponding full FRG starting values are taken from Ref. [71], the sMFA values from Ref. [84], the rMFA starting values have been fitted via a differential evolution (DE) global minimization algorithm [96]. For $N_f = 2$, the obvious simplifications happen (all parameters related to strangeness drop out) and we have less starting parameters:

$$\tilde{U}_\Lambda = U_\Lambda(\rho) - h_l\sigma \tag{D.9}$$

with

$$U_\Lambda(\rho) = m^2\rho + \lambda\rho^2 \tag{D.10}$$

in mean field approximation and

$$U_\Lambda(\rho) = a_1\rho + \frac{a_2}{2}\rho^2 \tag{D.11}$$

in the FRG solution. All other parameters have the same value as the corresponding ones in the 2+1-flavor case. All two-flavor couplings have been fitted via the differential evolution algorithm. The couplings and starting parameters are displayed in Tab. 2.

$N_f = 2$	m^2 [MeV^2]	λ
sMFA	$-(358.1)^2$	17.25
rMFA	901.09^2	-5.38

$N_f = 2$	a_1 [MeV^2]	a_2
FRG	711.98^2	10.11

$N_f = 2+1$	m^2 [MeV^2]	λ_1	λ_2
sMFA	384.71^2	-0.36	46.48
rMFA	1040.89^2	-2.65	11.73

$N_f = 2+1$	a_{10} [MeV^2]	a_{20}	a_{01}
FRG	542.22^2	36	50

Table 2: Couplings for different approaches towards the QM model with $m_\sigma = 560\,\text{MeV}$ and explicitly broken $U(1)_A$ symmetry.

References

[1] S. M. Carroll, "Spacetime and geometry. An introduction to general relativity", Pearson, 2004.

[2] S. L. Glashow, "The renormalizability of vector meson interactions", *Nuclear Physics* **10** (1959) 107–117.

[3] A. Salam and J. Ward, "Weak and electromagnetic interactions", *Il Nuovo Cimento* **11** (1959), no. 4, 568–577.

[4] S. Weinberg, "A model of leptons", *Physical review letters* **19** (1967), no. 21, 1264.

[5] K. C. Gendreau *et al.*, "The neutron star interior composition explorer (NICER): design and development", in "SPIE Astronomical Telescopes+ Instrumentation", p. 99051H, International Society for Optics and Photonics. 2016.

[6] B. P. Abbott *et al.*, "GW170817: Observation of Gravitational Waves from a Binary Neutron Star Inspiral", *Phys. Rev. Lett.* **119** (2017) 161101, 1710.05832v1.

[7] M. A. McLaughlin, "The International Pulsar Timing Array: A Galactic Scale Gravitational Wave Observatory", *M. Gen Relativ Gravit* **46** (2014) 1810, 1409.4579v2.

[8] B. Friman, C. Höhne, J. Knoll, S. Leupold, J. Randrup, R. Rapp, and P. Senger, eds., "The CBM Physics Book", Springer, 2011.

[9] D. B. Blaschke, T. Klahn, and F. Sandin, "Color superconducting quark matter in compact stars", *Exotic States of Nuclear Matter*, 2008 256–263, 0712.0117v1.

[10] J. Antoniadis, P. C. Freire, N. Wex, T. M. Tauris, R. S. Lynch, M. H. van Kerkwijk, M. Kramer, C. Bassa, V. S. Dhillon, T. Driebe, *et al.*, "A massive pulsar in a compact relativistic binary", *Science* **340** (2013), no. 6131, 1233232.

[11] H. Djapo, B.-J. Schaefer, and J. Wambach, "On the appearance of hyperons in neutron stars", *Phys. Rev. C* **81** (2010) 035803, 0811.2939v3.

[12] M. Alford, M. Braby, M. Paris, and S. Reddy, "Hybrid stars that masquerade as neutron stars", *Astrophys. J.* **629** (2005) 969–978, nucl-th/0411016v2.

[13] D. E. Alvarez-Castillo and D. Blaschke, "Supporting the existence of the QCD critical point by compact star observations", *PoS CPOD 2014* **045** (2014) 1503.05576v1.

[14] G. Beccari and G. Carraro, "Introduction to the Theory of Stellar Evolution", in "Ecology of Blue Straggler Stars", B. G. Boffin H., Carraro G., ed., vol. 413 of *Astrophysics and Space Science Library*, pp. 1–16. Springer, 2015. 1406.3462v1.

[15] S. Chandrasekhar, "XLVIII. The density of white dwarf stars", *The London, Edinburgh, and Dublin Philosophical Magazine and Journal of Science* **11** (1931), no. 70, 592–596.

[16] G. Baym, T. Hatsuda, T. Kojo, P. D. Powell, Y. Song, and T. Takatsuka, "From hadrons to quarks in neutron stars", *RIKEN-QHP-316*, 2017 1707.04966v1.

[17] J. B. Hartle, "Bounds on the mass and moment of inertia of non-rotating neutron stars", *Physics Reports* **46** (1978), no. 6, 201–247.

[18] C. Pethick, D. Ravenhall, and C. Lorenz, "The inner boundary of a neutron-star crust", *Nuclear Physics A* **584** (1995), no. 4, 675–703.

[19] Y. Nambu and G. Jona-Lasinio, "Dynamical model of elementary particles based on an analogy with superconductivity. I", *Physical Review* **122** (1961), no. 1, 345.

[20] Y. Nambu and G. Jona-Lasinio, "Dynamical model of elementary particles based on an analogy with superconductivity. II", *Physical Review* **124** (1961), no. 1, 246.

[21] S. Klevansky, "The Nambu–Jona-Lasinio Model of Quantum Chromodynamics", *Reviews of Modern Physics* **64** (1992) 649–708.

[22] G. Pagliara and J. Schaffner-Bielich, "Stability of color-flavor-locking cores in hybrid stars", *Physical Review D* **77** (2008), no. 6, 063004.

[23] R. C. Pereira, P. Costa, and C. Providência, "Two-solar-mass hybrid stars: a two model description with the Nambu-Jona-Lasinio quark model", *Phys. Rev. D* **94** (2016), no. 9, 094001, 1610.06435v2.

[24] C. J. Horowitz, E. J. Moniz, and J. W. Negele, "Hadron structure in a simple model of quark/nuclear matter", *Physical Review D* **31** (1985), no. 7, 1689.

[25] G. Röpke, D. Blaschke, and H. Schulz, "Pauli quenching effects in a simple string model of quark/nuclear matter", *Physical Review D* **34** (1986), no. 11, 3499.

[26] N.-U. F. Bastian, D. B. Blaschke, M. Cierniak, T. Fischer, M. A. R. Kaltenborn, M. Marczenko, and S. Typel, "Strange matter prospects within the string-flip model", 1710.09189v1.

[27] R. C. Tolman, "Effect of inhomogeneity on cosmological models", *Proceedings of the National Academy of Sciences* **20** (1934), no. 3, 169–176.

[28] R. C. Tolman, "Static solutions of Einstein's field equations for spheres of fluid", *Physical Review* **55** (1939), no. 4, 364.

[29] J. R. Oppenheimer and G. M. Volkoff, "On massive neutron cores", *Physical Review* **55** (1939), no. 4, 374.

[30] I. Sagert, M. Hempel, C. Greiner, and J. Schaffner-Bielich, "Compact Stars for Undergraduates", *Eur. J. Phys.* **27** (2006) 577–610, astro-ph/0506417v1.

[31] J. M. Lattimer and M. Prakash, "Neutron Star Observations: Prognosis for Equation of State Constraints", *Phys. Rept.* **442** (2007) 109–165, astro-ph/0612440v1.

[32] M. Srednicki, "Quantum Field Theory", Cambridge University Press, 2007.

[33] C.-N. Yang and R. L. Mills, "Conservation of isotopic spin and isotopic gauge invariance", *Physical review* **96** (1954), no. 1, 191.

[34] M. Gell-Mann, "Symmetries of baryons and mesons", *Physical Review* **125** (1962), no. 3, 1067.

[35] M. Gell-Mann, "A Schematic Model of Baryons and Mesons", *Phys.Lett.* **8** (1964) 214–215.

[36] Y. Nambu, "Quasi-particles and gauge invariance in the theory of superconductivity", *Physical Review* **117** (1960), no. 3, 648.

[37] J. Goldstone, "Field theories with ≪Superconductor≫ solutions", *Il Nuovo Cimento (1955-1965)* **19** (1961), no. 1, 154–164.

[38] J. Goldstone, A. Salam, and S. Weinberg, "Broken symmetries", *Physical Review* **127** (1962), no. 3, 965.

[39] J. Braun, "Fermion Interactions and Universal Behavior in Strongly Interacting Theories", *Journal of Physics G: Nuclear and Particle Physics* **39** (2012), no. 3, 1108.4449v1.

[40] G. Hooft, "How instantons solve the U (1) problem.", *Physics Reports* **142** (1986), no. 6, 357–387.

[41] H. D. Politzer, "Reliable perturbative results for strong interactions?", *Physical Review Letters* **30** (1973), no. 26, 1346.

[42] D. J. Gross and F. Wilczek, "Ultraviolet behavior of non-abelian gauge theories", *Physical Review Letters* **30** (1973), no. 26, 1343.

[43] A. Ukawa, "Kenneth Wilson and lattice QCD", *J. Stat. Phys.* **160** (2015), no. 5, 1081–1124, 1501.04215v2.

[44] F. J. Dyson, "The S matrix in quantum electrodynamics", *Physical Review* **75** (1949), no. 11, 1736.

[45] J. Schwinger, "On the Green's functions of quantized fields I", *Proc. Nat. Acad. Sci* **37** (1951) 452–455.

[46] J. Schwinger, "On the Green's functions of quantized fields II", *Proc. Nat. Acad. Sci* **37** (1951) 455–459.

[47] R. Alkofer and L. von Smekal, "The Infrared Behavior of QCD Green's Functions - Confinement, Dynamical Symmetry Breaking, and Hadrons as Relativistic Bound States", *Phys. Rept.* **353** (2001) 281, hep-ph/0007355v2.

[48] J. M. Pawlowski, "Aspects of the Functional Renormalisation Group", *Annals Phys.* **322** (2007) 2831–2915, hep-th/0512261.

[49] H. Gies, "Introduction to the functional RG and applications to gauge theories", in "Renormalization Group and Effective Field Theory Approaches to Many-Body Systems", P. J. Schwenk A., ed., vol. 852 of *Lecture Notes in Physics*, pp. 287–348. Springer, 2012. hep-ph/0611146.

[50] D. U. Jungnickel and C. Wetterich, "Effective Action for the Quark-Meson Model", *Phys. Rev. D* **53** (1996) 5142–5175, hep-ph/9505267v1.

[51] C. S. Fischer and J. Luecker, "Propagators and phase structure of Nf=2 and Nf=2+1 QCD", *Phys. Lett. B* **718** (2013) 1036–1043, 1206.5191v2.

[52] C. S. Fischer, J. Lücker, and J. M. Pawlowski, "The phase structure of QCD for heavy quarks", *Phys. Rev. D* **91** (2015) 014024, 1409.8462v1.

[53] B.-J. Schaefer and J. Wambach, "The Phase Diagram of the Quark-Meson Model", *Nucl.Phys. A* **757** (2005) 479–492, nucl-th/0403039.

[54] B.-J. Schaefer and J. Wambach, "Renormalization Group Approach towards the QCD Phase Diagram", *Phys. Part. Nucl.* **39** (2008) 1025–1032, hep-ph/0611191.

[55] C. Ratti, S. Roessner, and W. Weise, "Quark number susceptibilities: lattice QCD versus PNJL model", *Phys. Lett. B* **649** (2007) 57–60, hep-ph/0701091v1.

[56] B.-J. Schaefer, J. M. Pawlowski, and J. Wambach, "The Phase Structure of the Polyakov–Quark-Meson Model", *Phys. Rev. D* **76** (2007) 074023, 0704.3234v2.

[57] V. Skokov, B. Stokic, B. Friman, and K. Redlich, "Meson fluctuations and thermodynamics of the Polyakov loop extended quark-meson model", *Phys. Rev. C* **82** (2010) 015206, 1004.2665v1.

[58] T. K. Herbst, J. M. Pawlowski, and B.-J. Schaefer, "The phase structure of the Polyakov–quark-meson model beyond mean field", *Phys. Lett. B* **696** (2011) 58–67, 1008.0081v1.

[59] R. Alkofer and H. Reinhardt, "Chiral quark dynamics", Springer Science & Business Media, 1995.

[60] L. D. Faddeev and V. N. Popov, "Feynman diagrams for the Yang-Mills field", *Physics Letters B* **25** (1967), no. 1, 29–30.

[61] M. Schaden, H. Reinhardt, P. Amundsen, and M. Lavelle, "An effective action for Yang-Mills field strengths", *Nuclear Physics B* **339** (1990), no. 3, 595–622.

[62] H. Reinhardt, "Bosonization of QCD in the field strength approach", *Physics Letters B* **257** (1991), no. 3-4, 375–382.

[63] R. Alkofer and H. Reinhardt, "Fermion condensation in the field strength approach to non-abelian Yang-Mills theories", *Zeitschrift für Physik A Hadrons and Nuclei* **343** (1992), no. 1, 79–101.

[64] R. T. Cahill, J. Praschifka, and C. J. Burden, "Diquarks and the Bosonisation of QCD", *Aust. J. Phys.* **42** (1989) 161.

[65] J. Hubbard, "Calculation of partition functions", *Physical Review Letters* **3** (1959), no. 2, 77.

[66] R. Stratonovich, "On a method of calculating quantum distribution functions", in "Soviet Physics Doklady", vol. 2, p. 416. 1957.

[67] J. Berges, N. Tetradis, and C. Wetterich, "Non-Perturbative Renormalization Flow in Quantum Field Theory and Statistical Physics", *Phys.Rept.* **363** (2002) 223–386, hep-ph/0005122.

[68] F. Rennecke, "The Chiral Phase Transition of QCD", PhD thesis, University of Heidelberg, 2015.

[69] J. T. Lenaghan, D. H. Rischke, and J. Schaffner-Bielich, "Chiral Symmetry Restoration at Nonzero Temperature in the SU(3) x SU(3) Linear Sigma Model", *Phys.Rev.D* **62:085008** (2000) nucl-th/0004006.

[70] B.-J. Schaefer and M. Wagner, "The three-flavor chiral phase structure in hot and dense QCD matter", *Phys.Rev.D* **79:014018,2009** (2008) 0808.1491.

[71] M. Mitter and B.-J. Schaefer, "Fluctuations and the axial anomaly with three quark flavors", *Phys. Rev. D* **89,** (2013) 054027, 1308.3176.

[72] J. I. Kapusta and C. Gale, "Finite-temperature field theory: Principles and applications", Cambridge University Press, 2006.

[73] A. Nieto, "Evaluating Sums over the Matsubara Frequencies", *Comput. Phys. Commun.* **92** (1995) 54, hep-ph/9311210.

[74] K. G. Wilson, "Renormalization group and critical phenomena. I. Renormalization group and the Kadanoff scaling picture", *Physical review B* **4** (1971), no. 9, 3174.

[75] K. G. Wilson, "Renormalization group and critical phenomena. II. Phase-space cell analysis of critical behavior", *Physical Review B* **4** (1971), no. 9, 3184.

[76] M. Scherer, "Renormalization Group Theory: The Physics of Scales". Lecture Notes (Heidelberg), 2013.

[77] K. G. Wilson, "The renormalization group and critical phenomena", *Reviews of Modern Physics* **55** (1983), no. 3, 583.

[78] J. Polchinski, "Renormalization and effective Lagrangians", *Nuclear Physics B* **231** (1984), no. 2, 269–295.

[79] C. Wetterich, "Average action and the renormalization group equations", *Nuclear Physics B* **352** (1991), no. 3, 529–584.

[80] C. Wetterich, "Improvement of the average action", *Zeitschrift für Physik C Particles and Fields* **60** (1993), no. 3, 461–469.

[81] C. Wetterich, "The Average action for scalar fields near phase transitions", *Zeitschrift für Physik C Particles and Fields* **57** (1993), no. 3, 451–469.

[82] D. F. Litim, "Optimised Renormalisation Group Flows", *Phys. Rev. D* **64** (2001) 105007, hep-th/0103195v2.

[83] J. M. Pawlowski, M. M. Scherer, R. Schmidt, and S. J. Wetzel, "Physics and the choice of regulators in functional renormalisation group flows", *Annals Phys.* **384** (2017) 165–197, 1512.03598v1.

[84] S. Resch, "Mass Sensitivity of the QCD Phase Structure", Master's thesis, Justus Liebig University Giessen, 2016.

[85] J. Adams, J. Berges, S. Bornholdt, F. Freire, N. Tetradis, and C. Wetterich, "Solving non-perturbative flow equations", *Mod.Phys.Lett. A* **10** (1995) 2367–2380, hep-th/9507093.

[86] B.-J. Schaefer and M. Mitter, "Three-flavor chiral phase transition and axial symmetry breaking with the functional renormalization group", *Acta Phys. Polon. Supp.* **7** (2014), no. 1, 81–90, 1312.3850v1.

[87] G. G. Barnafoldi, A. Jakovac, and P. Posfay, "Harmonic expansion of the effective potential in Functional Renormalization Group at finite chemical potential", *Phys. Rev. D* **95** (2017) 025004, 1604.01717v1.

[88] W. H. Press, "Numerical recipes 3rd edition: The art of scientific computing", Cambridge University Press, 2007.

[89] R.-A. Tripolt, B.-J. Schaefer, L. von Smekal, and J. Wambach, "The low-temperature behavior of the quark-meson model", 1709.05991v1.

[90] N. Strodthoff, B.-J. Schaefer, and L. von Smekal, "Quark-meson-diquark model for two-color QCD", *Phys. Rev. D* **85** (2012) 074007, 1112.5401.

[91] N. Strodthoff and L. von Smekal, "Polyakov-Quark-Meson-Diquark Model for two-color QCD", *Physics Letters B* **731C** (2013) 350–357, 1306.2897.

[92] P. Pósfay, G. G. Barnaföldi, and A. Jakovác, "The effect of quantum fluctuations in compact star observables", 1710.05410v1.

[93] C. G. van Weert, "Statistical Field Theory - An Introduction to Real- and Imaginary-time Thermal Field Theory". Lecture Notes, 2001. https://staff.fnwi.uva.nl/c.g.vanweert/Lecnotes/thermal_notes.pdf.

[94] M. Laine and A. Vuorinen, "Basics of Thermal Field Theory - A Tutorial on Perturbative Computations", Springer, 2016.

[95] N. P. van der Aa, H. G. ter Morsche, and R. R. M. Mattheij, "Computation of eigenvalue and eigenvector derivatives for a general complex-valued eigensystem", *Electronic Journal of Linear Algebra* **16** (2007) 300–314, https://www.emis.de/journals/ELA/ela-articles/articles/vol16_pp300-314.pdf.

[96] R. Storn and K. Price, "Differential evolution–a simple and efficient heuristic for global optimization over continuous spaces", *Journal of global optimization* **11** (1997), no. 4, 341–359.

Selbstständigkeitserklärung

Hiermit versichere ich, die vorgelegte Thesis selbstständig und ohne unerlaubte fremde Hilfe und nur mit den Hilfen angefertigt zu haben, die ich in der Thesis angegeben habe. Alle Textstellen, die wörtlich oder sinngemäß aus veröffentlichten Schriften entnommen sind, und alle Angaben die auf mündlichen Auskünften beruhen, sind als solche kenntlich gemacht. Bei den von mir durchgeführten und in der Thesis erwähnten Untersuchungen habe ich die Grundsätze gute wissenschaftlicher Praxis, wie sie in der ‚Satzung der Justus-Liebig-Universität zur Sicherung guter wissenschaftlicher Praxis' niedergelegt sind, eingehalten. Gemäß § 25 Abs. 6 der Allgemeinen Bestimmungen für modularisierte Studiengänge dulde ich eine Überprüfung der Thesis mittels Anti-Plagiatssoftware.

Datum	Unterschrift